8-24-2011

The Structural Response of a Frame-Membrane Lunar Habitat Subjected to Impact and Thermal Loads

Thomas G. Gionet
thomasgionet@gmail.com

The Structural Response of a Frame-Membrane Lunar Habitat Subjected to Impact and Thermal Loads

Thomas Gionet

B.S., University of Connecticut, Department of Civil and Environmental Engineering

Storrs, CT

A Thesis

Submitted in Partial Fulfillment of the

Requirements for the Degree of

Master's of Science in Civil Engineering

at the

University of Connecticut

September, 2011

APPROVAL PAGE

Master's of Science Thesis

The Structural Response of a Frame-Membrane Lunar Habitat Subjected to Impact and Thermal Loads

Presented by

Thomas Gionet

Major Advisor 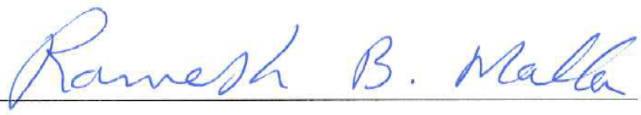

Prof. Ramesh B. Malla, Ph.D.

Associate Advisor 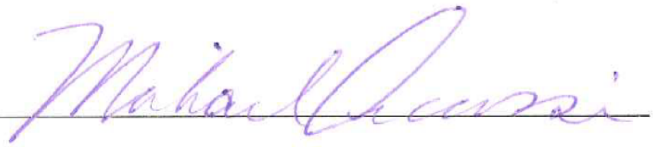

Prof. Michael Accorsi, Ph.D.

Associate Advisor 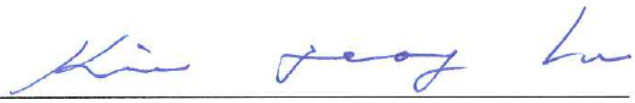

Prof. Jeong-Ho Kim, Ph.D.

University of Connecticut

August, 2011

ACKNOWLEDGEMENTS

First, I would like to thank Dr. Ramesh B. Malla, my Major Faculty Advisor, for his assistance and direction on this project. He has helped me tremendously on this project for the past two years and this report is a result of his dedication and devotion to this project. I am also very thankful for his guidance during my undergraduate and graduate programs.

I would like to thank my Associate Advisors, Dr. Michael Accorsi and Dr. Jeong-Ho Kim, for reviewing and providing valuable comments on this thesis.

I am very thankful for the financial support from the Connecticut Space Grant Consortium, Hamilton-Sundstrand, New England Transportation Consortium, and the Department of Civil & Environmental Engineering. In particular, I would like to thank the funding of the Connecticut Space Grant Consortium for the travel grant they awarded me, which funded my trip to the 52nd AIAA/ASME/ASCE/AHS/ASC Structures, Structural Dynamics and Materials Conference in Denver, CO.

Sincere thanks go out to the faculty and staff of the Department of Civil and Environmental Engineering at University of Connecticut, especially Ms. Kristina Ashley, Ms. Tiffany Thibodeau, and Ms. Jessica Zoldak.

Finally, I would like to thank my family and friends both at and away from the University of Connecticut for their much needed help and moral support.

ABSTRACT

Due to their lightweight, ease of construction, and sturdy design, three-dimensional frame-membrane structures have often been used as semi-permanent structures by the military and disaster relief agencies. The membrane provides a fully enclosed space for the people or equipment inhabiting the structure, while the frame adds extra structural support for any harsh loading such as impact, blast, or heavy wind loads. Because of their success on Earth, frame-membrane structures have also been proposed as possible lunar habitat. However, for any proposed lunar habitat, including frame-membrane structures, to be successful, it must be able to withstand the harsh lunar environment including, but not limited to, lack of atmosphere/hard vacuum, extreme temperature (daytime temperature = +123°C; nighttime temperature = -233°C), radiation, and space debris impact.

This research presents the structural response of an internally pressurized and regolith covered frame-membrane design. The structure is subjected to impact and thermal loading and incorporates the effects of the added mass due to the regolith cover and the stress stiffening from the internal pressurization. The impact loading was analytically determined considering a moving projectile, for example space debris, hitting the midpoint of a frame member at the crest of the structure. Results from the static, frequency, and dynamic nonlinear (large deformation) finite element analyses are presented.

Results from this research show that frequency is affected by the external temperature, internal pressurization, and added regolith mass. The increasing the external temperature increases the natural frequencies and conversely decreasing the temperature

decreases the frequencies. The addition of internal pressure is seen to increase the frequencies slightly, whereas the addition of the mass from the regolith cover drastically reduces the frequency. The static analysis shows that the external temperature and the internal pressurization have a significant effect on the static displacements and stresses. The dynamic results due to impact load shows that the application of the extreme lunar temperatures reduces the dynamic amplitude (compared to cases where the outside temperature is the same as the inside temperature). The internal pressurization is seen to have little effect on the dynamic amplitude and oscillation. The added mass due to the regolith is seen to reduce the oscillation amplitude and increase the period.

TABLE OF CONTENTS

LIST OF TABLES

LIST OF FIGURES

CHAPTER 1

INTRODUCTION

This chapter presents the motivation, objectives and scope for this thesis project. In addition a literature review on proposed lunar structures and the lunar environment are provided.

1.1 RESEARCH MOTIVATION

While conceived by the Eisenhower administration, the Apollo program did not truly until 1961 when President John F. Kennedy declared before congress that the United States of America "should commit itself to achieving the goal, before this decade is out, of landing a man on the moon and returning him safely to the earth (John F. Kennedy Presidential Museum and Library, 1961)." After numerous successes of a moderate nature throughout the decade, the ultimate goal was achieved when Apollo 11 became the first successful lunar landing in 1969. Additionally, the Apollo program would successfully land on the moon five more times throughout the early 1970s (NASA, 2011). While the United States interest in the moon waned considerably in the late 1970s through the 1990s, it peaked again in 2004. On January 4, President George Bush announced a new plan to return to the moon and establish a permanent base by 2020 (Ruess et al., 2006).

The reasons to return to the moon are numerous and diverse. They include (Ruess et. al, 2006; Siegfried, 1999):

a) Scientific studies. The moon would offer a pristine view of the surround space making it an ideal location for observatories. Additionally, the lack

of atmosphere and minimal seismic activity provides preserved geological landscape, which could be used to study lunar geology and asteroid threat analysis.

b) Economic Commercialization. The obvious commercial benefit would be the possibility of lunar tourism, but the moon could offer other commercial possibilities. The Moon has a wealth of raw materials, including iron, aluminum, silicon, and titanium. These materials could be mined and then exported to Earth. Also, the Moon is constantly exposed to sunlight creating an inexhaustible energy source. If this energy could be sent back to Earth, it could be sold as cheaper and more environmentally friendly energy source.

c) Technology Transfer. Space programs have designed technologies that were designed for space exploration, but that later have been used throughout society, for example the satellite. A permanent lunar colony could lead to the creation of new technologies, which will benefit both earth and space societies.

d) International Cooperation. While the space race was a competition between the USA and the USSR, the International Space Station was a collaborative effort between nations. The ISS helped improve international relations and the possibility of an International Lunar Space Station could do the same.

e) Stepping Stone to Mars. Many believe that a Moon base would be a stepping stone to Mars. Leaving Earth's orbit is an expensive challenge

due to its gravity, but the Moon has 1/6 the gravity on Earth and thus, it would be an easier take off point.

Over the past several decades, many lunar base concept designs have been proposed. A few engineering concepts (Sowerby, 1954; Rinehart, 1959; Szilard, 1959) were designed in the 1950s, before the Apollo program had even been conceived. However, the inspiration to the vast majority of lunar base concepts were the Apollo missions. Some potential lunar structures are those investigated in Benaroya and Ettouney (2002), Ruess et al. (2006), Lin et al. (1988), Vanderbilt et al. (1988), Drake and Richter (1990), Chow and Lin (1988), Sherwood and Toups (1992), Malla et al. (1995), and Dayal (2009).

Due to their light weight and ease of transport, the most common of these design concepts have proposed fabric shelters as future extraterrestrial habitats on the Moon and Mars (Vanderbilt et al., 1988; Malla, 1991; Sadeh and Criswell, 1994). Fabric shelters are inflatable structures that are commonly used in military bases on Earth for temporary storage of equipment, personnel, vehicles, and other military goods (AFRL, 2007). Additionally, light-weight fabric structures that can sustain extreme loading (such as impact and blast loading) are in development at the present(Kapoor et al, 2005; Quigley et al., 2006).

For any structure, including inflatable structure, to be successful as a lunar habitat it must withstand the harsh lunar environment, which includes the challenges of (Ruess et al., 2006):

a) Lack of atmosphere. Thus, any structure located on the moon must be pressurized and have oxygen present for humans to survive. While

atmospheric pressure on Earth is 101.4 kPa (14.7 psi), NASA has successfully experimented at pressures of 34.5 kPa (5 psi).

b) Radiation shielding. Earth's atmosphere limits the levels of harmful radiation, but since the Moon has no atmosphere and thus is bombard with solar radiation. A radiation dosage of 4-6 Sv is fatal for humans and the Moon experiences about 10 solar events that producing 4 Sv or more each year. A lunar structure must provide shielding from this radiation. Typically, concept designs use lunar regolith as a radiation shield. It has been determined that a 2 m thick layer of regolith reduce radiation to safe levels. Additionally, polymer sheets have been developed that absorb radiation reducing the amount of regolith required for shielding.

c) Temperature. The lunar temperature ranges from -233°C during the lunar night to +123°C during the lunar day. Additionally, the lunar day and night are each about 15 days.

d) Reduced gravity. Gravity on the Moon is $1/6^{th}$ the gravity of Earth. Thus, structures have six times the capacity.

e) Lunar dust. The Moon has a fine layer of regolith dust, which is easily displaced. Additionally, the dust statically clings to all surfaces and cause damage to equipment.

f) Ease of construction. Any lunar structure must be easily assembled, because the construction will be done by fully suited astronauts. Additionally, these astronauts likely will not be skilled construction workers and have access to all the construction equipment available on Earth.

g) Weight and use of in-situ materials. Due to the remoteness of the Moon and the cost of transporting building supplies, the majority of the construction material used to build the habitat should be lightweight or readily available on the Moon (in-situ materials).

Until recently, the majority of research on lunar base structures published is in the concept design stage. The exact static and dynamic responses of proposed lunar structures are unknown. Since the design codes used for earth based structures do not adequately address the requirements of a lunar base, these responses are crucial to knowing the structural stability and safety of a proposed base. Additionally, once these responses are ascertained and then, uniform lunar building codes can be developed.

In previous papers, an internally pressurized three-dimensional (3-D) frame-membrane structure covered with regolith shielding has been proposed by Malla and Chaudhuri (2006, 2007, 2008). The membrane of the structure contains the internal pressurization. The frame helps support the pressurization load and provides greater stiffness with low mass to the structural system (due to its inherent characteristics of high rigidity and mass ratio). The frame structure also helps to retain the regolith cover, which serves in protecting the structure from radiation, temperature extremes, and direct impact of moving debris/projectile on the membrane. The inside of the structure is fully pressurized (96.5 kPa), room temperature (21°C), and shielded from impact and radiation.

The research presented in this thesis is the structural response of this proposed frame-membrane lunar structure. The structure is subjected to lunar temperature extremes and impact loading due to flying debris (such as broken equipment falling from a lunar lander spacecraft) striking a key location, the mid-point of a frame member of the

structure. Frequency, non-linear static, and non-linear dynamic analysis results have been obtained using the finite element method. The impact force was analytically and computationally derived and applied as a forcing function to the finite element model. In order to evaluate the effects of internal pressurization, added mass of the regolith cover, and the extreme lunar temperature are examined with respect to the frequency, deformation, and stress of the structure.

1.2 RESEARCH OBJECTIVES

The main goal of this research project is to determine the structural response of a proposed internally pressurized lunar structure with a regolith layer when subjected impact loading and extreme lunar temperatures. This goal was achieved by attained the following objectives:

- Estimate the natural frequencies and mode shapes of the proposed lunar structure;
- Analyze the static deformation and stress of the proposed habitat;
- Analytically and computationally determine an accurate impact loading;
- Apply the impact loading to the structure and determine the dynamic displacements and stresses of the system;
- Determine the effects of internal pressurization, added mass of the regolith layer, and the extreme lunar temperatures on the proposed structure's frequency, static, and dynamic responses.

1.3 STRUCTURE OF THESIS

Chapter 1 of this thesis covers the background information, motivation, and project objectives. Chapter 2 presents "Dynamic Response of a Pressurized Frame-Membrane Lunar Structure with Regolith Cover Subjected to Impact Load." An analytically calculated impact load is applied to the midspan of a frame member of the proposed structure and the effect of added mass of regolith and internal pressurization on frequency, static, and dynamic response are provided. Chapter 3 presents "Frequency and Impact Analysis of a Proposed Frame-Membrane Lunar Structure at Extreme Temperatures." An analytically calculated impact load is again applied to the midspan of a frame member of the proposed structure and the effect of extreme temperature and internal pressurization on frequency, static, and dynamic response are provided. Chapter 4 covers the frequency and impact analysis of a single panel of the proposed lunar structure. In this chapter, the effects of temperature, added mass, and internal pressure on frequency are examined. Additionally, the impact force examined is found computationally, not analytically like in Chapters 2 and 3. The conclusions and recommendations for future research are provided in Chapter 5. Finally, all the references are displayed in Chapter 6.

CHAPTER 2

DYNAMIC RESPONSE OF A PRESSURIZED FRAME-MEMBRANE LUNAR STRUCTURE WITH REGOLITH COVER SUBJECTED TO IMPACT LOAD

Abstract

A three-dimensional frame-membrane structure covered with regolith shielding and internally pressurized has been proposed as a possible lunar habitat. This paper presents results from the static, frequency, and dynamic impact analysis of the structure using nonlinear (large deformation) finite element technique. The results are presented take into account the effect of the added mass of regolith and stress stiffening due to applied internal pressurization load as well. The impact loading is analytically derived by considering the impact of a moving object/debris/projectile hitting the midpoint of one of the frame members at the crest of the structure. For the frequency analysis, the results show that both pressurization and added regolith mass affect the frequency and mode shape characteristics, where the effects due to the added mass of regolith are observed to be substantially larger than that due to the pressurization. For the static and dynamic analyses, the mid-span impact results show that both pressurization and added regolith mass affect the displacement and stress of the structure. The internal pressurization (prestressing) causes the structure to statically expand and stresses it, but has little effect on the dynamic amplitude of oscillation of the displacement and stress. The added mass of regolith also influences the static displacement and stress slightly contracting and stressing the structure. However, it has a much larger impact on the transient analysis reducing the oscillation amplitude and increasing the period.

2.1 INTRODUCTION

There are many challenges engineers have to face in designing and constructing a lunar base for human habitation since the Moon has an extreme and harsh environment. The challenges include, but are not limited to, the complete lack of atmosphere (hard vacuum), micrometeorite impact, reduced gravity, dust, severe temperature extremes, and radiation exposure (ASCE Task Committee, 1992; Benaroya et al, 2002; Heiken et al, 1991; Malla, 1991).

There have been numerous concept designs proposed for lunar base structures in the past several decades (See, for examples, ASCE Task Committee on Lunar Base Structures, 1992; Benaroya et al, 2002; Malla, 1991). The first major concepts were conceived in 1950s, well before the manned Apollo missions to the Moon in late 1960's and early 1970's (Rinehart, 1959; Sowerby, 1954; and Szilard, 1959). However, the vast majority of lunar base concepts and their studies were triggered by the Apollo missions to the Moon. Some of these investigations on potential lunar structures include those by Benaroya and Ettouney (1992), Chow and Lin (1988), Dayal (2009); Drake and Richter (1990), Lin et al. (1988), Malla et al. (1995), Sherwood and Toups (1992), Ruess et al. (2006), and Vanderbilt et al. (1988) .

Many design concepts have proposed fabric shelters as future extraterrestrial habitats on the Moon and Mars (e.g. see Malla, 1991; Sadeh and Criswell, 1994; Vanderbilt *et al*., 1988). Fabric shelters are inflatable structures that are commonly used in military bases on Earth for temporary storage of equipment, personnel, vehicles and other military goods (for example, see AFRL, 2007). Recently, attention is being paid to the development of light weight fabric structures that meet impact and blast protection

requirements (e.g. see Kapoor *et al*., 2005; Quigley *et al*., 2006). On the Moon, these structures must be designed to withstand impact load from moving debris/projectiles.

For any lunar base to be successful, it must be internally pressurized and use local material. Because of the Moon lacks atmosphere, internal pressurization is essential for sustaining human life in a lunar structure. However, this could lead to prestressing/stress stiffening of the structure, which in turn affects the structural response. For economy and construction efficiency, it is a necessity that as much local material as possible be used for building structures on the Moon. Covering the structure with regolith (lunar soil) has been proposed to shield against extreme temperature, radiation exposure and impact (Land, 1985; Malla et al, 1985; Benaroya et al, 2002; Ruess et al, 2006). The regolith cover, however, can introduce a host of new challenges in the design and analysis of the structures for engineers. One of these challenges is the increase in the total mass of the structural system, which could have substantial effects on the structural response, especially dynamic response.

Most research on lunar base structures published until recently are in the conceptual stage and needs further quantification. The exact static and dynamic responses of proposed lunar structures are unknown. Additionally, design codes used for earth based structures do not adequately address the requirements of a lunar base. In order to successfully inhabit the moon, these responses must be ascertained and codes must be developed.

In previous papers, an internally pressurized three-dimensional (3-D) frame-membrane structure covered with regolith shielding has been proposed by the authors as a possible lunar habitat that would maintain a short-sleeve environment (Malla and

Chaudhuri, 2006, 2007, 2008). The membrane of the structure contains the internal pressurization. The 3-D frame structure helps support the pressurization load and provides greater stiffness with low mass to the structural system due to its inherent characteristics of high rigidity and mass ratio. The frame structure also helps to retain regolith, which serves in protecting the structure from radiation, temperature extremes, and direct impact of moving debris/projectile on the membrane.

This paper presents the response of the proposed frame-membrane lunar structure caused by the impact loading due to flying debris (such as broken equipment falling from a lunar lander spacecraft) striking a key location, the mid-point of a frame member of the structure. Frequency, non-linear static, and non-linear dynamic analysis results have been obtained using the finite element method. The impact force was analytically derived and then applied as a forcing function to the finite element model. In order to evaluate the effects of internal pressurization and added mass of the regolith cover on the structural response of the habitat, the frequency, deformation, and stress results are presented for the following four load cases: (a) no internal pressure and no added regolith mass, (b) internal pressure and no added regolith mass, (c) no internal pressure and added regolith mass, and (d) internal pressure and added regolith mass.

2.2 PROPOSED LUNAR HABITAT STRUCTURE DESIGN

The lunar habitat structure analyzed herein consists of a combination of 0.0075 m thick Kevlar membrane enclosed by four connected three-dimensional (3-D) aluminum frame modules. The membrane has a high modulus of elasticity to be able to carry/contain an internal pressurization load of one atmosphere and the frame increases

the structures stiffness while keeping the mass low. Figure 2.1(a) shows the front elevation of the proposed structural system. The 3-D frame is composed of 2014-T6 aluminum and has 467 tubular cross-section members with an outer diameter of 0.075 m and an inner diameter of 0.04 m (See Figure 2.1(c)). The clear height (h) of the structure equals to 5.83 m, the clear span (w) is 9.8 m, and the length of the structure (perpendicular to the plane of the paper) is 4.2 m. Additionally, the surface area of the membrane is 70.56 m^2 (four panels each with a 4.2 m x 4.2 m membrane spanning the inner chords).

Additionally, Figures 2.1(b) and 2.1(d) shows the top and side views of each of the frame modules (ABDC, CDEF, EFHG, and GHJI). Each frame module is a truncated square pyramid made up of 40 outer chords and 24 inner chords of length 1.4 m, and 64 diagonal members, each 1.8 m long. The length of frame elements must be such that they can be stored in a space shuttle cargo bay, since they are to be transported from earth. The minimum length of elements should be such to optimize the number of joints and costs associated with the increased construction time. Table 2.1 presents the structural parameters and material properties for the system. The foundation of the structure proposed was considered to be pinned on at the designated support points (Figure 2.1(a)). The pinned support is representative of many traditional foundations; for example, the membrane periphery being held down by a number of cables anchored into the regolith and the three dimensional frame members attached to the regolith.

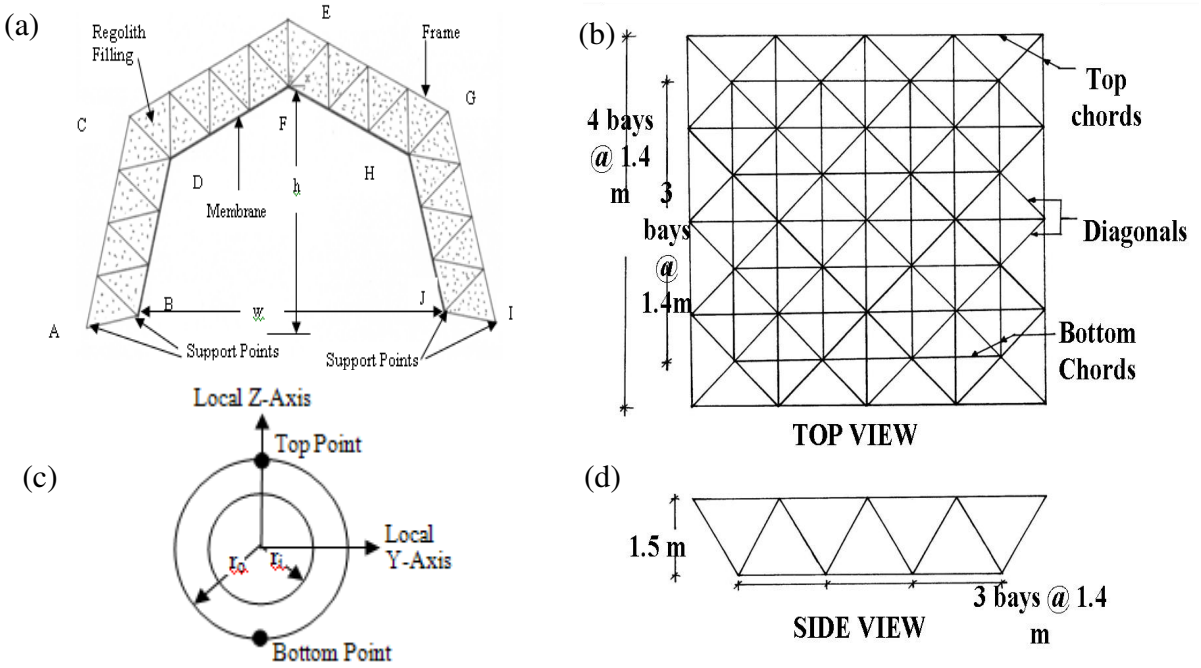

Figure 2.1. View of proposed structure: (a) Front view; (b) Top view; (c) Frame member cross-section with top and bottom of cross section marked; and (d) Side view.

Table 2.1. Structural dimensions and material properties and finite element model

Parameter	**Membrane**	**Frame**
(A) Frame-Membrane Structure:		
Material used	Kevlar	2014-T6 Aluminum
Young's Modulus (E)	70.5 GPa	72.5 GPa
Density (ρ)	1440 kg/m^3	2800 kg/m^3
Poisson's ratio (ν)	0.35	0.3
Thickness/ Cross-sec Area	0.0075 m	0.00316 m^2
Yield Strength	2920 MPa	410 MPa
(B) Finite Element Model :		
ANSYS Element Type	SHELL181	BEAM4
No. of Elements & Nodes (Frequency Analysis)	3600 (elements), 976 (nodes)	4640 (elements),4313 (nodes)
No. of Elements & Nodes (Impact Analysis)	576 (elements), 637 (nodes)	2048 (elements), 1556 (nodes)

In order to make the inside environment of the habitat hospitable, the system is internally pressurized and shielded from the external temperatures, solar radiation, and space debris impact. The system is considered internally pressurized to 96.5 kPa (14 psi) to maintain a short sleeve environment. The shielding provided a 1.5 m thick regolith layer (density = 1580 kg/m^3) that fills the spaces in the frame and covers the outside of the membrane (Heiken et al, 1991).

Furthermore, the following construction related considerations were taken into account designing the proposed structure: (a) use of indigenous (in situ) materials as much as possible for construction (thus, reducing the payload to be carried from the earth); (b) components which are easily deployed/assembled/connected to make the structure; (c) it is feasible to build the habitat entirely under or above the ground as well as partly under and partly above the ground; (d) a structural system which can be expanded easily to accommodate increased needs in the future.

2.3 ANALYSIS METHODOLOGY

Membrane structures are expected to undergo significant amount of stress stiffening due to applied pressurization and one must consider the stress state of the system during its service life for dynamic analysis (Bedri and Al-Nais, 2005). The frame-membrane system considered is subjected to internal pressurization load and thus, can also undergo stress stiffening. Additionally, the stress state influences the values of the stiffness matrix, and can therefore change the natural frequencies and response (Donadson *et al.*, 2002). Similarly, the added mass of regolith changes the mass matrix of the structure and hence, also changes the frequencies and the response.

The equation of motion of a structure is given by

$$\left[M + M_a\right]\{\ddot{\delta}\} + [C]\{\dot{\delta}\} + [K + K_G]\{\delta\} = \{P\} \tag{2.1}$$

where [K] is the stiffness matrix, [K_G] is the geometric stiffness matrix, [M] is the mass matrix; [M_a] is the added mass of regolith, [C] is the damping matrix, {P} is the external force applied, which may include the impact force, {δ} is the nodal degree of freedom, and a dot above a character is the derivative with respect to time. The [K_G] matrix will be augmented/modified initially to account for prestress due to application of internal pressurization load.

Restricting our study to undamped case, the above equation reduces to

$$\left[M + M_a\right]\{\ddot{\delta}\} + [K + K_G]\{\delta\} = \{P\} \tag{2.2}$$

2.3.1 Frequency/Modal Analysis

By setting *{P} = 0* in Eq. (2.2) and considering the free vibration motion as a simple harmonic,

$$\{\delta(t)\} = \{\delta_0\}\sin(\omega t + \phi) \tag{2.3}$$

where t is the time, $\{\delta_0\}$ is the shape of the system (which does not change with time; only the amplitude varies), ω is the natural frequency of the structure, and φ is the phase angle, the equation of motion can be expressed in the form of the eigenvalue problem as given below

$$\left([K + K_G] - \omega^2[M + M_a]\right)\{\delta_0\} = \{P\} \tag{2.4}$$

From Eq. (4), the characteristic frequency equation can be formed and is given by

$$\left|[M + M_a]^{-1}[K + K_G] - \omega^2[I]\right| = \{0\} \tag{2.5}$$

Where *[I]* is the identity matrix. Equation (2.5) is used to compute the natural frequencies of the structure.

2.3.2 Impact Force Dynamic Analysis

For the impact analysis, the 3-D frame-membrane structure is considered to be hit by a moving object (debris/projectile) at the mid-span of an outer chord of the frame. The impact load acting on the structure was calculated considering the transverse collision of a rigid mass, m_2, with initial velocity, $v_{2,0}$, striking a simply supported beam (AB) of mass, m_1, and length, L, as shown in Figure 2.2 (Goldsmith, 1960). The stiffness, k, of a simply supported beam subjected to central loading is $48EI/L^3$. It is assumed that the rigid mass and a certain fraction of the beam mass (χm_1) will undergo completely inelastic impact and attain the same velocity, v, immediately after impact. The law of conservation of momentum for the system gives,

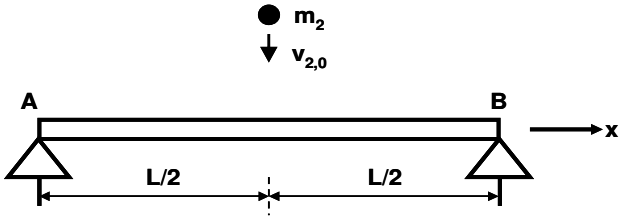

Figure 2.2. Central impact on a simply supported beam.

$$m_2 v_{2,0} = (m_2 + \chi m_1) v \; ; \qquad \text{or} \qquad v = m_2 v_{2,0} / (m_2 + \chi m_1) \tag{2.6}$$

It is assumed that the dynamic deflection curve is geometrically similar to the static deflection curve, $f(x)$. The static deflection curve is a function of position x measured along the beam length (with the origin at the left end, A, of the beam and with point of impact at x = c), and time, t. This is expressed in the following form,

$$w = w(c,t) f(x) = \overline{\eta}(t) f(x) \tag{2.7}$$

Where w is the transverse displacement, $\bar{\eta}(t)$ is the dynamic deflection at impact point x = c, and $f(L/2)=1$. For central impact on a simply supported beam, we have,

$$w=\bar{\eta}(t)\left[\frac{3L^2x-4x^3}{L^3}\right] \text{ for } 0\le x\le\frac{L}{2} \tag{2.8}$$

$$\text{and } w=\bar{\eta}(t)\left[\frac{4x^3-12Lx^2-9L^2x-L^3}{L^3}\right] \text{ for } \frac{L}{2}\le x\le L \tag{2.9}$$

The kinetic energy, T, and potential energy ,V, of the beam can now be written as

$$T=\frac{1}{2}\rho A\int_0^L\left(\frac{\partial w}{\partial t}\right)^2dx=\frac{17}{35}m_1\dot{\bar{\eta}}^2 \tag{2.10}$$

$$V=\frac{1}{2}EI\int_0^L\left(\frac{\partial^2 w}{\partial x^2}\right)^2dx=\frac{48EI\bar{\eta}^2}{L^3} \tag{2.11}$$

Where ρ is the density of the beam, A is the area of the beam, E is Young's Modulus of the beam, I is the moment of inertia of the beam, and a dot above a character represents the time derivative of that function. From equation (2.10), the certain fraction of the beam mass (χm_1) that attains the same velocity as the impactor is $(17/35)m_1$. The Lagrange's equation for impulsive motion can be written in the form

$$\frac{d}{dt}\left[\frac{\partial T}{\partial\dot{q}_i}\right]-\frac{\partial T}{\partial\dot{q}_i}+\frac{\partial V}{\partial q_i}=\bar{Q}_i \qquad i=1,2,.....n \tag{2.12}$$

Where $\bar{Q}_i$ is the generalized external force corresponding to generalized coordinate q_i. Substitution of the expressions for kinetic and potential energies (equation (2.10) and (2.11)) into equation (2.12) yields the expression for the generalized impact force,

$$\bar{Q}=(17/35)m_1\ddot{\bar{\eta}}+(48EI/L^3)\bar{\eta} \tag{2.13}$$

Since m_1 and m_2 move together after impact, the equation of motion for m_2 can be expressed in terms of $\bar{Q}$ and $\bar{\eta}(t)$ as follows,

$$m_2 g - \bar{Q} = m_2 \ddot{\bar{\eta}} \tag{2.14}$$

Where g is the acceleration due to gravity. Substituting the expression for $\bar{Q}$ from equation (2.13), equation (2.14) takes the form

$$m_2 g = \left[m_2 + (17/35)m_1\right]\ddot{\bar{\eta}} + k\bar{\eta} \qquad \text{where, } k = 48EI/L^3 \tag{2.15}$$

Solving equation (2.15) with initial conditions

$$\bar{\eta}_0 = 0,\ \dot{\bar{\eta}} = v = m_2 v_{2,0} \big/ (m_2 + (17/35)m_1) \tag{2.16}$$

$\bar{\eta}$ and $\ddot{\bar{\eta}}$ can be obtained as

$$\bar{\eta}(t) = w\left(\frac{L}{2}, t\right) = \frac{m_2 g}{k}\left\{1 - \cos\alpha t\right\} + \frac{m_2 v_{2,0}}{\sqrt{\beta k}}\sin\alpha t \tag{2.17}$$

and

$$\ddot{\bar{\eta}}(t) = \frac{\alpha^2 m_2 g}{\beta}\cos\alpha t - \frac{\alpha^2 m_2 v_{2,0}}{\sqrt{\beta k}}\sin\alpha t \tag{2.18}$$

where α and β are respectively defined by the expressions

$$\alpha = \sqrt{\frac{k}{m_2 + \frac{17}{35}m_1}} \tag{2.19}$$

and

$$\beta = m_2 + \frac{17}{35}m_1 \tag{2.20}$$

Equations (2.13), (2.17), and (2.18) are used to compute the impact force, $\bar{Q}$, at any time. The impact force is in turn used as the forcing function *{P}* in equation (2.2) to solve the equation of motion for the structural response (deformations and stresses). The value of interest in equation (2.13) is the maximum impact force, Q_{max}, which is defined by the following expression

$$Q_{\max} = \frac{17}{35} m_1 \ddot{\bar{\eta}}_{\max} + k\bar{\eta}_{\max} \tag{2.21}$$

Where $\bar{\eta}_{\max}$ and $\ddot{\bar{\eta}}_{\max}$ are the maximum beam deflection and acceleration, respectively. The times that maximum beam deflection and maximum beam acceleration occur at are determined by setting the derivative of equations (2.17) and (2.18) equal to zero and solving for the time. The maximum beam deflection and maximum beam acceleration are found to happen at the same time, t_{max}. Hence, the maximum force also occurs at the time, t_{max}. Time t_{max} is given by the equation

$$t_{\max} = \frac{1}{\alpha} \tan^{-1}\left(-\frac{\alpha v_{2,0}}{g} \right) \tag{2.22}$$

The maximum beam deflection, $\bar{\eta}_{\max}$, and maximum beam acceleration, $\ddot{\bar{\eta}}_{\max}$, are obtained using equations (2.17), (2.18), and (2.22). They are

$$\bar{\eta}_{\max}(t_{\max}) = w_{\max}\left(\frac{L}{2}, t_{\max} \right) = \frac{m_2 g}{k} \left\{ 1 + \sqrt{1 + \frac{{v_{2,0}}^2 k}{\beta g^2}} \right\} \tag{2.23}$$

and

$$\ddot{\bar{\eta}}_{\max}(t_{\max}) = \left(\frac{m_2 g}{m_2 + \frac{17}{35} m_1} \right) \left[\frac{1}{\sqrt{1 + \frac{\alpha^2 {v_{2,0}}^2}{g^2}}} \right] - \frac{\alpha^2 m_2 v_{2,0}}{\sqrt{k\left(m_2 + \frac{17}{35} m \right)}} \left[\frac{\frac{\alpha v_{2,0}}{g}}{\sqrt{1 + \frac{\alpha^2 {v_{2,0}}^2}{g^2}}} \right] \tag{2.24}$$

Another value of interest is the impact duration. Setting the impact force of equation (2.13) equal to zero, the following expression results

$$-m_2 g + \left[m_2 g - \frac{17}{35} m_1 \left(\frac{m_2 g}{\beta} \right) \right] \cos \alpha t = \left[\alpha m_2 v_{2,0} + \frac{17}{35} m_1 \left(\frac{\alpha m_2 v_{2,0}}{\beta} \right) \right] \sin \alpha t \tag{2.25}$$

This equation can be solved for the impact duration by iterative methods.

For the present study, the impact loading is considered to come from debris impact, such as broken equipment falling off a spacecraft during takeoff or landing and the debris then colliding with the structure. As there is no information on possible debris that might impact lunar habitats at the current time, the FAA's airplane-debris impacts codes (Wilde, 2010) were used to obtain the debris mass and velocity. Following the FAA code, a 1.2 kg projectile traveling at a velocity of 240 m/s was used for the impactor in the analysis (Wilde, 2010). The projectile was considered to strike the mid-span of an outer frame member of the structure. With these parameters, the theoretical impact force shown in Figure 2.3 was calculated by equation (2.4) and found to be sinusoidal with a maximum force of 24.9 kN and an impact duration of 6.2 ms. These values match well with that obtained from equations (2.21) and (2.25), respectively.

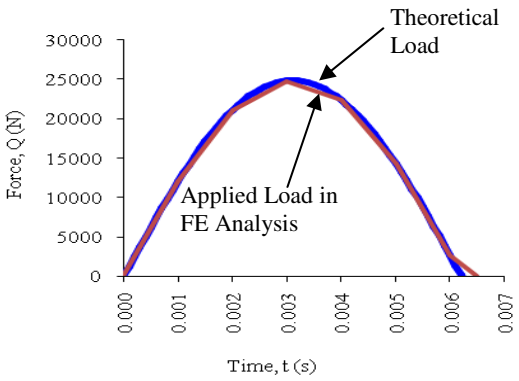

Figure 2.3. Impact load used in analysis.

2.3.3 Static, Frequency and Dynamic Response Solution Technique

Static, frequency/modal, and dynamic analyses of a finite element (FE) model of the 3-D frame-membrane structure was performed using ANSYS (2009). SHELL181 elements available in the ANSYS code were used to model the membrane in the structural system. Both bending and membrane stiffness capabilities of SHELL181

elements were accounted for in the model. However, since the membrane in the structure selected herein has a very small thickness (0.0075 m), the SHELL181 elements accurately simulate the response of the membrane. This was verified by comparing the results from the FE analysis obtained in previous studies (Malla and Chaudhuri, 2007 and 2008) with those from an analytical model developed by Maier-Schneider, *et al.* (1995) for load-deflection characteristic of a membrane. BEAM4 elements with tension, compression, torsion, and bending capabilities were used to model the frame elements. Both SHELL181 and BEAM4 are 3-D elements and have the option for stress stiffening and large deflection capabilities. Table 2.1 shows the parameters used for the FE model.

To study the effect of the regolith cover on the structure in the dynamic and frequency analyses, the regolith mass was applied in the model as a "non-structural added mass" via the "Real Constants" parameter option in ANSYS. The added regolith mass

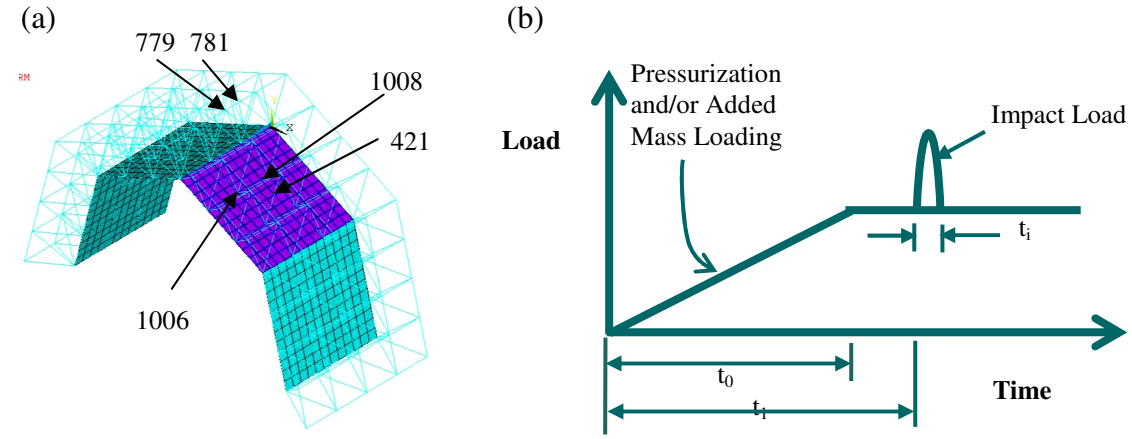

781: Mid-span of outer chord and point of impact
779: Joint of outer chord
1008: Mid-span of inner chord
1006: Joint of inner chord
421: Central node of membrane panel

Figure 2.4. (a) Finite element mesh model of the structure with some key nodes from the membrane impact analysis identified; (b) Scheme used to apply pressurization, added mass, and impact loads.

was computed to be 167,227 kg by considering a regolith shielding cover 1.5 m deep applied over the membranes surface area of 70.56 m^2. One-half of the regolith mass was added to the frame members (112 kg/m) and half of it was added to the membrane (1180 kg/m^2).

ANSYS uses a stress stiffness matrix that is analogous to $[K_G]$ in equations (2.1), (2.2), (2.4), and (2.5) to account for the stiffening effect as a result of prestressing (ANSYS, 2009). There are two prestressing loads on the habitat. First, the internal pressurization load of 96.5 kPa is applied on the structure pushing outward. Also, the added mass of regolith on the outside of the membrane pushes inward on the habitat due to gravity. The regolith load was calculated by finding the pressure component perpendicular to the membrane panel CDEF created by the regolith mass applied to the membrane (1180 kg/m^2). The regolith pressure was found to be 1.752 kPa (0.25 psi). Thus, any case that accounts for the added mass of regolith must also account for its corresponding pressure load in addition to the internal pressure load.

Four internal pressurization and/or added regolith mass loadings were considered: (a) no internal pressure and no added regolith mass; (b) internal pressure and no added regolith mass; (c) no internal pressure and added regolith mass; and (d) internal pressure and added regolith mass (Table 2.2). The resulting effective pressures (sum of the internal pressure load and regolith pressure loads) for cases (a), (b), (c), and (d) are 0 kPa, 96.5 kPa, -1.752 kPa, and 94.748 kPa, respectively. These effective pressures were applied as the prestressing loads.

The frequency analysis was performed in two steps. First, static analysis was run to calculate the prestressing caused by the internal pressurization and the regolith cover loads, where applicable. Then, in the second step, the modal (frequency) analysis was performed on the structural model with the "prestressing" option on. Block Lanczos method was used to solve the characteristic frequency equation in the previous section (Equation (2.5)) to determine the frequencies and mode shapes. For frequency analysis, each frame member in the FE model was divided into 10 elements and each membrane panel of size 4.2 m x 4.2 m was divided into 30 x 30 grids (Table 2.1).

Table 2.2. Load cases used in analysis.

Load Case Number	Load Case Identification*	Internal Pressure	Regolith Added Mass
Load Case 1	NP_NA	No	No
Load Case 2	P_NA	Yes	No
Load Case 3	NP_A	No	Yes
Load Case 4	P_A	Yes	Yes

Note: *Load Case Identification: NP = No internal pressure, NA = No added regolith mass, P = Internal Pressure, A = Added Regolith Mass

Static analysis (response due to internal pressure and regolith cover) and dynamic analyses (response due to impact force in conjunction with internal pressure and regolith cover) were performed taking into account large deformation and stress stiffening effects from the applied loads on the structure. For the static and dynamic analyses, due to computational time constraints, each frame member in the FE model was divided into 4 elements, and each membrane panel (4.2 m x 4.2 m) was meshed into 16 X 16 grids (Table 2.1). Additionally, the effect of the self-weight of the frame and membrane was found to negligible in the no pressure and no added mass with self-weight case of the

static analysis (see Tables 2.4(a) and 2.6(a)). Hence, self-weight was not included in any further analysis cases.

For the static and dynamic analyses, three time steps were used spanning 1 s (Figure 2.4(b)). Step one takes place from 0.00 – 0.25 s and has a time step of 0.01 s. In step one, the internal pressure and regolith loads (if any) are ramped up to their full values over 0.2 s, t_0. The pressure and regolith loads (if any) are then kept constant for the remainder of the step and for all subsequent steps. This first step was performed with the time integration off and, therefore, was equivalent to a static loading. Thus, the static results were acquired after this step.

Step two began at 0.25 s, t_i, which was the start of the impact loading, and ended at 0.2565 s, t_1, the end of the impact loading (Figure 2.4(b)). The time step for step two was 0.0005 s to accurately capture the impact phenomenon. The time integration was turned on in ANSYS for this step and after, meaning the dynamic effects were captured. The impact force, $\{P\}$ in Equations (2.1) and (2.2), while analytically found to be sinusoidal, was applied as a piecewise linear function (Fig. 2.3). The end point points of each linear segment were chosen coincide with the theoretical curve. The applied load accurately captured the theoretical amplitude of 24.9 kN. However, applied duration, t_i, of 6.5 ms was longer than the analytical duration of 6.2 ms, because the loading cannot end in the middle of a time step (which would happen if the analytical duration was use). The piecewise linear forcing function was applied to the mid-point of an outer chord of the structure (node 781, Figure 2.4(a)).

The final step proceeds from 0.2565 s until 1 s and has a time step of 0.001 s. Step three shows the habitat's structural response after the impact load duration.

For the dynamic analysis, the Newmark solution method with Newton-Raphson iteration technique was used to solve the equation of motion (Eq. (2.2)) for displacement, $\{\delta\}$, incorporating non-linear (large deformation) dynamic analysis. Displacement and stress time histories were generated for a total of 1 s.

2.4 RESULTS AND DISCUSSION

The static, frequency/modal and impact analyses of the 3-D frame-membrane structure were conducted for the following 4 distinct cases shown in Table 2.2. The results obtained from these analyses are presented in this section. The finite element mesh of the structure is shown in Figure 2.4(a) with some of the key nodes identified.

2.4.1 Static Analysis Results

In static analysis, displacement and stress results have been presented at five nodes of interest, in order to give representative results for the full structure. The nodes that were tracked were: (a) the point of impact and mid-span of an outer chord, (node 781); (b) the joint of an outer chord (779); (c) the mid-span of an inner chord (1008); (d) the joint of an inner chord (1006); and (e) the center of a membrane panel (421). These nodes are shown in Figure 2.4(a). The maximum displacement and stress results in the outer chord members, inner chord members, diagonal members, and membrane panel are provided as well.

2.4.1.1 Static Displacement

Tables 2.4 and 2.5 show the static displacement results for the structure for cases: (a) no pressure and no added mass of regolith including the effects of self weight; (b) pressure and no added mass of regolith not including the effects of self weight; (c) no pressure and added mass of regolith not including the effects of self weight; and (d) pressure and added mass regolith not including the effects of self weight. For the displacement results, positive x-direction means the node is moving to the right, a positive y-displacement means the node of structure is moving upward, and a positive z-displacement

Table 2.3. Maximum static displacements of the structure for Load Cases: (a) Load Case 1 with self-weight and (b) Load Case 2 without self-weight.

(a) No Pressure, No Added Mass, Self Weight			
Representative Nodes *	Max X Displacement (m)	Max Y Displacement (m)	Max Z Displacement (m)
781	5.94E-11	-1.85E-05	1.53E-07
779	5.55E-11	-1.73E-05	-1.67E-09
1008	-3.66E-07	-1.83E-05	-7.94E-11
1006	5.79E-07	-1.64E-05	5.60E-08
421	-1.09E-05	-4.06E-05	-6.36E-11
Maxima of the Frame-Membrane Structure			
Membrane +	-1.19E-05 Node 373 Panel EFGH	-4.31E-05 Node 373 Panel EFGH	6.31E-07 Node 488 Panel GHIJ
Outer Chords +	4.94E-06 Node 1280 Panel GHIJ	-1.94E-05 Node 777 Junction EF	9.01E-07 Node 1093 Panel ABCD
Inner Chords +	-6.46E-06 Node 956 Junction CD	-1.89E-05 Node 978 Junction CD	6.31E-07 Node 2135 Panel GHIJ
Diagonals +	7.81E-06 Node 1947 Panel GHIJ	2.06E-05 Node 1737 Panel EFGH	3.61E-06 Node 1857 Panel EFGH
(b) Pressure, No Added Mass, No Self Weight			
Representative Nodes *	Max X Displacement (m)	Max Y Displacement (m)	Max Z Displacement (m)
781	-7.26E-08	2.09E-03	-5.93E-07
779	-6.27E-08	2.17E-03	3.52E-07
1008	4.34E-03	1.03E-02	1.62E-07
1006	1.35E-03	3.79E-02	-3.61E-04
421	1.83E-02	3.99E-02	1.22E-07
Maxima of the Frame-Membrane Structure			
Membrane +	4.26E-02 Node 621 Panel GHIJ	4.16E-02 Node 221 Panel CDEF	1.50E-03 Node 199 Panel CDEF
Outer Chords +	2.80E-03 Node 881 Panel GHIJ	3.74E-03 Node 745 Panel CDEF	2.81E-04 Node 1215 Panel EFGH
Inner Chords +	1.26E-02 Node 1043 Panel GHIJ	1.30E-02 Node 978 Panel CDEF	1.50E-03 Node 2153 Panel CDEF
Diagonals +	3.41E-03 Node 1938 Panel GHIJ	4.38E-03 Node 1677 Panel CDEF	3.08E-03 Node 1641 Panel CDEF

Note: *For location of representative nodes see Figure 4(a)
+For location of panels see Figure 1(a)

means the node is moving out of the page (Figure 2.4(a)).

The results show the effects of self weight of the structure alone (Table 2.4(a)) were found to be negligible (maximum displacement of only -4.31E-5 m in the y-direction for node 373 (membrane)) and thus, the effects of self-weight were neglected for all other static analysis cases and for the frequency and dynamic analyses.

Examining the pressure and no added regolith mass case (with no self-weight) (Table 2.4(b)), the internal pressure can be seen to cause the structure to expand outward in the x- and y-directions. In the y-

Table 2.4. Maximum static displacements of the structure for Load Cases: (a) Load Case 3 without self-weight and (b) Load Case 4 without self-weight.

(a) No Pressure, Added Mass, No Self Weight			
Representative Nodes *	Max X Displacement (m)	Max Y Displacement (m)	Max Z Displacement (m)
781	3.89E-09	-8.18E-05	1.93E-06
779	3.61E-09	-8.40E-05	9.64E-09
1008	-7.44E-04	-2.14E-04	-4.48E-09
1006	-2.61E-05	-1.08E-04	3.62E-07
421	-1.34E-03	-2.91E-03	-3.64E-09
Maxima of the Frame-Membrane Structure			
Membrane +	-3.12E-03 Node 537 Panel GHIJ	-2.97E-03 Node 465 Panel EFGH	-2.02E-06 Node 59 Panel ABCD
Outer Chords +	-4.92E-05 Node 1282 Panel GHIJ	-9.97E-05 Node 1222 Panel CDEF	-7.28E-06 Node 1110 Panel ABCD
Inner Chords +	-2.29E-04 Node 1043 Panel GHIJ	-2.74E-04 Node 1004 Panel EFGH	-1.72E-06 Node 2135 Panel EFGH
Diagonals +	-7.14E-05 Node 1937 Panel GHIJ	-1.26E-04 Node 1799 Panel EFGH	7.74E-05 Node 1974 Panel GHIJ
(b) Pressure, Added Mass, No Self Weight			
Representative Nodes *	Max X Displacement (m)	Max Y Displacement (m)	Max Z Displacement (m)
781	-7.33E-08	2.04E-03	-1.90E-07
779	-6.37E-08	2.12E-03	3.46E-07
1008	4.26E-03	1.01E-02	1.59E-07
1006	1.32E-03	3.71E-03	-3.56E-04
421	1.81E-02	3.96E-02	1.20E-07
Maxima of the Frame-Membrane Structure			
Membrane +	4.23E-02 Node 621 Panel GHIJ	4.16E-02 Node 221 Panel CDEF	-7.56E-04 Node 199 Panel CDEF
Outer Chords +	2.75E-03 Node 881 Panel GHIJ	3.67E-03 Node 745 Panel CDEF	2.75E-04 Node 1215 Panel EFGH
Inner Chords +	1.24E-02 Node 1043 Panel GHIJ	1.28E-02 Node 978 Panel CDEF	1.48E-03 Node 2153 Panel CDEF
Diagonals +	3.35E-03 Node 1938 Panel GHIJ	4.30E-03 Node 1677 Panel CDEF	3.03E-03 Node 1641 Panel CDEF

Note: *For location of representative nodes see Figure 4(a)
+For location of panels see Figure 1(a)

directions, all nodes (representative and maxima) move upwards. In the x-direction, nodes 1008, 1006, and 421 are all located on panel EFGH (right side of structure; Figure 2.1(a)) and have positive x-displacements (moving right). The maximum x-displacements are all on panel GHIJ (right side of structure; Figure 2.1(a)) and also move to the right. Additional results not presented show panel ABCD moves to the left at a value equivalent to panel GHIJ displacement and likewise panel CDEF moves at an equal magnitude but opposite direction at panel EFGH. Nodes 781 and 779 (junction EF; Figure 2.1(a)) are seen to have negligible movement in the x-direction (-7.33E-08 m and -6.37E-08 m, respectively). In the z-direction, the displacement is seen to be almost 10 times smaller in all nodes except the diagonals. This is expected since the pressure force acts perpendicular to the z-direction. There is significant z-displacement in the diagonals (which are not orthogonal to the pressure load), since the diagonals take pressure load axially and are displaced outwards in all directions.

For the no pressure and added regolith mass case (with no self-weight) (Table 2.5(a)), the structure is seen to reduce in size in the x- and y-directions, which is expected as the regolith load pushes inwards on the structure. The y-displacements are negative (downward movement). The x-displacements show the right side of the structure moving left and the EF junction (Figure 2.1(a)) as stationary. Conversely, the left side of the structure moves right (not shown in table). Additionally, like with the pressure and no regolith mass (with no self-weight), the z-displacements are seen to be significantly smaller than the x- and y-displacements except in the diagonals. In comparison to the pressure and no added mass case (with no self-weight), the displacement magnitudes are

much smaller, which is expected since the internal pressure load is significantly than the pressure load.

Table 2.5(b) shows that the structure expands outward in the x- and y-direction for the internal pressure and added regolith mass case (with no self-weight). The y-displacements are positive. The EFGH and GHIJ panels (nodes 1008, 1006, 421, and the maxima) move to the right (positive x-displacement), whereas the ABCD and CDEF panel move to the left (negative x-displacement; not shown in a table). The nodes 781 and 779 (junction EF) remain motionless in the x-direction. Again, the z-displacement is small compared to the x and y-displacement except in the diagonals. While both the pressure and no added mass case (not including self-weight) and the pressure and added mass case (not including self-weight) expand outwards in the x- and y-directions, the load case with pressure and no added mass (without self-weight) has larger displacements. This is expected, since the pressure load is greater than the pressure and added regolith mass load.

The largest static displacements are during the pressure and no added regolith mass case (with no self-weight) (Table 2.4(b)). For the x-direction, the maximum displacement is 4.26E-02 m at node 621 (membrane). The maximum y-displacement is 4.16E-02 m at node 221 (membrane). The largest displacement in the z-direction is 3.08E-03 m at a diagonal (node 1641).

2.4.1.2 Static Stress

Table 2.6 presents the static stress results for the structure for the four load cases: (a) no pressure and no added mass of regolith including the effects of self-weight; (b)

pressure and no added mass of regolith not including the effects of self-weight; (c) no pressure and added mass of regolith not including the effects of self-weight; and (d) pressure and added mass regolith not including the effects of self-weight. The static stress results are provided for the representative cross-sections (the point of impact and mid-span of an outer chord, (node 781); the joint of an outer chord (779); the mid-span of an inner chord (1008); the joint of an inner chord (1006); and the center of a membrane panel (421)) and the maximum stresses in the outer frame members, inner frame members, diagonals, and membrane. The first principal stress is presented for the membrane. For all frame members (beam elements), the total normal stress (axial stress plus bending stress) is presented. For the representative cross-sections 781, 779, 1008, and 1006, the larger of the maximum stresses at the top and the bottom of the cross-section (See Figure 2.1(c)) is recorded. Additionally, the values presented for frame members under "Maxima of the Frame-Membrane Structure" are the largest values of the normal stresses for the entire cross section (not just at the top or bottom of the cross-section) of the whole structure during the analysis. As per usual, positive stress means the element is in tension and negative stress means the element is in compression.

Table 2.5. Maximum static stresses of the structure for Load Cases: (a) Load Case 1 with self-weight; (b) Load Case 2 without self-weight; (c) Load Case 3 without self-weight; and (d) Load Case 4 without self-weight.

(a) No Pressure, No Added Regolith Mass, Self Weight			**(b) Pressure, No Added Regolith Mass, No Self Weight**		
Element Location	Element (**Node**)	Stress (Pa)	Element Location	Element (**Node**)	Stress (Pa)
Stress at Representative Nodes			Stress at Representative Nodes		
Representative Nodes *	867 (**781**)	1.41E+04	Representative Nodes *	867 (**781**)	4.32E+05
	868 (**779**)	-7.12E+03		868 (**779**)	8.90E+05
	1078 (**1008**)	5.52E+04		1078 (**1008**)	-1.55E+08
	1080 (**1006**)	4.66E+04		1080 (**1006**)	-1.30E+08
	367 (**421**)	6.93E+04		367 (**421**)	1.64E+08
Maxima of the Frame-Membrane Structure			*Maxima of the Frame-Membrane Structure*		
Membrane +	219 (**221**) Panel CDEF	7.09E+04	Membrane +	34 (**149**) Panel ABCD	1.65E+08
Outer Chord +	1373 (**830**) Panel EFGH	1.57E+05	Outer Chord +	1273 (**745**) Panel CDEF	5.12E+07
Inner Chord +	605 (**30**) Junction CD	1.45E+05	Inner Chord +	1093 (**1019**) Panel EFGH	2.91E+08
Diagonal +	1829 (**1592**) Panel CDEF	2.17E+05	Diagonal +	2417 (**1071**) Panel GHIJ	1.13E+08
(c) No Pressure, Added Regolith Mass, No Self Weight			**(d) Pressure, Added Regolith Mass, No Self Weight**		
Element Location	Element (**Node**)	Stress (Pa)	Element Location	Element (**Node**)	Stress (Pa)
Stress at Representative Nodes			Stress at Representative Nodes		
Representative Nodes *	867 (**781**)	-2.14E+05	Representative Nodes *	867 (**781**)	3.85E+05
	868 (**779**)	-2.18E+05		868 (**779**)	8.32E+05
	1078 (**1008**)	2.00E+06		1078 (**1008**)	-1.52E+08
	1080 (**1006**)	1.72E+06		1080 (**1006**)	-1.28E+08
	367 (**421**)	7.88E+06		367 (**421**)	1.62E+08
Maxima of the Frame-Membrane Structure			*Maxima of the Frame-Membrane Structure*		
Membrane +	495 (**533**) Panel GHIJ	7.99E+06	Membrane +	34 (**149**) Panel ABCD	1.63E+08
Outer Chord +	1153 (**643**) Panel ABCD	1.05E+06	Outer Chord +	1273 (**745**) Panel CDEF	5.02E+07
Inner Chord +	1037 (**962**) Panel CDEF	5.53E+06	Inner Chord +	1045 (**967**) Panel CDEF	2.85E+08
Diagonal +	2353 (**1062**) Panel GHIJ	2.63E+06	Diagonal +	2417 (**1071**) Panel GHIJ	1.11E+08

Note: *For location of representative nodes see Figure 4(a)
+For location of panels see Figure 1(a)

As with the static displacement results, the stress for the no pressure and no added regolith mass case including the self-weight shows the effects due to the self-weight of the structure are minimal (Table 2.6(a)). The maximum stress from self weight alone is 2.17E+05 Pa (diagonal, node 1592), which is significantly less than the next smallest maximum value in any of the other three cases of 1.05E+06 Pa (outer chord, node 1062 for case no pressure and added regolith masses not including self weight). Thus, the self-weight of the lunar base was neglected in the all other static analysis cases as well as the frequency and dynamic analyses.

For the pressure and no added regolith mass (without self-weight), the maximum stresses at the representative cross-sections and the maximum in the structure are of the magnitude 10^8 Pa, except the outer chords (cross-sections 781, 779, and the maximum outer chord stress) (Table 2.6(b)). Thus, the internal pressure load has much less prestressing effect on the outer chord of the frame than on any other structural component. Additionally, all cross-sections are in tension, except at cross-sections 1008 and 1006, which are in compression.

Examining the no pressure and added regolith mass (with no self-weight effect) (Table 2.6(c)), the stresses are seen to be in tension, except at cross-sections 781 and 779. The largest stress is 7.99E+06 and occurs in the membrane panel (cross-section 533). The stress are seen to be far less than those of the pressure and no added mass case (without self-weight). This is expected since the internal pressure load is much larger than the added regolith load.

Table 2.6(d) shows the stresses for the pressure and added mass case (not including the self-weight). The results are almost identical to those of the pressure and no

added mass case (not including the self-weight) (Table 2.6(b)), which is expected since the two loads are very close.

In both cases, the stresses are significantly lower at the outer chords and all stresses are tension, except at cross-section 1008 and 1006. However, the stress for the pressure and no added mass case (not including self-weight) are slightly higher than the pressure and added mass case (not including self-weight), since the pressure alone load is larger than the pressure and self-weight load.

The largest stresses, both at the representative nodes and maximum of the full structure, are found during the pressure and no added mass of regolith (not including self weight) case (Table 2.6). The largest stress overall is 2.91E+08 Pa at the inner chord (node 1019).

2.4.2 Frequency Analysis Results

The first 20 natural frequencies and mode shapes of the frame-membrane structure were computed. Table 2.3 and Figure 2.5 present these natural frequencies and the corresponding to the mode numbers. Table 2.3 also shows the percent change in natural frequencies caused by the addition of internal pressure and the ratio of the natural frequency without added mass to the natural frequency with added mass. The results from the frequency/modal analysis indicate that internal pressurization increases the frequencies slightly due to prestressing effects. The maximum increase in natural frequencies of the frame-membrane system due to pressurization are found to be 1.470% (7^{th} mode) in the absence of added regolith mass and 5.203% (19^{th} mode) in the case with added regolith mass. It can be observed that the added mass of regolith reduces the

frequencies of the structure significantly. The ratios of the fundamental frequency of the system without added regolith mass to the fundamental frequency with added regolith is found to be 4.548 times in the cases without pressure and 4.545 times in the cases with pressure. The maximum increase in the ratio of the natural frequencies of the frame-membrane system due to added regolith mass are 5.601 (13^{th} mode) without pressurization and 5.502 (12^{th} mode) with the pressurization.

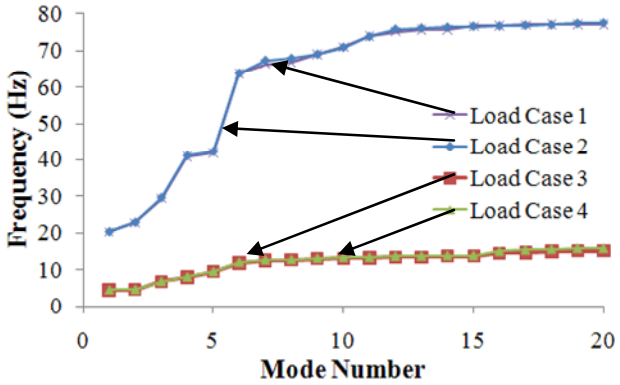

Figure 2.5. First twenty natural frequencies for Load Cases: Load Case 1 (NP_NA); Load Case 2 (P_NA); Load Case 3 (NP_A); and Load Case 4 (P_A).

Table 2.6. Natural frequencies of frame-membrane composite system.

Mode Number	Frequency without Added Regolith Mass (Hz)			Frequency with Added Regolith Mass (Hz)			Ratio of Frequency with and without Added Regolith Mass	
	Frequency without Pressure	Frequency with Pressure	Percent Change with and without Pressure	Frequency without Pressure	Frequency with Pressure	Percent Change with and without Pressure	Ratio without Pressure	Ratio with Pressure
1	20.356	20.510	0.757	4.476	4.513	0.827	4.548	4.545
2	22.826	23.072	1.078	4.624	4.682	1.254	4.936	4.928
3	29.460	29.741	0.954	6.813	6.889	1.116	4.324	4.317
4	40.940	41.237	0.725	7.989	8.119	1.627	5.125	5.079
5	41.856	42.356	1.195	9.489	9.577	0.927	4.411	4.423
6	63.856	63.862	0.009	11.840	12.131	2.458	5.393	5.264
7	66.405	67.381	1.470	12.570	12.766	1.559	5.283	5.278
8	66.940	67.922	1.467	12.697	12.877	1.418	5.272	5.275
9	68.957	69.051	0.136	13.094	13.175	0.619	5.266	5.241
10	71.036	70.913	-0.173	13.211	13.505	2.225	5.377	5.251
11	74.077	73.828	-0.336	13.238	13.508	2.040	5.596	5.466
12	75.203	75.800	0.794	13.486	13.778	2.165	5.576	5.502
13	75.758	76.104	0.457	13.525	13.841	2.336	5.601	5.498
14	75.854	76.341	0.642	13.763	13.929	1.206	5.511	5.481
15	76.651	76.612	-0.051	13.785	13.948	1.182	5.560	5.493
16	76.791	76.700	-0.119	14.515	15.069	3.817	5.290	5.090
17	77.008	76.859	-0.193	14.707	15.412	4.794	5.236	4.987
18	77.054	76.975	-0.103	15.038	15.668	4.189	5.124	4.913
19	77.143	77.360	0.281	15.146	15.934	5.203	5.093	4.855
20	77.213	77.469	0.332	15.179	15.934	4.974	5.087	4.862

2.4.3 Dynamic Analysis Results

Like the static results, the dynamic displacement and stress results have been presented at five representative nodes (the point of impact and mid-span of an outer chord, (node 781); the joint of an outer chord (779); the mid-span of an inner chord (1008); the joint of an inner chord (1006); and the center of a membrane panel (421)). These nodes are shown in Figure 2.4(a). The maximum displacements and stresses in the inner chord members, outer chord members, diagonal members, and membrane are also provided.

2.4.3.1 Dynamic Displacement

Figures 6 through 10 show the dynamic vertical displacement time histories for the representative nodes for load cases: (a) no pressure

Table 2.7. Maximum dynamic displacements of the structure for Load Cases: (a) Load Case 1 and (b) Load Case 2.

(a) No Pressure, No Added Regolith Mass			
Representative Nodes *	Max X Displacement (m)	Max Y Displacement (m)	Max Z Displacement (m)
781	6.05E-08	-7.26E-03	7.49E-05
779	2.58E-08	-1.97E-04	-7.06E-05
1008	4.75E-05	-1.86E-04	3.73E-05
1006	-2.19E-05	-1.07E-04	3.50E-05
421	-2.53E-04	-5.89E-04	3.38E-05
Maxima of the Frame-Membrane Structure			
Membrane +	4.92E-04 Node 529 Panel GHIJ	-7.25E-04 Node 399 Junction GH	4.72E-05 Node 182 Junction EF
Outer Chords +	1.10E-03 Node 798 Panel EFGH	-7.26E-03 Node 781 Junction EF	1.20E-03 Node 1191 Panel CDEF
Inner Chords +	1.28E-04 Node 2159 Panel EFGH	3.23E-04 Node 2156 Panel CDEF	4.72E-05 Node 988 Junction EF
Diagonals +	4.74E-04 Node 1803 Panel EFGH	-1.35E-03 Node 1710 Junction EF	-3.22E-03 Node 1716 Junction EF
(b) Pressure, No Added Regolith Mass			
Representative Nodes *	Max X Displacement (m)	Max Y Displacement (m)	Max Z Displacement (m)
781	-2.61E-07	5.66E-03	9.14E-05
779	-9.50E-08	2.35E-03	8.47E-05
1008	4.41E-03	1.05E-02	-3.20E-05
1006	1.37E-03	3.90E-03	-3.97E-04
421	1.84E-02	4.03E-02	4.22E-05
Maxima of the Frame-Membrane Structure			
Membrane +	4.28E-02 Node 533 Panel GHIJ	4.19E-02 Node 221 Panel CDEF	1.55E-03 Node 199 Panel CDEF
Outer Chords +	2.85E-03 Node 881 Panel GHIJ	5.66E-03 Node 781 Junction EF	1.29E-03 Node 1191 Panel CDEF
Inner Chords +	-1.27E-02 Node 939 Panel ABCD	1.32E-02 Node 978 Panel CDEF	-1.55E-03 Node 2153 Panel CDEF
Diagonals +	3.48E-03 Node 1968 Panel GHIJ	4.61E-03 Node 1677 Panel CDEF	-3.37E-03 Node 1638 Panel CDEF

Note: *For location of representative nodes see Figure 4(a)
+For location of panels see Figure 1(a)

and no added mass of regolith (Load Case 1); (b) pressure and no added mass of regolith (Load Case 2); (c) no pressure and added mass of regolith (Load Case 3); and (d) pressure and added mass regolith (Load Case 3). Additionally, the maximum displacements of the representative nodes and the full structure are presented in Tables 2.7 and 2.8. As with the static displacement results, positive x-displacement means the node is moving to the right, a positive y-displacement means the node of structure is moving upward, and a positive z-displacement means the node is moving out of the page (Fig. 2.4(a)).

The time histories for the no pressure and no added regolith mass case (Load Case 1) shows no change in displacement until the impact load is applied. Once the

Table 2.8. Maximum dynamic displacements of the structure for various cases: (a) Load Case 3 and (b) Load Case 4.

(a) No Pressure, Added Regolith Mass			
Representative Nodes *	Max X Displacement (m)	Max Y Displacement (m)	Max Z Displacement (m)
781	-1.55E-07	-5.03E-03	-3.39E-05
779	1.44E-07	-2.36E-04	-3.54E-05
1008	-1.03E-04	-2.83E-04	-1.24E-05
1006	-3.04E-05	-1.46E-04	-1.67E-05
421	-7.27E-05	-2.96E-03	-1.36E-05
Maxima of the Frame-Membrane Structure			
Membrane +	-3.15E-03 Node 533 Panel GHIJ	-3.02E-03 Node 221 Panel CDEF	-3.03E-05 Node 170 Junction EF
Outer Chords +	-4.05E-04 Node 798 Panel EFGH	-5.03E-03 Node 781 Junction EF	-8.84E-04 Node 1191 Panel CDEF
Inner Chords +	-2.44E-04 Node 1056 Panel EFGH	-3.44E-04 Node 978 Panel CDEF	-3.03E-05 Node 997 Junction EF
Diagonals +	-1.47E-04 Node 1775 Panel EFGH	-8.33E-04 Node 1710 Junction EF	-1.77E-03 Node 1716 Junction EF
(b) Pressure, Added Regolith Mass			
Representative Nodes *	Max X Displacement (m)	Max Y Displacement (m)	Max Z Displacement (m)
781	-1.49E-07	5.30E-03	-3.61E-05
779	-7.09E-08	2.20E-03	-3.38E-05
1008	4.29E-03	1.02E-02	-1.23E-05
1006	1.33E-03	3.72E-03	-3.71E-04
421	1.82E-02	3.96E-02	1.30E-05
Maxima of the Frame-Membrane Structure			
Membrane +	-4.23E-02 Node 65 Panel ABCD	4.13E-02 Node 221 Panel CDEF	-1.49E-03 Node 176 Panel CDEF
Outer Chords +	2.77E-03 Node 667 Panel ABCD	5.30E-03 Node 781 Junction EF	-8.75E-04 Node 1191 Panel CDEF
Inner Chords +	-1.24E-02 Node 939 Panel ABCD	1.28E-02 Node 978 Panel CDEF	1.49E-03 Node 2153 Panel CDEF
Diagonals +	3.38E-03 Node 1938 Panel GHIJ	4.30E-03 Node 1677 Panel CDEF	-3.07E-03 Node 1638 Panel CDEF

Note: *For location of representative nodes see Figure 4(a)
+For location of panels see Figure 1(a)

impact load is applied, the displacement amplitude increases and oscillates rapidly, at the point of impact (node 781) (Figure 2.6(a)). At the other representative nodes, however, the displacement amplitude is quite small (Part (a) of Figures 2.6 through 2.10). At all nodes, the displacement amplitude reduces as time goes on, caused by the impact force being distributed throughout the structure and not staying localized at a single node. The maximum displacement is -5.03E-03 m at the point of impact in the y-direction (Table 2.7(a)).

Examining the pressure and no added mass case (Load Case 2), a large upward static displacement from the internal pressure can be seen between 0.0 – 0.2 s, which the dynamic displacement oscillates about from 0.25 – 1.00 s (Part (a) of Figures 2.6 through 2.10). The largest displacement amplitude is seen at the point of impact. The other nodes have much smaller y-displacement amplitudes, especially compared to the initial static displacement. At all nodes, the displacement amplitudes can be seen to reduce towards their static level as the time increases. Additionally, the displacement amplitude and amplitude reduction to the static level for Load Case 2 is very similar to Load Case 1 (no pressure and no added regolith mass).

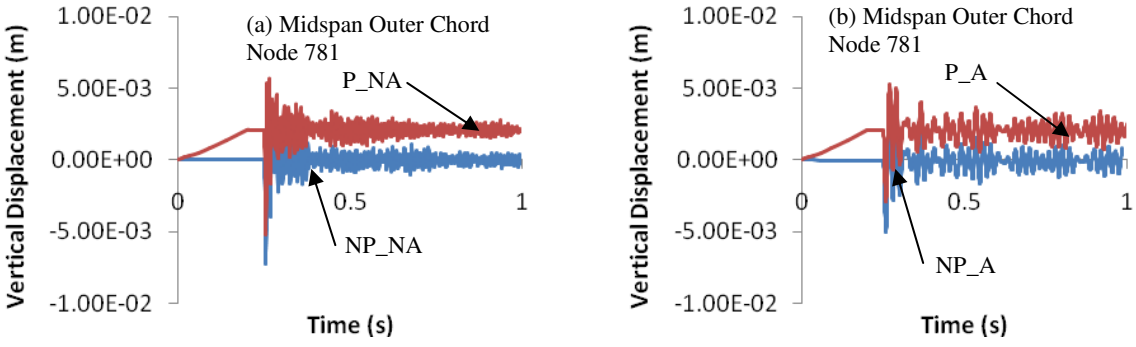

Figure 2.6. Displacement time history of node 781, midspan of an outer chord, for Load Cases: (a) Load Case 1 (NP_NA) and 2 (P_NA); (b) Load Case 3 (NP_A) and 4 (P_A).

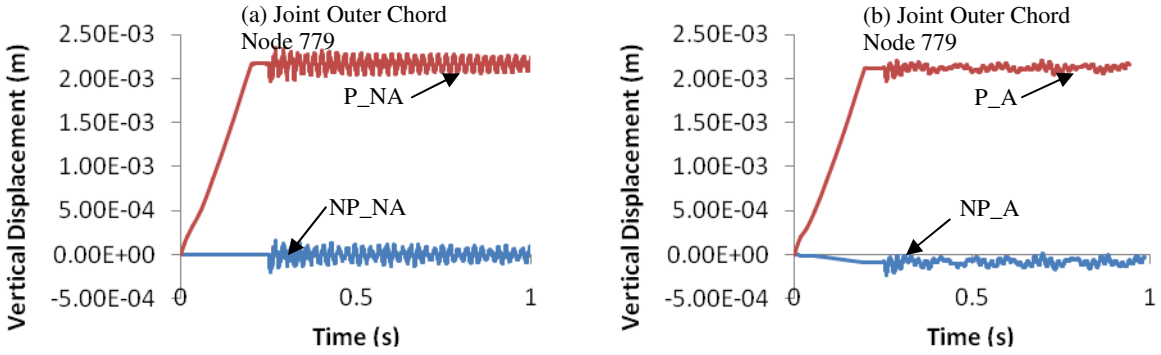

Figure 2.7. Displacement time history of node 779, joint of an outer chord, for Load Cases: (a) Load Case 1 (NP_NA) and 2 (P_NA); (b) Load Case 3 (NP_A) and 4 (P_A).

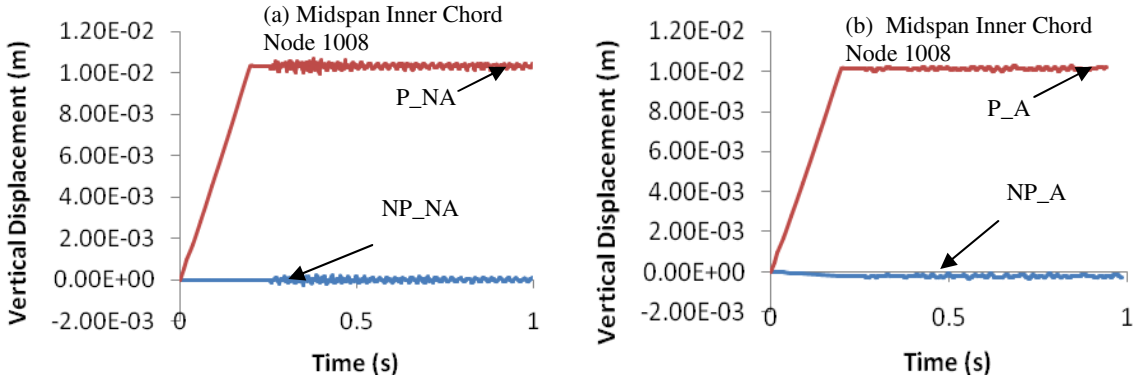

Figure 2.8. Displacement time history of node 1008, midspan of an inner chord, for Load Cases: (a) Load Case 1 (NP_NA) and 2 (P_NA); (b) Load Case 3 (NP_A) and 4 (P_A).

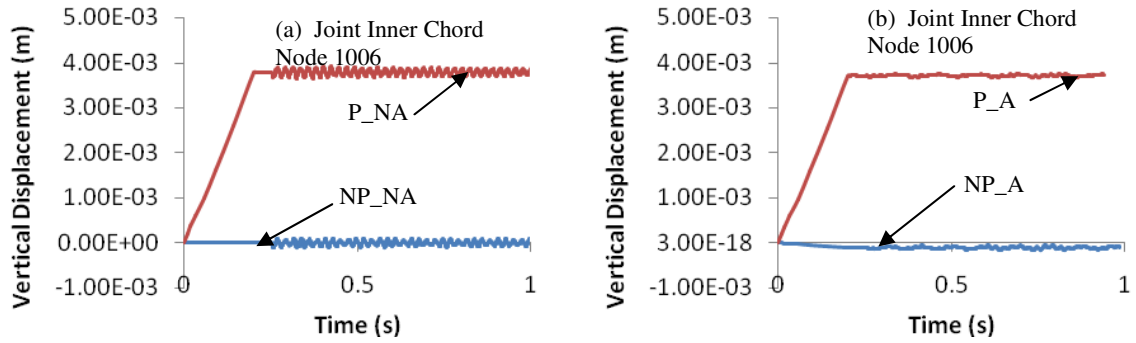

Figure 2.9. Displacement time history of node 1006, joint of an inner chord, for Load Cases: (a) Load Case 1 (NP_NA) and 2 (P_NA); (b) Load Case 3 (NP_A) and 4 (P_A).

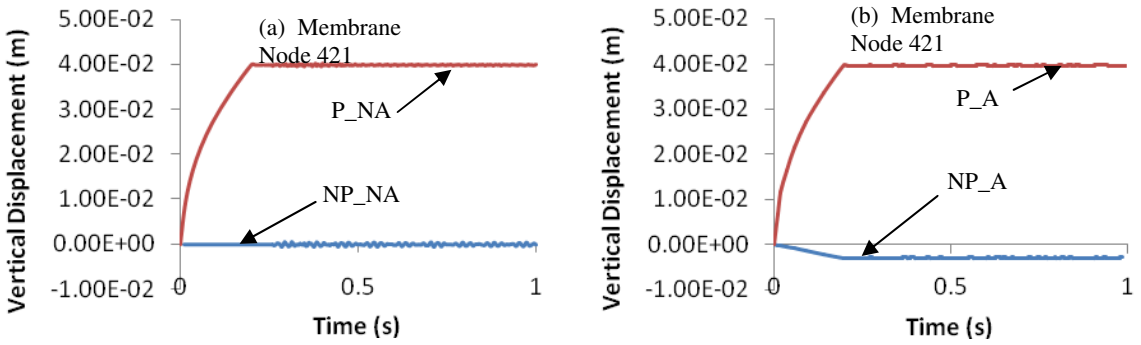

Figure 2.10. Displacement time history of node 421, center of a membrane panel, for Load Cases: (a) Load Case 1 (NP_NA) and 2 (P_NA); (b) Load Case 3 (NP_A) and 4 (P_A).

For the no pressure and added regolith mass case (Load Case 3), the static displacement is small and downward. Again, the displacement amplitude is significant at the point of impact (node 781), but much smaller at the other nodes. The displacement amplitude reduces towards the static level as time increases. Beat phenomenon can be seen in parts (b) of Figures 2.6 through 2.10, especially in Figure 2.6(b). In comparison to the cases without added mass (Load Cases 1 and 2), Load Case 3 has a smaller oscillation amplitude and a larger oscillation period.

For the internal pressure and added regolith mass case (Load Case 4), the large static displacement can be seen from 0.0 - 0.2 s (Part (b) of Figures 2.6 through 2.10). The dynamic displacement amplitude oscillates about this static value. Again, the largest y-displacement amplitude is at the point of impact and the amplitude is significantly less than the static displacement at all other nodes. The displacement amplitude is similar to the no pressure and added regolith mass case and less than the two cases without added regolith mass (Load Cases 1 and 2). The period of oscillation is also similar to Load Case 3 (no pressure and added regolith mass) and greater than the Load Cases 1 (no pressure and no added regolith mass) and 2 (pressure and no added regolith mass). As

with the other cases, the dynamic displacement amplitude reduces as the time after impact increases.

The largest displacements occur during the pressure and no added mass case (Table 2.7(b)). For the x- and y-direction, the maximum displacement is in the membrane with values of 4.28E-02 m (node 533) and 4.19E-02 m (node 221), respectively. The largest displacement in the z-direction is -3.37E-03 m at a diagonal (node 1638).

2.4.3.2 Dynamic Stress

The stress time histories for the representative nodes (nodes 781, 779, 1008, 1006, and 421) are presented in Figures 2.11 through 2.17, respectively. The maximum stresses that occur at the representative nodes and overall in the structure are presented in Table 2.9. For the membrane, the first principal stress is presented in both the time history response in Figure 2.17 and the stress values given in Table 2.9. The stress presented for all frame members (beams elements) is the total normal stress (axial stress plus bending stress) in a cross-section. Figures 2.11 through 2.16 are the stress time histories at the top and the bottom of the beam cross-section (see Figure 2.1(c)) for representative cross-sections 781, 779, 1008, and 1006. It should be noted that the axial stress component is the difference between the top and bottom stresses. For these four representative cross-sections, the larger of the maximum stresses at the top and the bottom of the cross-section is recorded in Table 2.9. Additionally, in Table 2.9, the values reported for frame members under "Maxima of the Frame-Membrane Structure" are the largest values of the normal stresses for the entire cross section (not just at the top or bottom of the cross-section) of the whole structure within the time duration of the response. Stress time

histories at these maximum values have not been reported, because the location (throughout the entire structure as well as location within a cross-section in case of a frame member) of the maximum value changes with time.

Table 2.9. Maximum dynamic stresses of the structure for Load Cases: (a) Load Case 1; (b) Load Case 2; (c) Load Case 3; and (d) Load Case 4.

(a) No Pressure, No Added Regolith Mass			**(b) Pressure, No Added Regolith Mass**		
Element Location	Element (**Cross-Section**)	Stress (Pa)	Element Location	Element (**Cross-Section**)	Stress (Pa)
Stress at Representative Nodes			Stress at Representative Nodes		
Representative Nodes *	867 (**781**)	-3.98E+07	Representative Nodes *	867 (**781**)	-3.94E+07
	868 (**779**)	-3.65E+07		868 (**779**)	-3.58E+07
	1078 (**1008**)	-3.88E+06		1078 (**1008**)	-1.59E+08
	1080 (**1006**)	-3.09E+06		1080 (**1006**)	-1.32E+08
	367 (**421**)	4.91E+05		367 (**421**)	7.75E+07
Maxima of the Frame-Membrane Structure			*Maxima of the Frame-Membrane Structure*		
Membrane +	261 (**302**) Panel CDEF	3.73E+06	Membrane +	27 (**61**) Panel ABCD	1.64E+08
Outer Chord +	855 (**768**) Panel CDEF	1.77E+08	Outer Chord +	985 (**902**) Panel GHIJ	2.57E+08
Inner Chord +	661 (**327**) Panel EFGH	1.30E+07	Inner Chord +	1025 (**949**) Junction CD	2.91E+08
Diagonal +	1981 (**1706**) Panel CDEF	8.12E+07	Diagonal +	2405 (**2024**) Panel GHIJ	1.15E+08
(c) No Pressure, Added Regolith Mass			**(d) Pressure, Added Regolith Mass**		
Element Location	Element (**Cross-Section**)	Stress (Pa)	Element Location	Element (**Cross-Section**)	Stress (Pa)
Stress at Representative Nodes			Stress at Representative Nodes		
Representative Nodes *	867 (**781**)	-5.14+07	Representative Nodes *	867 (**781**)	-5.08E+07
	868 (**779**)	-4.84E+07		868 (**779**)	-4.74E+07
	1078 (**1008**)	-4.39E+06		1078 (**1008**)	-1.53E+08
	1080 (**1006**)	4.19E+06		1080 (**1006**)	-1.28E+08
	367 (**421**)	1.02E+06		367 (**421**)	7.66E+07
Maxima of the Frame-Membrane Structure			*Maxima of the Frame-Membrane Structure*		
Membrane +	255 (**225**) Panel CDEF	8.40E+06	Membrane +	27 (**61**) Panel ABCD	1.63E+08
Outer Chord +	853 (**762**) Panel CDEF	1.32E+08	Outer Chord +	985 (**902**) Panel GHIJ	2.52E+08
Inner Chord +	1045 (**967**) Panel CDEF	7.50E+06	Inner Chord +	1033 (**954**) Junction CD	2.84E+08
Diagonal +	1981 (**1706**) Panel CDEF	5.24E+07	Diagonal +	2405 (**2024**) Panel GHIJ	1.13E+08

Note: *For location of representative nodes see Figure 4(a)
+For location of panels see Figure 1(a)

The no pressure and no added regolith mass (Load Case 1) time histories show the stress constant at 0 Pa until the impact load is applied. At 0.25 s when the impact occurs, the amplitude of the stress increases and oscillates. At cross-section 781 (Figure 2.11(a) and (b)) and cross-section 779 (Figure 2.13(a) and (b)), the amplitude is very large. However, at the other representative cross-sections the stress amplitude is much smaller (Parts (a) and (b) of Figure 2.15 and 2.16; and Part (a) of Figure 2.17). At all representative nodes, the stress amplitude can be seen to reduce as time increase. This is a result of the impact force being distributed throughout the structure. The maximum stress for the no pressure and no added mass case is 1.77E+08 Pa at an outer chord (cross-section 768) (Table 2.9(a)).

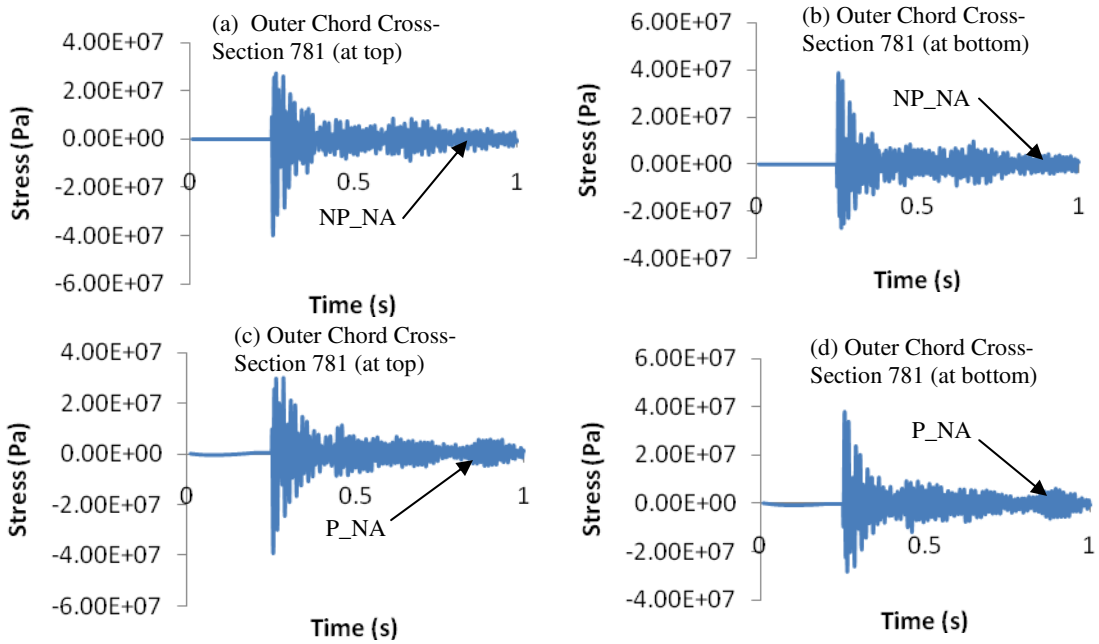

Figure 2.11. Stress time history at the top and bottom of cross-section 781, midspan of an outer chord and impact location, for Load Cases: (a) Load Case 1 (NP_NA) top of cross-section, (b) Load Case 1 (NP_NA) bottom of cross-section, (c) Load Case 2 (P_NA) top of cross-section, and (d) Load Case 2 (P_NA) bottom of cross-section.

For the pressure and no added mass case (Load Case 2), a large static stress (from the ramping of the internal pressure) is prominent between 0.0 s – 0.2 s at cross-sections 1008, 1006, and 421 (Parts (a) and (b) of Figures 2.15 and 2.16; and Part (a) of Figure 2.17). This static stress is not present at cross-sections 781 (Parts (c) and (d) of Figure 2.11) and 779 (Parts (c) and (d) of Figure 2.13). After impact occurs, at all cross-sections, the stress oscillates about it static level. The amplitude of this stress though is only significant compared to the static stress at cross-sections 781 and 779. Stress amplitude and period are very similar to the values in the no pressure and no added regolith mass case (Load Case 1). Also, the stress amplitude is seen to reduce toward the static stress as time increases. The maximum stress of the structure is 2.91E+08 Pa (inner chord, cross-section 949) (Table 2.9(b)), which is the same value as the static stress.

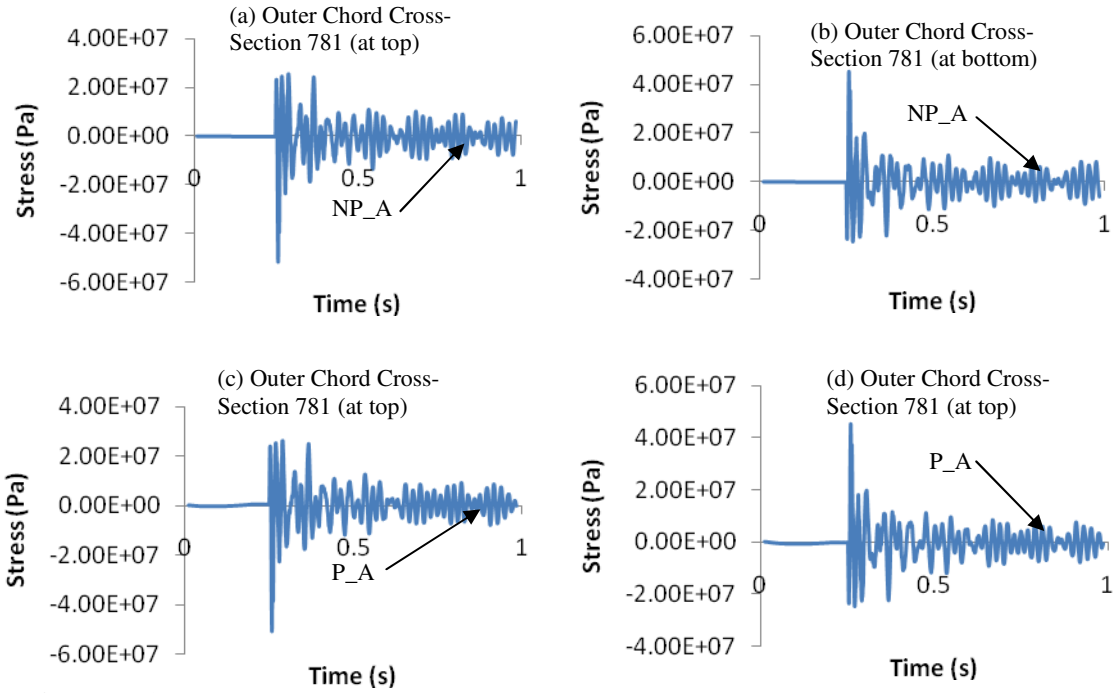

Figure 2.12. Stress time history at the top and bottom of cross-section 781, midspan of an outer chord and impact location, for Load Cases: (a) Load Case 3 (NP_A) top of cross-section, (b) Load Case 3 (NP_A) bottom of cross-section, (c) Load Case 4 (P_A) top of cross-section, and (d) Load Case 4 (P_A) bottom of cross-section.

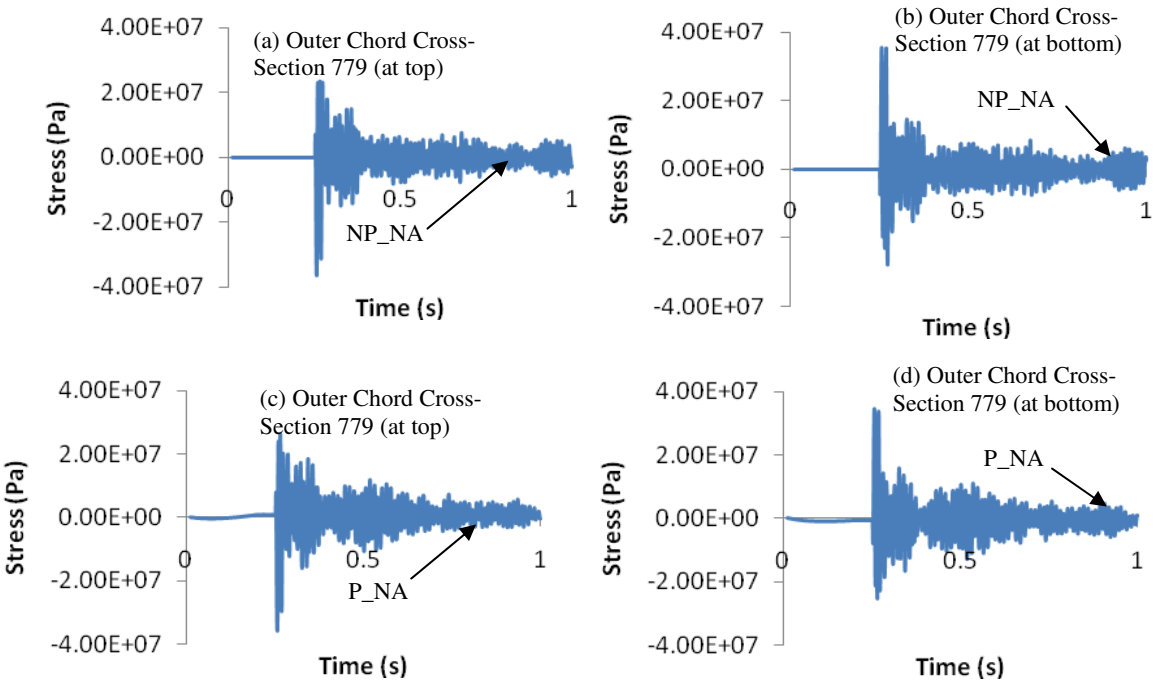

Figure 2.13 Stress time history at the top and bottom of cross-section 779, joint of an outer chord, for Load Cases: (a) Load Case 1 (NP_NA) top of cross-section, (b) Load Case 1 (NP_NA) bottom of cross-section, (c) Load Case 2 (P_NA) top of cross-section, and (d) Load Case 2 (P_NA) bottom of cross-section.

The dynamic stress results for no pressure with added regolith mass case (Load Case 3) shows very little static stress at any of the representative nodes (Parts (a) and (b) of Figures 2.12 and 2.14; Part (c) and (d) of Figures 2.15 and 2.16; and Part (b) of Figure 2.17). The stress amplitude is very small for cross-sections 1008, 1006, and 421, but large for cross-sections 781 and 779. For cross-sections 781 and 779, the stress amplitude is seen to be larger for Load Case 3 than Load Cases 1 (no pressure and no added regolith mass) and 2 (pressure and no added regolith mass). For the other representative cross-sections (1008, 1006, and 421), the amplitude is smaller. For all cross-sections, the period of oscillation is larger for Load Case 3. As with the Load Cases 1 and 2, the stress amplitude is seen to reduce as time increases. The maximum

stress for Load Case 3 is 1.32E+08 Pa at cross-section 762, an outer chord member (Table 2.9(c)).

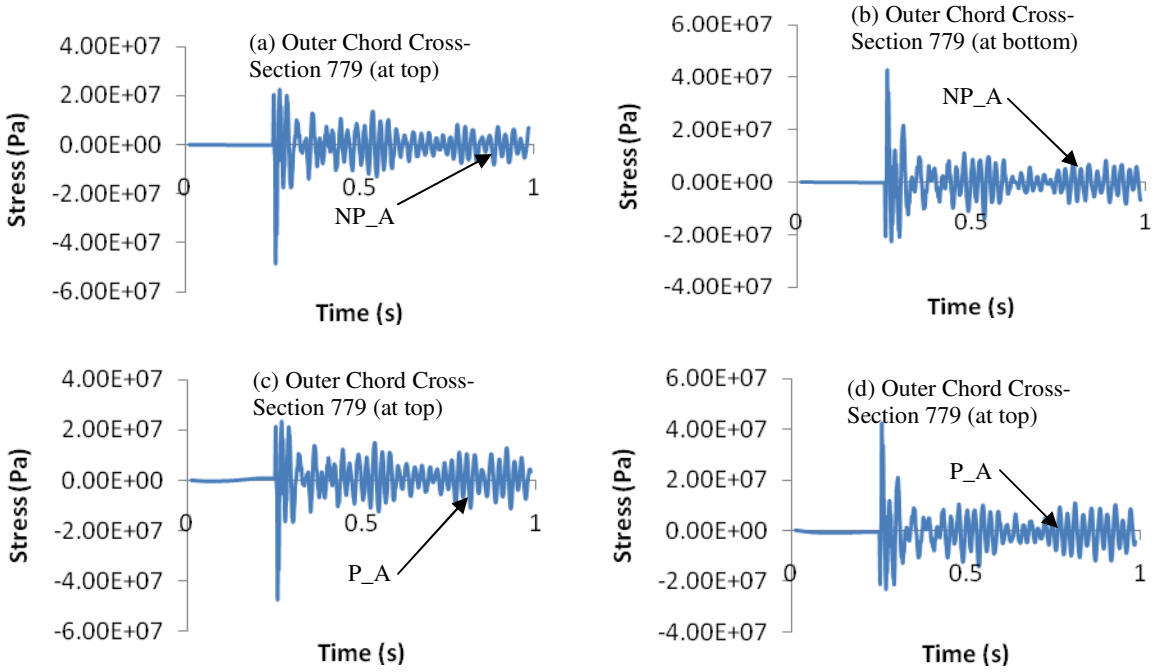

Figure 2.14. Stress time history at the top and bottom of cross-section 779, joint of an outer chord, for Load Cases: (a) Load Case 3 (NP_A) top of cross-section, (b) Load Case 3 (NP_A) bottom of cross-section, (c) Load Case 4 (P_A) top of cross-section, and (d) Load Case 4 (P_A) bottom of cross-section.

The load case with both internal pressure and added regolith mass (Load Case 4) shows the static stress occurring from 0.0 s - 0.2 s at cross-sections 1008 (Part (c) and (d) of Figure 2.15), 1006 (Part (c) and (d) of Figure 2.16), and 421 (Part (b) of Figure 2.17). The static stressing is about 0 Pa at cross-sections 781 (Figure 2.12(c) and (d)) and 779 (Figure 2.14(c) and (d)). As expected, the dynamic stress oscillates about the static stress levels. The amplitude of the stress oscillations and period are similar to Load Case 3 (no pressure and added regolith mass). Thus, the stress amplitude is greater than the amplitudes for Load Cases 1 and 2 for cross-sections 781 and 779. Additionally, the stress amplitude is lower than those two cases for cross-sections 1008, 1006, and 421.

The period is greater for the representative nodes compared to Load Cases 1 (no pressure and no added regolith mass) and 2 (pressure and no added regolith mass). As with the previous three cases, the stress amplitude is seen to reduce as time goes on. The maximum stress is 2.84E+08 Pa at cross-section 954 (an inner chord member).

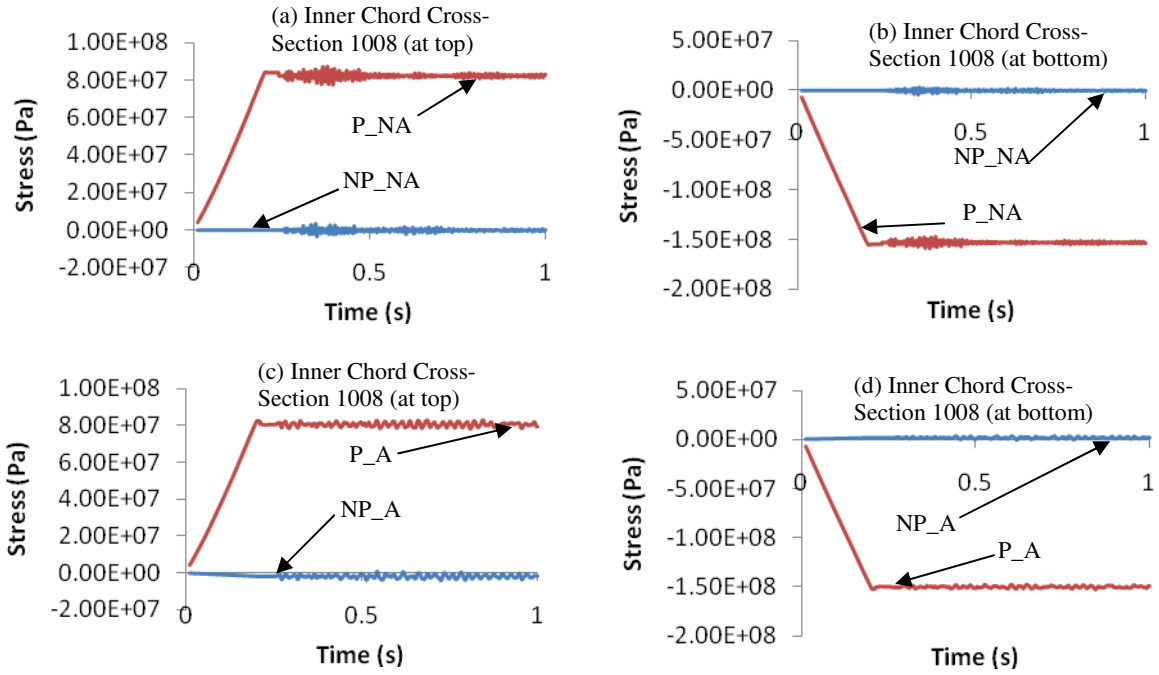

Figure 2.15. Stress time history at top and bottom of cross-section 1008, midspan of an outer chord, for Load Cases: (a) Load Case 1 (NP_NA) and 2 (P_NA) top of the cross-section; (b) Load Case 1 (NP_NA) and 2 (P_NA) bottom of the cross-section; (c) Load Case 3 (NP_A) and 4 (P_A) top of the cross-section; (d) Load Case 3 (NP_A) and 4 (P_A) bottom of the cross-section.

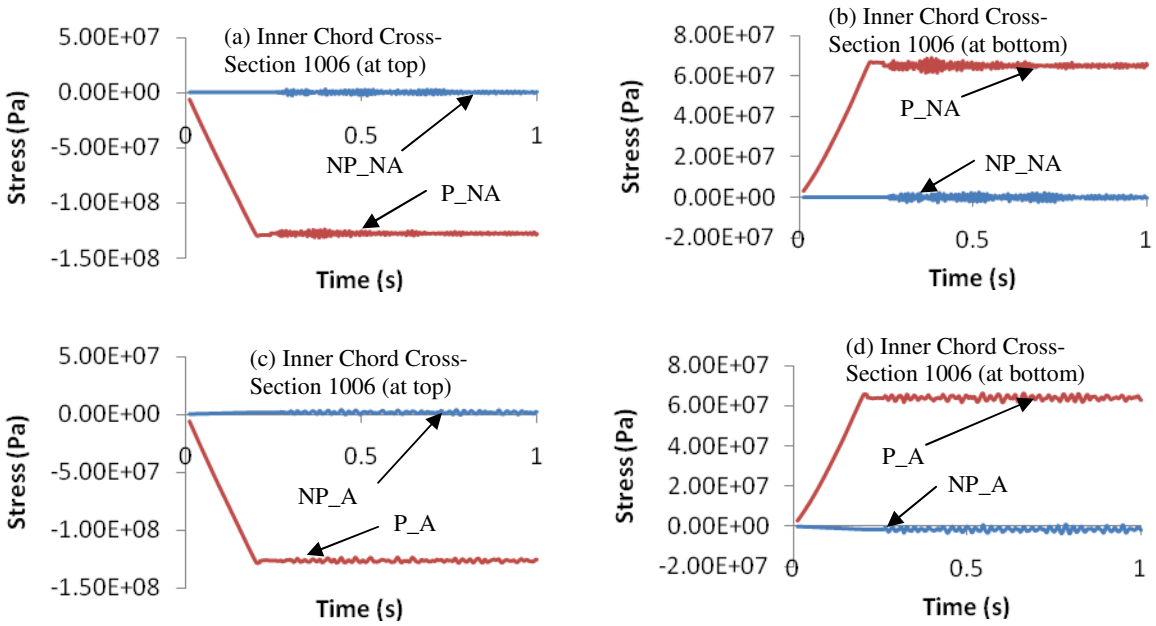

Figure 2.16. Stress time history at top and bottom of cross-section 1006, joint of an outer chord, for Load Cases: (a) Load Case 1 (NP_NA) and 2 (P_NA) top of the cross-section; (b) Load Case 1 (NP_NA) and 2 (P_NA) bottom of the cross-section; (c) Load Case 3 (NP_A) and 4 (P_A) top of the cross-section; (d) Load Case 3 (NP_A) and 4 (P_A) bottom of the cross-section.

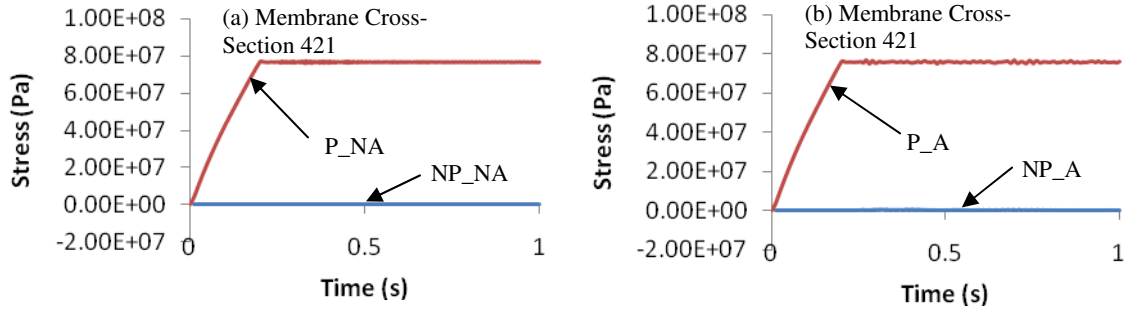

Figure 2.17. Stress time history of node 421, middle of a membrane panel, for Load Cases: (a) Load Case 1 (NP_NA) and 2 (P_NA); (b) Load Case 3 (NP_A) and 4 (P_A).

2.5 CONCLUSIONS

Within the range of parameters used in this study, the internal pressurization of the frame-membrane structure was found to increase the structural frequencies slightly, while the added mass of regolith was found to decrease the frequencies of the system significantly. For example, natural frequencies of the structure with prestressing are found to increase by a maximum of 1.470% and 5.203%, without and with the added regolith mass, respectively. The fundamental frequency of the system without added mass of regolith is about 4.5 times greater than of the fundamental frequency with the mass of regolith for both the pressurized and unpressurized cases.

Static analysis of the habitat shows the internal pressurization load causes the structure to expand outward greatly and the added regolith load causes the structure to contract inward slightly. The internal pressure is also seen to stress the inner chord members, diagonal members, and the membrane, but does not significantly stress the outer chord members. The added regolith mass does not significantly stress the structure. The maximum static deformations and stresses occur during the pressure and no added mass case at the membrane and inner chords, respectively.

For the dynamic analysis under impact force on a mid-span of a frame member, the dynamic displacements are only significant at the point of impact. At other nodes, the static loads are more important. The added regolith mass reduces the displacement amplitude and increase the oscillation period, but the internal pressure has little effect on the displacement amplitude and period. The maximum total displacement occurs in the pressure and no added regolith mass case at the membrane.

The dynamic stress effects are similar to the static. The dynamic stresses are only significant at or near the point of impact and elsewhere, the static loads are more important. The addition of the regolith mass causes the stress amplitude to increase at the outer chords and decrease at the membrane and inner chords. However, the internal pressure has no appreciable effect on the dynamic stress amplitude. Also, the added mass is seen to increase the stress oscillations periods, whereas the pressure has no noticeable effect on the period.

The results from this study show that the effects of added regolith mass and the prestressing effects from the internal pressurization are critical parameters to consider while designing frame-membrane pressurized structural system. The pressurization effects the initial static displacement tremendously, while the added mass of regolith drastically reduces the natural frequencies of the lunar habitat. Additionally, the key areas of concern are the membrane, where the maximum displacement occurs, and the inner chords, where the stress levels are the highest. Both of these maxima occur during the pressure and no added mass case.

2.6 REFERENCES

AFRL (2007). "Inflatable Structures Can Reduce Logistics And Setup Time For Bare-based Operations." *Air Force Research Laboratory, Materials & Manufacturing Directorate*, Dayton, OH. http://www.ml.afrl.af.mil/stories/mlq-01124.html (date referred 09April2007).

ANSYS (2009). *User's Guide, Release 12.0*, ANSYS Inc., Pennsylvania, USA, 2009.

ASCE Task Committee (1992). "Overview of Existing Lunar Base Structural Concepts." *J. of Aerospace Engineering*, 5(2), 159-174.

Bedri, R. and Al-Nais, M.O. (2005). "Prestressed Modal Analysis Using Finite Element Package ANSYS." *Numerical Analysis and Its Applications*, Third International Conference, NAA 2004, Revised Selected Papers, 3401/2005, Springer Berlin / Heidelberg, 171-178.

Benaroya, H., and Ettouney, M. (1992). "Framework for Evaluation of Lunar Base Structural Concepts." *J. of Aerospace Engineering*, 5(2), 187-198.

Benaroya, H., Bernold, L., and Chua K. (2002). "Engineering, Design and Construction of Lunar Bases." *J. of Aerospace Engineering*, 15(2), 33-45.

Castellano, A. J., Caltagirone, J. P., Sock, F. E., Dobbs, N. (1990), "Structures to Resist the Effects of Accidental Explosions." *TM 5-1300*, Departments of the Army, Navy, and the Air Force, Alexandria, VA, USA.

Chow, P. Y., Lin, T. Y. (1988). "Structures for the Moon." *Engineering, Construction and Operations in Space- Procs. of Space 88*, 362–374.

Dayal, V. (2009). "Conceptual Design of Unpressurized Shelters on Lunar Surface." *J. of Aerospace Engineering*, 22(4), 396-402.

Donadon, M.V., Almeida, S.F.M. and de Faria, A.R. (2002). "Stiffening effects on the natural frequencies of laminated plates with piezoelectric actuators." *Composites: Part B*, **33**, 335–342.

Drake, R. M., and Richter, P. J. (1990). "Design and Construction of a Lunar Outpost Assembly Facility." *Engineering, Construction and Operations in Space II- Volume 1, Procs. of Space 90*, 449- 457.

Goldsmith, W. (1980). *Impact*, Courier Dover Publications, London, U.K.

Heiken, G., Vaniman, D. and French B. M., eds. (1991). *The Lunar Source Book*, Cambridge University Press, Cambridge, England, U.K.

Kapoor, H., Chun, S., Kapania, R. K., and Plaut, R. H. (2005). "Nonlinear Dynamic Response of Highly Flexible Membrane Structures to Blast Load." *Procs.*, *3rd International Conference on Structural Stability and Dynamics,* June 19-22, 2005, 6 pages.

Land, P. (1985). "Lunar Base Design." *In Lunar Bases and Space Activities of the 21st century* (W. W. Mendell, ed.), Lunar and Planetary Institute, Houston, Texas, 363-373.

Lin, T. D., Senseney, J. A., Arp, L. D., and Lindbergh, C. (1988). "Concrete Lunar Base Investigations." *Engineering, Construction and Operations in Space- Proceedings of Space-88*, 148-156.

Maier-Schneider, D., Maibach, J., Obermeier, E. (1995). "A new analytical solution for the load-deflection of square membranes." J. *of Microelectromechanical Systems,* 4(4), 238-241.

Malla, R. (1991). "Earthbound Civil Engineering Experience for Space Applications." *J. of Aerospace Engineering*, 4(4), 330-346.

Malla, R., Adib-Jahromi, H., and Accorsi, M.L. (1995). "A Simplified Design Method for Braced Double Skinned Structure in Lunar Application." *J. of Aerospace Engineering*, 8(4), 189-195

Malla, R. B. and Chaudhuri, D. (2006). "Analysis of a 3D Frame – Membrane structure for Lunar Base." *Engineering, Construction and Operations in Challenging*

Environments (Procs., Earth & Space 2006 Conference), ASCE, Reston, VA , March 2006, 8 pages.

Malla, R. B. and Chaudhuri, D. (2007). "Effects of Pressurization on Frequencies and Impact response of Frame-Membrane Composite Structure." *Procs., ASCE Engineering Mechanics Division (EMD) conference*, Blacksburg, VA; June, 2007, 12 pages.

Malla, R. B. and Chaudhuri, D. (2008). "Dynamic Analysis of a 3-D Frame-Membrane Lunar Structure Subjected to Impact." *Engineering, Science, Construction and Operations in Challenging Environments- Procs., Earth & Space 2008 Conf.*, ASCE, Reston, VA, March, 10 pages.

Quigley, C., Horak, K., Devine, R., Dagher, H., Parent, L., Landis, E., Goslin, K, and Cassidy, E. (2006). "The Development and Evaluation of Modular Ballistic Panels for Fabric Shelters." *25th Army Science Conf.*, Orlando, Florida, November 27-30, 2006.

Rinehart, J.S. (1959). "Basic Design Criteria for Moon Building." *J. of the British Interplanetary Soc*., 17, 126-129.

Ruess, F., Schaenzlin, J., and Benaroya, H. (2006). "Structural Design of a Lunar Habitat." *J. of Aerospace Engineering*, 19(3), 133-157.

Sadeh, W. Z., and Criswell, M. E. (1994). "A generic inflatable structure for a lunar/martian base." *Engineering, Construction, and Operations in Space – Procs., SPACE 94 conf., ASCE,* Reston, Va., 1146–1156.

Sherwood, B., and Toups, L. (1992). "Technical Issues for Lunar Base Structures", J. *of Aerospace Engineering*, 5(2), 175-186.

Sowerby, P.L. (1954). "Structural Problems of the Lunar Base." *J. of the British Interplanetary Soc*., 13, 36-40.

Szilard, R. (1959). "Structures for the Moon." *Civil Engineering,* 29, 46-49.

Vanderbilt, M. D., Criswell, M. E., Sadeh, W. Z. (1988). "Structures for a lunar base", *Engineering, Construction and Operations in Space- Procs. of Space 88*, 352-361.

Walker, J. D. (1998). "Turning Bullets into Baseballs," *Technology Today*®. Southwest Research Institute, San Antonio, TX.

Wilde, P. D. and Draper, C. (2010). "Aircraft Protection Standards and Implementation Guidelines for Range Safety." *48th AIAA Aerospace Science Meeting Including the New Horizon Forum and Aerospace Exposition*, Orlando, Florida, January 4-7, 2010.

CHAPTER 3

FREQUENCY AND IMPACT ANALYSIS OF A PROPOSED FRAME-MEMBRANE LUNAR STRUCTURE AT EXTREME TEMPERATURES

Abstract

This paper presents results from large deformation non-linear finite element frequency, static, and dynamic analyses of a proposed three-dimensional frame-membrane lunar habitat structure in presence of lunar temperature extremes. The prestressing effect from two causes are included in the analysis: one from applied internal pressurization load of one atmosphere and the other from the temperature differential caused by the extreme lunar diurnal temperature of -233°C (night) and +123°C (day) applied outside the structure and room temperature (21°C) maintained inside the structure. The load for the dynamic analysis has been analytically determined by considering the impact of a moving projectile/debris hitting the mid-point of one of the outer chord frame members. The study shows that both the internal pressurization and the temperature differential affect the frequency and mode shape characteristics of the structure. It is seen that the temperature differential caused by the lunar day causes small increases in the frequencies, whereas the lunar night temperature differential causes a large reduction in the frequencies. The static analysis results show that both pressurization and temperature differential give significant static displacements and stresses in the structure. The dynamic results due to the impact load show that the

application of extreme daytime hot and night time cold lunar diurnal temperatures outside and room temperature inside the structure reduces the dynamic amplitude of the displacement and stress compared to the case with no temperature differential (room temperature inside as well as the structure).

3.1 INTRODUCTION

There are many reasons to return to and inhabit the Moon(ASCE Task Committee, 1992; Benaroya et al, 2002; Ruess et al., 2006). For scientists, a lunar habitat would provide an unimpeded and pristine view into space as well as a geological surface that has not decayed, since seismic activity is minimal, there is no atmosphere, and biological life is not present. Thus, a lunar base would be an ideal laboratory for astronomy, geology, and asteroid threat analysis. Economically, the Moon offers the possibility of valuable mineral resources, solar power generation, and even tourism. Finally, a permanent lunar base would just further inspire man's quest for exploration and discovery of the universe working as a steppingstone for travel to Mars and beyond. However, the first step to inhabiting the Moon is the proper design of a lunar base.

Over the past several decades, numerous lunar base concept designs have been proposed. A few engineering concepts (Sowerby, 1954; Rhinehart, 1959; Szilard, 1959) were conceived as early as 1950s, well before the manned Apollo missions to the Moon in late 1960's and early 1970's. However, the Apollo missions to the Moon were the inspiration to the vast majority of lunar base concepts. Some of these investigations on potential lunar structures include those by Benaroya and Ettouney (2002), Ruess et al.

(2006), Lin et al. (1988), Vanderbilt et al. (1988), Drake and Richter (1990), Chow and Lin (1988), Sherwood and Toups (1992), Malla et al. (1995), and Dayal (2009).

Due to their light weight and ease of transport, many of these design concepts have proposed fabric shelters as future extraterrestrial habitats on the Moon and Mars (Vanderbilt, 1988; Malla, 1991; Sadeh and Criswell, 1994). Fabric shelters are inflatable structures that are commonly used in military bases on Earth for temporary storage of equipment, personnel, vehicles, and other military goods (AFRL, 2007). Additionally, light-weight fabric structures that can sustain extreme loading (such as impact and blast loading) are in development at the present (Kapoor et al., 2005; Quigley et al., 2006).

However, so far the vast majority of published research on lunar base structures is in the conceptual stage and needs further quantification. Detailed static, thermal, and dynamic responses of these proposed lunar structures are not available. In order to successfully inhabit the moon, first, these responses must be ascertained so that, building and construction codes can be developed to meet the challenges of the lunar environment.

The lunar environment presents many varied challenges including, but are not limited to, radiation exposure, reduced gravity, electrostatic dust, micrometeorite impact, the complete lack of atmosphere (hard vacuum), debris impact, and temperature extremes ranging from 123°C during the lunar day to -233°C during the lunar night (ASCE Task Committee, 1992; Benaroya et al., 2002; Malla, 1991; Heiken et al., 1991). Overcoming these significant challenges is imperative to the success of a lunar base for human occupation.

This paper focuses on three of these major challenges: the complete lack of atmosphere (hard vacuum), severe temperature extremes, and debris impact. First, the

presence of a hard vacuum on the Moon makes internal pressurization of any human habitat built on the Moon essential to support life. However, this could lead to prestressing/stress stiffening of the structure, which in turn affects the structural response. Second, the extreme lunar temperatures may have considerable effects on the structure, because of thermal expansion. As with the internal pressurization, the thermal expansion may lead to prestressing of the structure. Finally, a lunar structure could at any time be subjected to an impact load caused by space debris. Regolith or broken equipment could fall from a lunar lander or other spacecrafts. This impact could pose a serious threat to the habitat's structural integrity.

In previous studies, an internally pressurized three-dimensional (3-D) frame-membrane structure has been proposed as a possible lunar habitat that would maintain a short-sleeve and room temperature environment (Batelle Memorial Institure, 2009; Dupont, 2001; Bedri and Al-Nais, 2005). The structure's livable space is enclosed by the inflated membrane. The livable space is kept at a one atmosphere internal pressure load and room temperature. The 3-D frame structure helps support the pressurization load and provides additional stiffness to help limit any structural response.

In this paper, results from modal, non-linear static, and non-linear dynamic impact finite element analyses. The frequency results are presented for three different structural cases: (a) the frame alone, (b) the unpressurized full frame-membrane structure, and (c) pressurized full frame-membrane structure. Static and dynamic deformation and stress results are presented for the pressurized full frame-membrane structure. All results are for two extreme external temperatures of lunar day and night (123°C and -233°C, respectively), while the inside temperature was maintained at the room temperature of

21°C. For comparison purpose, a baseline case where both the outside and inside of the structure are at room temperature (21°C) has also been analyzed.

3.2 PROPOSED LUNAR HABITAT

The lunar habitat structure analyzed herein consists of a combination of 0.0075 m thick Kevlar membrane enclosed by four connected 3-D aluminum frame modules (Fig. 3.1). The Kevlar membrane has a high modulus of elasticity allowing it to contain a one atmosphere pressure load. The frame modules possess low mass and high stiffness, which will increase the structure's overall rigidity and strength. Figure 3.1(a) shows the front elevation of the proposed structural system. The full 3-D frame is composed of 467 tubular cross-section members. Each member is made of 2014-T6 aluminum and has an outer radius, r_o, of 0.0375 m and an inner radius, r_i, of 0.02 m (See Fig. 3.1(c)). The clear height (h) of the structure equals 5.83 m, the clear span (w) is 9.8 m, and the length of the structure (perpendicular to the plane of the paper) is 4.2 m. The surface area of the membrane is 70.56 m^2 (four panels each with a 4.2 m x 4.2 m membrane spanning the inner chords).

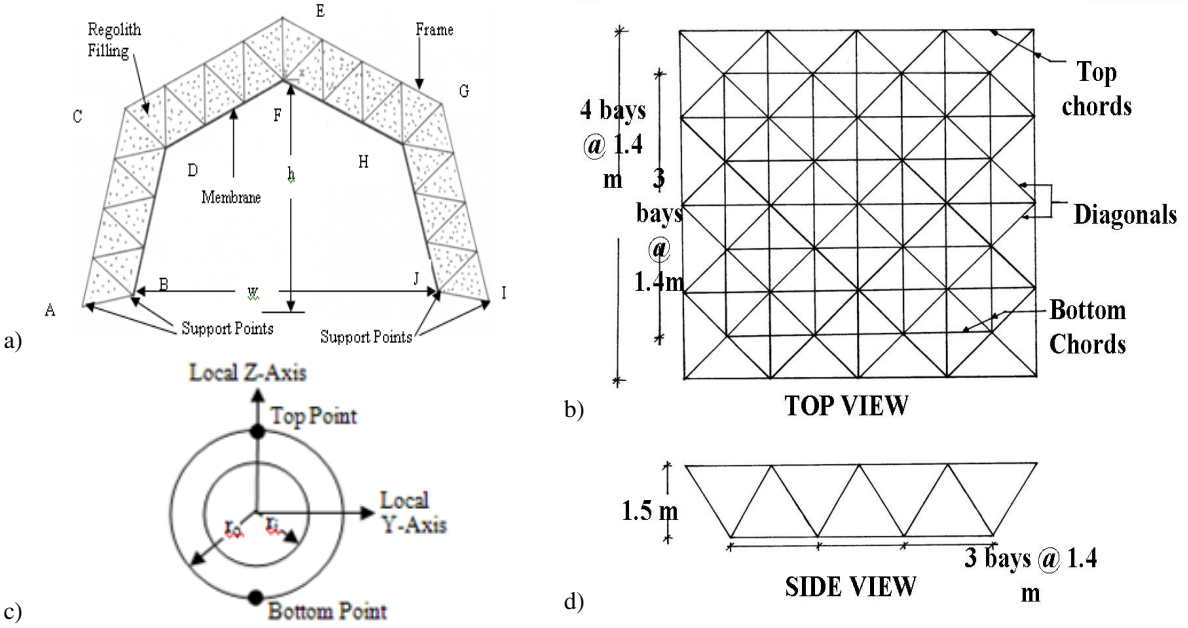

Figure 3.1. Proposed structure. a) Front view; b) Top view; c) Frame member cross-section with top and bottom of cross section marked; and d) Side view.

Table 3.1. Structural dimensions, material properties at normal temperature, and finite element model information.

Parameter	Membrane	Frame
(A) Frame-Membrane Structure:		
Material Used	Kevlar	2014-T6 Aluminum
Young's Modulus[21, 22]	70.5 GPa	72.5 GPa
Density[21, 22]	1440 kg/m^3	2800 kg/m^3
Poisson's Ratio[21, 22]	0.35	0.3
Thickness/ Cross-Sectional Area	0.0075 m	0.00316 m^2
Yield Strength[21, 22]	2920 MPa	410 MPa
Coefficient of Thermal Expansion[21, 22]	-3.96E-06 m/m	23E-06 m/m
(B) Finite Element Model :		
ANSYS Element Type	Shell181	Beam4
No. of Elements & Nodes (Frequency Analysis)	3600 (elements), 976 (nodes)	4640 (elements), 4313 (nodes)
No. of Elements & Nodes (Static and Dynamic Analysis)	576 (elements), 637 (nodes)	2048 (elements), 1556 (nodes)

Figs. 3.1(b) and 3.1(d) show the top and side views of each of the frame modules (ABDC, CDEF, EFHG, and GHJI). Each frame module is a truncated square pyramid made up of 40 outer chords and 24 inner chords, each of length 1.4 m, and 64 diagonal members, each 1.8 m long. The minimum length of the members was chosen such to optimize the number of joints and costs associated with the increased construction time. However, the length of frame member also takes in to account the fact that they must be able to be stored in a spacecraft cargo bay, since they are to be transported from earth. Table 3.1 presents the structural parameters and material properties for the system. Material properties were assumed to be constant at all temperatures, since the change in properties with respect to the temperature range considered here is not significant and the purpose of this paper is to examine the effects of temperature on the structural prestressing (not the material properties). For aluminum (2014-T6) exposed to the extreme temperatures for 1,000 hours, the yield strength ranges from 476 MPa (at -233°C) to 377 MPa (+123°C) and Young's Modulus ranges from 82.7 GPa (-233°C) to 71 GPa (+123°C) (Batelle Memorial Institute, 2009). The values for Poisson's ratio (0.33) and density (2800 kg/m^3) are constant for this temperature range (Batelle Memorial Institute, 2009). For Kevlar exposed to the temperatures for 1,000 hours, the yield strength varies from 2942 GPa (-233°C) to 2905 GPa (+123°C), and Young's Modulus varies from 72.5 GPa (-233°C) to 67.4 GPa (+123°C), the density range is 1498 kg/m^3 (-233°C) to 1411 kg/m^3 (+123°C) (Dupont, 2011). The Poisson's ratio (0.35) is constant for the temperature range (Dupont, 2011).

Furthermore, the following construction related considerations were taken into account when designing the proposed structure: (a) easily deployed/assembled/connected

components for constructing the structure; (b) a habitat that is feasible to be built entirely under or above the ground as well as partly under and partly above the ground; (c) an easily expandable structural system to accommodate an increased in future needs; and (d) an open frame that can be filled with regolith, which can be used as a thermal insulator and radiation shield (thus, utilizing in-situ material to reduce the payload to be carried from the earth).

The bottom of the proposed structure is taken as pinned at the support points marked in Figure 3.1(a). The pinned boundary conditions simulate a few possible practical foundations. For example, for the membrane, it may represent a number of cables holding down the periphery of the membrane, which are then anchored into the regolith, and for the frame, its bottom anchored to the regolith.

To maintain a short sleeve environment, the internal space of the habitat is considered pressurized to 96.5 kPa (14 psi). The internal environment of the structure is kept at room temperature (21°C) compared to extreme external temperatures (123°C during lunar daytime and -233°C lunar night time.).

3.3 ANALYSIS METHODOLOGY

Membrane structures are expected to undergo significant amount of stress stiffening due to applied pressurization and one must consider the stress state of the system during its service life for dynamic analysis (Bedri and Al-Nais, 2005). The frame is also subjected to the internal pressurization load as well as thermal loads and thus, it too can also undergo stress stiffening. The stress state influences the values of the stiffness matrix, and can therefore change the natural frequencies (Donadson et al., 2002). As a consequence of these factors, the dynamic response of the system will be affected.

The equation of motion of a structure subjected to an external excitation is given by

$$[M]\{\ddot{\delta}\} + [C]\{\dot{\delta}\} + [K + K_G]\{\delta\} = \{P\} \tag{3.1}$$

where *[K]* is the stiffness matrix, *[K_G]* is the geometric stiffness matrix, *[M]* is the mass matrix, *[C]* is the damping matrix, *{P}* is the external force applied, which may include the impact force, *{δ}* is the nodal degree of freedom, and a dot above a character is the derivative with respect to time. The *[K_G]* matrix will be augmented/modified initially to account for prestress due to application of internal pressurization load and thermal load.

Restricting the study to undamped case, the above equation reduces to

$$[M]\{\ddot{\delta}\} + [K + K_G]\{\delta\} = \{P\} \tag{3.2}$$

3.3.1 Frequency/Modal Analysis

By setting *{P} = 0* in equation (3.2) and considering the free vibration motion as a simple harmonic,

$$\{\delta(t)\} = \{\delta_0\}\sin(\omega t + \phi) \tag{3.3}$$

where t is the time, $\{\delta_0\}$ is the shape of the system (which does not change with time; only the amplitude varies), ω is the natural frequency of the structure, and φ is the phase angle, the equation of motion can be expressed in the form of the eigenvalue problem as given below

$$\left(\left[K + K_G\right] - \omega^2\left[M\right]\right)\{\delta_0\} = \{0\} \tag{3.4}$$

From equation (3.4), the characteristic frequency equation can be formed and is given by

$$\left|[M]^{-1}[K + K_G] - \omega^2[I]\right| = 0 \tag{3.5}$$

Where *[I]* is the identity matrix. Equation (3.5) is used to compute the natural frequencies of the structure.

3.3.2 Impact Force Dynamic Analysis

For the impact analysis, an outer chord of the frame is considered to be struck by a moving projectile (debris) at its midspan. As formulated by Goldsmith (1960), the impact load acting on the structure was calculated bearing in mind the transverse collision of a rigid mass, m_2, with initial velocity, $v_{2,0}$, striking a simply supported beam

(*AB*) of mass, m_1, and length, *L*, at the mid-length as shown in Figure 3.2. The stiffness of a simply supported beam subjected to central loading is $48EI/L^3$ (where *E* and *I* are the beams modulus of elasticity and moment of inertia, respectively). It is assumed that the rigid mass and a certain fraction of the beam mass (χm_1), undergo completely inelastic (plastic) impact and attain the same velocity, *v*, immediately after impact.

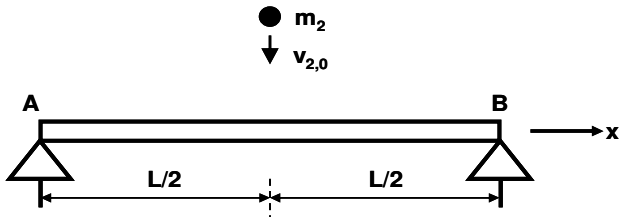

Figure 3.2. Central impact on a simply supported beam.

It is assumed that the dynamic deflection curve is given by

$$w(x,t) = w(c,t)f(x) = \bar{\eta}(t)f(x) \tag{3.6}$$

Where the static deflection curve *f(x)* is a function of time, *t*, and position *x* measured along the beam length (with the origin at the left end, *A*, of the beam and with point of impact at $x = c$) and $\eta(t)$ is the dynamic deflection at the impact point. Therefore, using the standard equations for the static center deflection of a simply supported beam, the kinetic energy, *T*, and potential energy, *V*, can be evaluated as

$$T = \rho A\int_0^L \left(\frac{\partial w}{\partial t}\right)^2 dx = \frac{17}{35} m_1 \dot{\bar{\eta}}^2 \tag{3.7}$$

and

$$V = EI\int_0^L \left(\frac{\partial^2 w}{\partial x^2}\right)^2 dx = \frac{48EI\bar{\eta}^2}{L^3} \tag{3.8}$$

respectively. ρ is the density of the beam material, A is the area of the beam cross-section, and $\dot{\bar{\eta}}$ is the velocity of the beam's midpoint. From the kinetic expression (Equation (3.2)), the fraction of the beam mass, χm_1, that undergoes completely inelastic (plastic) impact and attains the same velocity as the projectile can be regarded as $(17/35)m_1$. Using Lagrange's equation of motion, the generalized impact force, Q, can be obtained as

$$\bar{Q} = (17/35)m_1\ddot{\bar{\eta}} + (48EI/L^3)\bar{\eta} \tag{3.9}$$

Where $\ddot{\bar{\eta}}$ is the dynamic acceleration of the beam's midpoint. Knowing that the beam and projectile move together after impact, the solutions for $\bar{\eta}$ and $\ddot{\bar{\eta}}$ with initial conditions

$$\bar{\eta}_0 = 0,\ \dot{\bar{\eta}} = v = m_2 v_{2,0}/(m_2 + (17/35)m_1) \tag{3.10}$$

Can be obtained from equation (3.9) using Newton's 2nd law of motion as

$$\bar{\eta}(t) = w\left(\frac{L}{2}, t\right) = \frac{m_2 g}{k}\left\{1 - \cos\alpha t\right\} + \frac{m_2 v_{2,0}}{\sqrt{\beta k}}\sin\alpha t \tag{3.11}$$

and

$$\ddot{\bar{\eta}}(t) = \frac{\alpha^2 m_2 g}{\beta}\cos\alpha t - \frac{\alpha^2 m_2 v_{2,0}}{\sqrt{\beta k}}\sin\alpha t \tag{3.12}$$

Where g is the acceleration due to gravity and where α and β are defined by the expressions

$$\alpha = \sqrt{\frac{k}{m_2 + \frac{17}{35} m_1}} \tag{3.13}$$

and

$$\beta = m_2 + \frac{17}{35} m_1 \tag{3.14}$$

Equations (3.11) and (3.12) are used in equation (3.9) to compute the impact force, Q, at any time. This impact force is used as the forcing function $\{P\}$ in equation (3.2) to solve the equation of motion for the structural response (deformations and stresses).

For the present study, the impact loading is considered to come from space debris impact, such as, debris falling off a spacecraft during takeoff or landing and the debris then colliding with the structure. As there is no information on possible debris that might impact lunar habitats at the current time, the FAA's airplane-debris impacts codes (Wilde, 2010) were used to obtain the debris mass and velocity. Following the FAA code, a 1.2 kg projectile traveling at a velocity of 240 m/s was used for the impactor in the analysis (Wilde, 2010). The projectile was considered to strike the midspan of an outer frame member of the structure. With these parameters, the

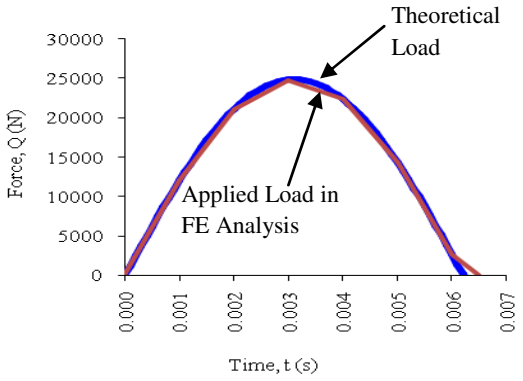

Figure 3.3. Impact load used in analysis.

theoretical impact force shown in Figure 3.3 was calculated by equation 3.4 and found to be sinusoidal with a maximum force of 24.9 kN and an impact duration of 6.2 ms.

3.3.3 Static, Frequency and Dynamic Response Solution Technique

The 3-D frame-membrane structure was modeled and analyzed (frequency, static, and dynamic analyses) using the finite element (FE) code ANSYS (ANSYS 2009). The membrane of the structure was model with SHELL181 elements. SHELL181 elements have both bending and membrane stiffness capabilities and thus, both were accounted for

Table 3.2. Loading cases used in analysis

Structural Case	Temperature Case	Load Case	Internal Temperature (°C)	External Temperature (°C)	Includes 3-D Frame	Includes Membrane	Includes Internal Pressure
1	1	1-1	21	21	Yes	No	No
1	2	1-2	21	123	Yes	No	No
1	3	1-3	21	-233	Yes	No	No
2	1	2-1	21	21	Yes	Yes	No
2	2	2-2	21	123	Yes	Yes	No
2	3	2-3	21	-233	Yes	Yes	No
3	1	3-1	21	21	Yes	Yes	Yes
3	2	3-2	21	123	Yes	Yes	Yes
3	3	3-3	21	-233	Yes	Yes	Yes

in the model. However, the membrane in the structure selected herein has a very small thickness (0.0075 m). Thin SHELL181 elements were verified to accurately simulate the response of a membrane by comparing the results from the FE analysis obtained in previous studies (Malla and Chaudhuri, 2007, 2008) with analytical results (Maier-Schneider et al., 1995). The frame was modeled using BEAM4 elements with tension, compression, torsion, and bending capabilities. Both SHELL181 and BEAM4 are 3-D

elements and have the option for stress stiffening and large deflection capabilities. Table 3.1 shows the parameters used for the FE model.

The frequency analysis was performed on a total of nine different cases (See Table 3.2). There are three structural cases: (a) the frame only (structural case 1); (b) the full frame-membrane structure without internal pressure (structural case 2); and (c) the full frame-membrane structure with internal pressure (structural case 3). The internal pressurization load of 96.5 kPa is applied on the structure's membrane pushing outward. Each of these structural cases were performed under three temperature cases: (a) room temperature both inside and outside (both 21°C) (temperature case 1); (b) room temperature inside (21°C) and hottest external temperature (lunar day temperature of 123°C) (temperature case 2); and (c) room temperature inside (21°C) and coldest external temperature (lunar night temperature of -223°C) (temperature case 3). The internal (room) temperature was applied to the inner chords and membrane, whereas the hottest and coldest external temperatures were applied to the outer chords. The temperature varied linearly along the diagonals connecting the outer chord and inner chord.

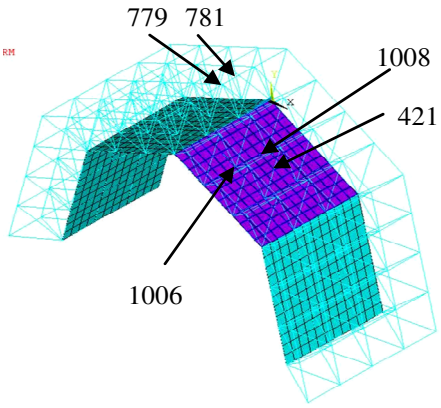

781: Midspan of outer chord and point of impact
779: Joint of outer chord
1008: Midspan of inner chord
1006: Joint of inner chord
421: Central node of membrane panel

a)

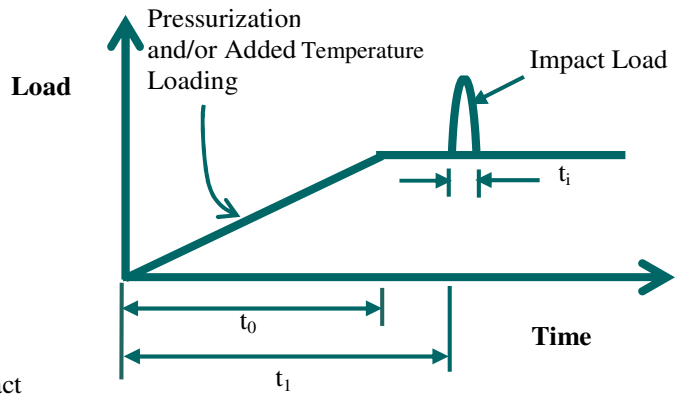

b)

Figure 3.4. a) Finite element mesh model of the structure with some key nodes identified; b) Scheme used to apply pressurization, added mass, and impact loads.

The applied temperature and pressure loads were the two prestressing loads on the structure. ANSYS uses a stress stiffness matrix that is analogous to $[K_G]$ in equations (3.1), (3.2), (3.4), and (3.5) to account for the stiffening effect as a result of prestressing (ANSYS, 2009). Static analysis was run with the internal pressure and temperature loads applied to determine the prestressing caused by the loads. For the frequency analysis, each frame member in the FE model was divided into 10 elements and each membrane panel of size 4.2 m x 4.2 m was divided into 30 x 30 grids. The prestressing loads were applied to this FE model and Block Lanczos method was used to solve the eigenvalue problem in a previous section (equaiton (3.5)) to determine the frequencies and mode shapes.

The static and dynamic analyses were performed only on the full frame-membrane structure with internal pressure (structural case 3, Table 3.2), however all

three temperature cases were examined. Due to computational time constraints, each frame member in the FE model was divided into 4 elements, and each membrane panel was meshed into 12 X 12 grids.

The FE analyses were done utilizing the non-linear geometry option to take into account large deformation and stress stiffening effects from the applied loads on the structure. In the dynamic analysis, there were three loading steps spanning 1 s. The first step occurred from 0 s to 0.25 s with a time step of 0.01s. In step one, the internal pressurization load and temperature were ramped to their full value over 0.2 s, t_0 (Figure 3.4(b)). The pressure and temperature were then kept constant for the remainder of the step and for all subsequent steps. This first step was performed with the time integration off and, therefore, was equivalent to a static loading. Thus, the static results were acquired after this step.

Step two began at 0.25 s, t_1, which was the start of the impact loading, and ended at 0.2565 s, the end of the impact loading. The time step for step two was 0.0005 s to accurately capture the impact phenomenon. The time integration was turned on in ANSYS for this step and after, meaning the dynamic effects were captured. The impact force, $\{P\}$ in equation (3.2), while analytically found to be sinusoidal, was applied as a piecewise linear function (Figure 3.3). The end point points of each linear segment were chosen coincide with the theoretical curve. The applied load accurately captured the theoretical amplitude of 24.9 kN. However, applied duration, t_i, of 6.5 ms was longer than the analytical duration of 6.2 ms, because the loading cannot end in the middle of a time step (which would happen if the analytical duration was use). The piecewise linear forcing function was applied to the mid-point of an outer chord (node 781, Figure 3.4(a)).

The final step proceeds from 0.2565 s until 1 s and has a time step of 0.001 s. Step three shows the habitat's structural response after the impact load duration.

For the dynamic analysis, the Newmark solution method with Newton-Raphson iteration technique was used to solve the equation of motion (equation (3.2)) for displacement, $\{\delta\}$, incorporating non-linear (large deformation) dynamic analysis. Displacement and stress time histories were generated for a total of 1 s.

3.4 RESULTS AND DISCUSSION

3.4.1 Frequency Analysis Results

The first 20 natural frequencies and mode shapes were computed for the nine cases noted in Table 2. Table 3 present these natural frequencies. Table 4 shows the percent change in natural frequencies between the each of the three temperature cases within each of the 3 structural cases.

Examining the frequency results for the frame only case (structural case 1), the highest frequency is for the hottest temperature case (load case 1-2), which is slightly higher (percent change in the fundamental frequency is 1.425 %) than the frequencies for the room temperature case (load case 1-1). The frequencies for the coldest case (load case 1-3) are significantly lower than the room and hottest temperature cases (load cases 1-1 and 1-2) (percent change in the fundamental frequency are -85.576 % and -85.779 %, respectively). For the full frame-membrane structure without internal pressure (structural case 2), the frequencies for the hottest case (load case 2-2) are a little greater (percent change in the fundamental frequency is 5.139 %) than the frequencies in the room temperature case (load case 2-1). When the coldest temperature

Table 3.3. Natural frequencies of the lunar structure.

Mode Number	Load Case 1-1	Load Case 1-2	Load Case 1-3	Load Case 2-1	Load Case 2-2	Load Case 2-3	Load Case 3-1	Load Case 3-2	Load Case 3-3
1	13.614	13.808	1.964	20.356	21.402	2.746	20.510	21.404	3.509
2	20.283	21.265	5.455	22.826	23.501	4.744	23.072	23.505	4.634
3	23.579	23.263	5.576	29.460	31.193	5.303	29.741	31.197	5.585
4	31.931	32.771	9.812	40.940	43.004	6.237	41.237	43.009	5.981
5	42.378	41.943	11.747	41.856	43.287	7.844	42.356	43.295	8.005
6	46.060	47.527	12.054	63.856	67.647	8.662	63.862	67.652	9.527
7	53.838	55.654	12.615	66.405	69.992	9.668	67.381	70.005	10.341
8	53.932	55.729	13.182	66.940	71.657	12.131	67.922	71.672	13.239
9	59.305	61.967	13.706	68.957	73.021	12.354	69.051	73.024	14.214
10	65.226	65.814	14.836	71.036	77.149	12.588	70.913	77.150	14.356
11	65.750	67.599	15.101	74.077	81.677	13.282	73.828	81.692	14.715
12	66.016	70.342	15.460	75.203	81.861	14.189	75.800	81.873	15.363
13	67.473	70.420	16.692	75.758	82.994	14.893	76.104	82.991	15.780
14	70.132	75.347	17.113	75.854	83.146	16.138	76.341	83.160	16.553
15	70.656	76.573	17.674	76.651	83.434	16.452	76.612	83.450	17.095
16	72.936	80.078	17.959	76.791	84.711	16.739	76.700	84.711	17.495
17	73.155	80.113	18.624	77.008	85.753	17.384	76.859	85.763	18.097
18	73.273	81.851	18.757	77.054	85.815	18.086	76.975	85.818	18.517
19	73.310	81.921	20.045	77.143	87.407	18.304	77.360	87.402	18.994
20	73.607	84.154	20.174	77.213	88.258	19.137	77.469	88.266	19.900

(load case 2-3) is applied the frequencies drastically reduce compared to load cases 2-1 and 2-2 (percent change for fundamental frequency -86.509 % and -87.168%, respectively). The full frame-membrane structure with internal pressure case follows the same pattern as the other two structural cases. The lowest frequencies are for the coldest temperatures (load case 3-3) and the highest frequencies are for the hottest temperature (load case 3-2). Therefore, regardless of the structure analyzed, the hottest temperature increases the frequencies slightly compared to the room temperature case (average percent change in the fundamental frequency is 3.641 %) and the coldest temperature drastically reduces the frequencies compared to the room temperature case (average percent change in the fundamental frequency is -84.992 %). Examining the room temperature frequencies, the lowest frequencies of any structural are for the frame alone

(load case 1-1). The frequencies for the full structure without pressurization (load case 2-1) and the full structure with pressure (load case 3-1) are significantly higher than load case 1-1. The greatest frequencies are in load case 3-1. For the hottest temperature case, the frequencies of the full structure with pressure (load case 3-2) are slightly higher than the frequencies of the full structure without the pressure (load case 2-2). The frequencies for the frame alone (load case 1-2) are much lower than for load cases 2-2 and 3-2. Examining the coldest temperature results, again the lowest frequency is for the frame alone (load case 1-3) and the highest is for the full structure with internal pressure (load case 3-3). Hence, for temperatures studied, the addition of the membrane increases the frequency by a large amount and the pressurization of the membrane creates a small increase in the frequency.

Table 3.4. Percent change in natural frequencies of the lunar structure.

Mode No.	Percent Change Case 1-1 to Case 1-2	Percent Change Case 1-1 to Case 1-3	Percent Change Case 1-2 to Case 1-3	Percent Change Case 2-1 to Case 2-2	Percent Change Case 2-1 to Case 2-3	Percent Change Case 2-2 to Case 2-3	Percent Change Case 3-1 to Case 3-2	Percent Change Case 3-1 to Case 3-3	Percent Change Case 3-2 to Case 3-3
1	1.425	-85.576	-85.779	5.139	-86.509	-87.168	4.359	-82.891	-83.606
2	4.841	-73.104	-74.346	2.957	-79.215	-79.812	1.877	-79.916	-80.286
3	-1.340	-76.353	-76.032	5.883	-81.999	-82.999	4.896	-81.220	-82.096
4	2.631	-69.273	-70.060	5.042	-84.766	-85.497	4.297	-85.496	-86.093
5	-1.026	-72.280	-71.993	3.419	-81.260	-81.880	2.217	-81.100	-81.510
6	3.185	-73.830	-74.638	5.937	-86.435	-87.195	5.935	-85.081	-85.917
7	3.373	-76.569	-77.333	5.402	-85.440	-86.187	3.894	-84.653	-85.228
8	3.332	-75.558	-76.346	7.047	-81.878	-83.071	5.521	-80.509	-81.528
9	4.489	-76.889	-77.882	5.894	-82.084	-83.082	5.754	-79.415	-80.535
10	0.901	-77.254	-77.458	8.605	-82.279	-83.684	8.795	-79.755	-81.392
11	2.812	-77.033	-77.661	10.260	-82.070	-83.738	10.652	-80.069	-81.987
12	6.553	-76.581	-78.022	8.853	-81.132	-82.667	8.012	-79.732	-81.236
13	4.368	-75.261	-76.297	9.551	-80.341	-82.055	9.049	-79.265	-80.986
14	7.436	-75.599	-77.288	9.613	-78.725	-80.591	8.932	-78.317	-80.095
15	8.374	-74.986	-76.919	8.849	-78.536	-80.281	8.925	-77.686	-79.515
16	9.792	-75.377	-77.573	10.314	-78.202	-80.240	10.445	-77.190	-79.347
17	9.511	-74.542	-76.753	11.356	-77.426	-79.728	11.585	-76.454	-78.899
18	11.707	-74.401	-77.084	11.370	-76.528	-78.924	11.488	-75.944	-78.423
19	11.746	-72.657	-75.531	13.305	-76.273	-79.059	12.981	-75.447	-78.268
20	14.329	-72.592	-76.027	14.305	-75.215	-78.317	13.937	-74.312	-77.455

3.4.2 Static Analysis Results

In static and dynamic analysis, displacement and stress time history results have been presented at five nodes of interest, in order to give representative results for the full structure. The nodes that were tracked were: (a) the point of impact and midspan of an outer chord, (node 781); (b) the joint of an outer chord (779); (c) the midspan of an inner chord (1008); (d) the joint of an inner chord (1006); and (e) the center of a membrane panel (421). These nodes are shown in Figure 3.4(a).

Table 3.5. Maximum static displacements of the full structure with pressure for temperature case 1.

Full Structure with Pressure - Temperature Case 1			
Representative Nodes	Max X Displacement (m)	Max Y Displacement (m)	Max Z Displacement (m)
781	-7.26E-08	2.09E-03	-5.93E-07
779	-6.27E-08	2.17E-03	3.52E-07
1008	4.34E-03	1.03E-02	1.62E-07
1006	1.35E-03	3.79E-03	-3.61E-03
421	1.83E-02	3.99E-02	1.22E-07
Maxima of the Frame-Membrane Structure			
Membrane	4.26E-02 Node 621 Panel GHIJ	4.16E-02 Node 221 Panel CDEF	1.50E-03 Node 199 Panel CDEF
Frame Outer Chords	2.80E-03 Node 881 Panel GHIJ	3.74E-03 Node 745 Panel CDEF	2.81E-04 Node 1215 Panel EFGH
Frame Inner Chords	1.26E-02 Node 1043 Panel GHIJ	1.30E-02 Node 978 Panel CDEF	1.50E-03 Node 2153 Panel CDEF
Frame Diagonals	3.41E-03 Node 1938 Panel GHIJ	4.38E-03 Node 1677 Panel CDEF	3.08E-03 Node 1641 Panel CDEF

Tables 3.5 and 3.6 show the static displacement results for the full frame-membrane structure with internal pressurization for all three temperature cases (load cases 3-1, 3-2, and 3-3). Results are presented for the representative nodes as well as at nodes where the maximum displacements occur in the membrane, inner chords, outer chords, and diagonals. For the displacement results, positive x-direction means the node is moving to the right, a positive y-displacement means the node of structure is moving upward, and a positive z-displacement means the node is moving out of the page (Figure 3.4(a)).

For load case 3-1 (room temperature applied to the full membrane-structure with pressure), the internal pressure causes the structure to expand outward. This can be seen by examining the x and y-displacement in Table 3.5. For the y-displacement, all the nodes (representative and maximum) are positive, meaning the structure is moving up. For the x-displacement, nodes 1008, 1006, and 421 and all the maximum nodes are located on panel EFGH and GHIJ (panels on the right side of the structure, Figure 3.1(a)) and are seen to move to the right. Additional results not presented show panel ABCD moves to the left at a value equivalent to panel GHIJ displacement and likewise panel CDEF moves at an equal magnitude but opposite direction at panel EFGH. The x-

Table 3.6. Maximum static displacements of the full structure with pressure for two temperature cases. a) Temperature Case 2; and b) Temperature Case 3.

a) Full Structure with Pressure - Temperature Case 2			
Representative Nodes	Max X Displacement (m)	Max Y Displacement (m)	Max Z Displacement (m)
781	3.67E-07	1.14E-02	-1.20E-03
779	3.19E-07	1.16E-02	4.87E-07
1008	5.66E-03	1.76E-02	1.94E-07
1006	2.43E-03	1.06E-02	-3.62E-04
421	1.76E-02	4.21E-02	1.42E-07
Maxima of the Frame-Membrane Structure			
Membrane	3.87E-02 Node 533 Panel GHIJ	4.36E-02 Node 221 Panel CDEF	1.60E-03 Node 332 Panel EFGH
Frame Outer Chords	5.81E-03 Node 881 Panel GHIJ	1.16E-02 Node 779 Junction EF	6.73E-03 Node 1095 Panel ABCD
Frame Inner Chords	1.38E-02 Node 1043 Panel GHIJ	1.91E-02 Node 1012 Panel EFGH	1.60E-03 Node 2162 Panel EFGH
Frame Diagonals	5.60E-03 Node 1951 Panel GHIJ	1.10E-02 Node 1717 Junction EF	6.37E-03 Node 1642 Panel CDEF
b) Full Structure with Pressure - Temperature Case 3			
Representative Nodes	Max X Displacement (m)	Max Y Displacement (m)	Max Z Displacement (m)
781	-1.57E-06	-2.26E-02	3.09E-03
779	-1.41E-06	-2.30E-02	7.32E-08
1008	5.46E-04	-9.99E-03	4.91E-08
1006	-1.41E-03	-1.43E-02	-3.71E-04
421	2.02E-02	3.46E-02	5.65E-08
Maxima of the Frame-Membrane Structure			
Membrane	5.55E-02 Node 581 Panel GHIJ	3.80E-02 Node 261 Panel CDEF	1.54E-03 Node 169 Panel ABCD
Frame Outer Chords	1.02E-02 Node 711 Junction CD	-2.30E-02 Node 779 Junction EF	1.56E-02 Node 808 Panel EFGH
Frame Inner Chords	1.69E-02 Node 1371 Panel GHIJ	-1.63E-02 Node 993 Junction EF	1.52E-03 Node 949 Junction CD
Frame Diagonals	-8.70E-03 Node 1885 Junction GH	-2.14E-02 Node 1717 Junction EF	-1.14E-02 Node 2065 Panel GHIJ

displacement of nodes 781 and 779 (located at the crest of the structure) have very small movement (-7.26E-08 m and -6.27E-08 m, respectively), so the crest of the structure is almost motionless. Therefore, the structure is expanding vertically and horizontally (x-direction) outward under internal pressure. The z-direction displacement is not seen to be significant in any nodes (about 10 times less than the x and y-displacement), except the diagonals (Table 3.5). Thus, the pressure does not move the structure significantly in the z-direction.

For load case 3-2 (hottest temperature applied to the full membrane-structure with pressure), the structure also expands vertically and horizontally outward. Table 3.6 shows the y-displacements are positive. The x-displacements are positive for panel EFGH and GHIJ (the right side of the structure moves right) and with minimal motion at the crest (node 781 and 779). Additionally, the left side of the structure displaces to the left (not shown). Comparing the hottest temperature (load case 3-2) with the room temperature (load case 3-1) (Table 3.5), the y-displacement is higher in all representative nodes for the hottest temperature and maximum y-displacements are also larger for the hottest temperature. The x-displacements are larger for load case 3-2 than load case 3-1 for all frame members as well. Conversely, the x-displacement in the membrane is larger for the room temperature case. The z-displacements are larger for the daytime case than the room temperature case. Therefore, the hottest external temperature causes to the frame of the structure to displace in all direction more than the room temperature case. The membrane displaces more in the y and z-direction, but less in the x-direction for the daytime case compared to the room temperature case.

For load case 3-3 (coldest temperature applied to the full membrane-structure with pressure), the frame nodes (representative and maximums) are negative in the y-direction, but the membranes displacement is positive (though less than room temperature case (load case 3-1)) (Table 3.6). Thus, the coldest temperature causes the frame to contract relative to its unloaded position and the membrane to contract relative to the baseline room temperature case. In the x-direction, the outer frame members and diagonal members contract (panels ABCD and CDEF have positive displacements and panels EFGH and GHIJ have negative displacements). For the inner chords, nodes 1008 and 1006 (Table 3.6) have values less than the room temperature case (Table 3.5), showing these nodes also contract. However, the maximum inner chord displacement (node 1371) for the load case 3-3 is greater than load case 3-1, so the inner chords are expanding at some positions and contracting at others. Examining the membrane's x-displacement, node 421 and the maximum x-displacement in the membrane (node 581) are larger for load case 3-3 than for load case 3-1 (room temperature). In the z-direction (Table 3.6), all representative nodes and all of the maximum displacement nodes move towards the center of the structure in the z-direction during the coldest temperature, so the structure is contracting in the z-direction. This is most noticeable in node 781 where the z-

Table 3.7. Maximum static stresses of the full structure with pressure for temperature case 1.

Full Structure with Pressure - Temperature Case 1		
Element Location	Element (Cross-section)	Stress (Pa)
Stress at Representative Nodes		
Representative Nodes	867 (781)	4.32E+05
	868 (779)	8.90E+05
	1078 (1008)	-1.55E+08
	1080 (1006)	-1.30E+08
	367 (421)	1.64E+08
Maxima of the Frame-Membrane Structure		
Membrane	34 (149) Panel ABCD	1.65E+08
Frame Outer Chord	1273 (745) Panel CDEF	5.12E+07
Frame Inner Chord	1093 (1019) Panel EFGH	2.91E+08
Frame Diagonal	2417 (1071) Panel GHIJ	1.13E+08

displacement went from -5.93E-07 m (moving away from the center) in the room temperature case to 3.09E-03 m (toward the center) in the nighttime case. Thus, the coldest temperature (load case 3-3) contracts the frame in the y and z-direction. The outer chords of the frame are contracted in the x-direction, but not all the inner chords of the frame contract (some expand and others contract). The membrane expands in the x and y-direction, but contracts in the z-direction.

The maximum displacement in the structure is 5.55E-02 m in the x-direction and occurs in the membrane (node 581) for the coldest temperature (load case 3-3) (Table 6). The maximum vertical displacement is 4.26E-02 m for node 421 in the membrane during the daytime case (load case 3-2) (Table 3.6). The maximum z-displacement is -1.14E-02 m at node 2065 (diagonal member) during the nighttime case.

Tables 3.7 and 3.8 show the maximum static stress values for the full frame-

Table 3.8. Maximum static stresses of the full structure with pressure for two temperature cases. a) Temperature Case 2; and b) Temperature Case 3.

a) Full Structure with Pressure - Temperature Case 2			b) Full Structure with Pressure - Temperature Case 3		
Element Location	Element (Cross-Section)	Stress (Pa)	Element Location	Element (Cross-Section)	Stress (Pa)
Stress at Representative Nodes			Stress at Representative Nodes		
Representative Nodes	867 (781)	-4.46E+07	Representative Nodes	867 (781)	1.03E+08
	868 (779)	-4.46E+07		868 (779)	1.03E+08
	1078 (1008)	1.25E+08		1078 (1008)	8.18E+07
	1080 (1006)	-9.53E+07		1080 (1006)	-8.90E+07
	367 (421)	1.79E+08		367 (421)	1.80E+08
Maxima of the Frame-Membrane Structure			*Maxima of the Frame-Membrane Structure*		
Membrane	14 (61) Panel ABCD	1.78E+08	Membrane	515 (621) Panel GHIJ	1.94E+08
Frame Outer Chord	2461 (2071) Panel GHIJ	-2.18E+08	Frame Outer Chord	733 (638) Panel ABCD	5.22E+08
Frame Inner Chord	1045 (967) Panel CDEF	-3.63E+08	Frame Inner Chord	1083 (1249) Panel EFGH	-2.98E+08
Frame Diagonal	2425 (2039) Panel GHIJ	1.58E+08	Frame Diagonal	2481 (2086) Panel GHIJ	3.33E+08

membrane structure with internal pressure for the three temperature cases (room temperature, lunar day, and lunar night extremes). For all frame members, the *total normal stress* (axial plus bending stresses) is presented. For the membrane, the *first principal stress* values are presented. For the representative frame nodes (the point of impact and midspan of an outer chord, node 781; the joint of an outer chord, 779; the midspan of an inner chord, 1008; the joint of an inner chord, 1006), the stress is presented at the *top* and the *bottom* points of the cross-section (See Figure 3.1(c)). For maximum stresses of the frame members, the stresses are for the *entire* cross-section (not just the top and bottom point), since the maximum stress often occurs on an angle in the cross-section (not at the top and bottom point).

Like the displacement results, the internal pressure in room temperature case (load case 3-1) is shown to cause a stress on the structure (Table 3.7). This stress is most significant at the inner chords members (cross-section 1008, cross-section 1006, and maximum inner chord stress) and membrane (cross-section 421 and maximum membrane stress), where the stress has an order of magnitude of 10^8 Pa. The static stress is much less significant for outer chords where the stress is on the order of 10^7 Pa at the maximum (cross-section 745) and 10^5 at the representative nodes (cross-section 781, cross-section 779). For load case 3-2 (hottest temperature), the magnitude of stress is greater for maxima compared to load case 3-1 (room temperature). The stress at the representative cross-sections 781, 779, 1008, and 421 is also increased. However, the stress is reduced for cross-section 1006 from -1.30E+08 Pa (Table 7) at room temperature to -9.53E+07 at the hottest temperature (Table 3.8). For load case 3-3 (coldest temperature), Tables 3.7 and 3.8 shows the maximum stresses in the structure are greater than load case 3-1 (room

temperature). For the representative cross-sections, the stresses at cross-sections 1008 and 1006 during the extreme cold (load case 3-3) were less than load case 3-1. The stresses at cross-sections 781, 779, 421 during the extreme cold (load case 3-3) were greater than those in room temperature case. Comparing the day and night temperature cases (Table 3.8), the stress at the inner chords (cross-section 1008, cross-section 1006, and the maximum inner chord stress) were largest in the daytime case (load case 3-2). However, the stresses for the outer chords (cross-section 781, cross-section 779, and the maximum outer chord stress), the diagonal (the maximum diagonal stress), and the membrane (cross-section 421 and maximum membrane stress) were larger during the coldest temperature (load case 3-3). The overall maximum static stress is 5.22E+08 Pa at cross-section 638 (outer chord, Panel ABCD) during load case 3-3 (Table 3.8).

3.4.3 Dynamic Analysis Results

The dynamic vertical displacement time histories for the representative nodes are presented in Figures 3.5 and 3.6. The maximum displacements of the representative nodes and the maximum displacement of the membrane, inner chord member, outer chord member, and diagonal members are presented in Tables 3.8 and 3.9. The time histories in Figures 3.5 and 3.6 shows a static displacement from 0 – 0.2 s, about which the dynamic results oscillates. For the room temperature case (load case 3-1, Figure 3.5), the displacement amplitude is most significant at node 781 (Figure 3.5(a)) with an amplitude far greater than the static displacement. For nodes 779, 1008, and 1006 (parts (b), (c), and (d) of Figure 3.5), the vibration effects are still noticeable, but static displacement has a larger impact on the displacement than the impact load. In the

membrane (node 421, Figure 3.5(e)), there is almost no vibration present. Therefore, the farther the node is from the point of impact the smaller the amplitude of vibration. In parts (a), (b), and (c) of Figure 3.5, the displacement vibration amplitude can also be seen to reduce with time, which is a result of the impact force spreading through the structure rather than staying localized at a single node. For the lunar day (load case 3-2) and night cases (load case 3-3) (Figure 3.6) similar results can be seen. In the extreme hot temperature case (load case 3-2), only at the point of impact (node 781) (Figure 3.6(a)) is the vibration amplitude prominent. Compared to the room temperature case (load case 3-1), the amplitude of displacement for the hottest temperature is less at node 781 and the amplitude reduces to the static level at a faster rate. For the other nodes (Figure 3.6 parts (b) through (e)), the static displacement is the only significant displacement during the lunar day. For the lunar night case, again the dynamic displacement is prominent only at node 781 (Figure 3.6(a)). The dynamic displacement at the point of impact for load case 3-3 has smallest amplitude and the amplitude reduces to the static level the fastest compared to the room temperature and daytime temperature cases. Nodes 779, 1008, 1006, and 421 during the lunar night all have large displacement from the static internal pressure and applied temperature, but negligible displacement caused by the impact load (Figure 3.6 parts (a) through (d)).

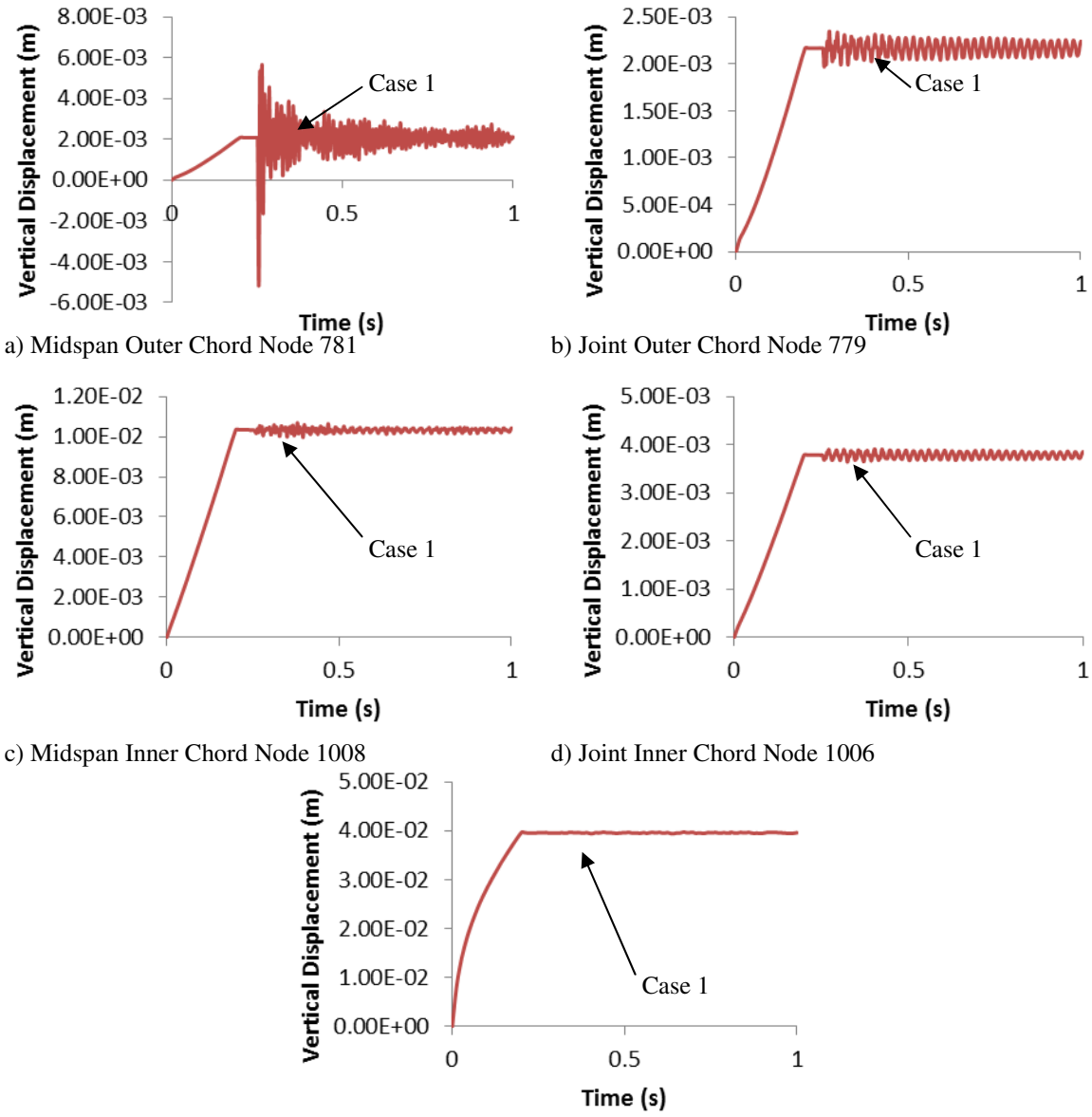

Figure 3.5. Displacement time history of the full structure with pressure for temperature case 1 for various nodes. a) Node 781; (b) Node 779; c) Node 1008; d) Node 1006; and e) Node 421.

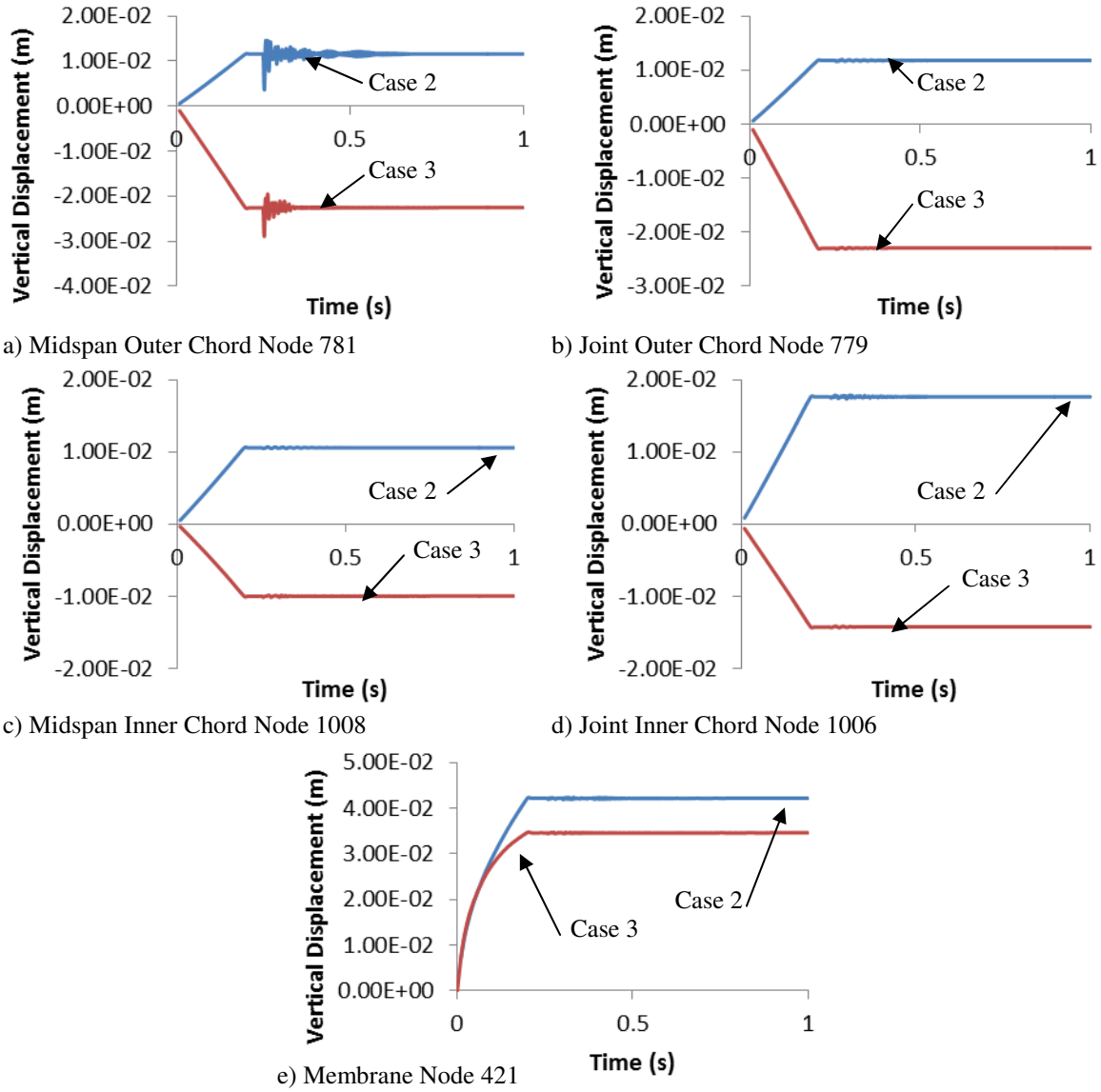

a) Midspan Outer Chord Node 781

b) Joint Outer Chord Node 779

c) Midspan Inner Chord Node 1008

d) Joint Inner Chord Node 1006

e) Membrane Node 421

Figure 3.6. Displacement time history of the full structure with pressure for temperature cases 2 and 3 for various nodes. a) Node 781; b) Node 779; c) Node 1008; d) Node 1006; and e) Node 421.

Examining all the nodes in the full frame-membrane structure with internal pressure for all three temperature cases (room, hottest, and coldest temperatures), all the maximum displacements occur shortly after impact (within the period of 0.25 s 0.275 s). The maximum overall displacement is 5.56E-02 m in the x-direction occurring at node 581, a membrane node, during load case 3-3 (lunar night) (Table 3.6). The maximum vertical displacement of 4.38E-02 is in membrane node 221 during load case 3-2 (lunar day) (Table 3.6). The maximum z-displacement is -1.14E-02 at node 2065 (diagonal member) during the lunar night. These maximum are mainly the result of static displacement (Table 3.6).

The stress time histories for the representative cross-sections (the point of impact and midspan of an outer chord, node 781; the joint of an outer chord, 779; the midspan of an inner chord, 1008; the joint of an inner chord, 1006; the center of a membrane panel, 421) are presented in Figure 3.7, 3.8, 3.9, and 3.10. For all frame members, the stress presented is the *total normal stress* (axial stress plus bending stress) in a cross-section. For the membrane, the *first principle stress* is reported (Figure 3.8). Figures 3.7, 3.9, and 3.10 are the total normal stresses time histories, where the stress presented is the stress at the *top* and the *bottom* of the member cross-section (see Figure 3.1(c)).

The maximum stress for the representative cross-sections and the maximum stresses occurring in the outer frame members, inner frame members, diagonal, and membrane are presented in Tables 3.11 and 3.12. The *total normal stress* is reported for the frame members and the *first principal stress* is reported for the membrane. The stress presented for the representative cross-section in the frame (781, 779, 1008, and 1006) is the total normal stress at either *top* or *bottom* of the cross-section (the larger of the two is

reported). Additionally, the maximum normal stress throughout the *entire* cross-section (not just the top or bottom of the member) is presented in Tables 3.11 and 3.12 for the maximum stress occurring in the outer frame members, the inner frame members, and diagonal frame members. The stress for the entire cross-section is presented, since the maximum stress in a frame member often does not occur at the top of bottom of the member, but on angle. These maximum stresses throughout the entire cross-sections are not shown in the time histories, since the location of the maximum normal stress changes depending on the position of the beam of the oscillating beam.

Table 3.9. Maximum dynamic displacements of the full structure with pressure for temperature case 1.

Full Structure with Pressure - Temperature Case 1			
Representative Nodes	Max X Displacement (m)	Max Y Displacement (m)	Max Z Displacement (m)
781	-2.61E-07	5.66E-03	9.14E-05
779	-9.50E-08	2.35E-03	8.47E-05
1008	4.41E-03	1.05E-02	-3.20E-05
1006	1.37E-03	3.90E-03	-3.97E-04
421	1.84E-02	4.02E-02	3.76E-03
Maxima of the Frame-Membrane Structure			
Membrane	4.28E-02 Node 533 Panel GHIJ	4.19E-02 Node 221 Panel CDEF	1.55E-03 Node 199 Panel CDEF
Frame Outer Chords	2.85E-03 Node 881 Panel GHIJ	5.66E-03 Node 781 Junction EF	1.29E-03 Node 1191 Panel CDEF
Frame Inner Chords	-1.27E-02 Node 939 Panel ABCD	1.32E-02 Node 978 Panel CDEF	-1.55E-03 Node 2153 Panel CDEF
Frame Diagonals	3.48E-03 Node 1968 Panel GHIJ	4.61E-03 Node 1677 Panel CDEF	-3.37E-03 Node 1638 Panel CDEF

Looking at Figure 3.7, 3.8, 3.9, and 3.10, the static stress can be seen from 0 – 0.2 s when the temperature and pressure are ramped up. However, for the room temperature (load case 3-1), the static stress is only present in nodes 1008 (midspan of an inner chord), 1006 (joint of an inner chord), and 421 (center of membrane panel) (Figure 3.7). The static stress is not present in the nodes 781 (midspan of an outer chord and the point of impact) and 779 (joint of an outer chord), suggesting that the pressure does not stress the outer chords (Figure 3.7). The static stress is present for all frame members and the

membrane in hottest temperature case (load cases 3-2) and the coldest temperature case (load case 3-3) (Figures 3.9 and 3.10). It should be noted though that for cross-sections 781 and 779 (Figure 3.9) during load cases 3-2 and 3-3, the static stress on the bottom of the member is very small likely due to the bending and direct axial stress canceling each other out. After the pressure and temperature reach their full values and the impact load is applied, the stress oscillates about its static stress in all three load cases (3-1, 3-2, and 3-3). In all three load cases (3-1, 3-2, and 3-3), the stress amplitude is largest for the top chords (cross-section 781 and 779) (Figure 3.7 and 3.9). The largest amplitude is at the bottom of cross-section 781 for load case 3-2 (Figure 3.9), when the bending stress and axial stress are in the same direction. However, for the top of the same cross-section in the same case the stress amplitude is very small, since the bending and axial stress are in opposite directions canceling each other out. Cross-section 779 in load case 3-2, cross-section 781 in load case 3-3, and cross-section 779 in load case 3-3 also have stress amplitudes that are very different at the top and bottom of the cross-section (Figure 3.9). For load case 3-1 though, the stress amplitude at the top and bottom of all the cross-sections are similar (Figure 3.7). Also, comparing the day and night cases (load cases 3-2 and 3-3, respectively) to the room temperature case (load case 3-1), the stress amplitude is smaller and the stress amplitude reduces at a faster rate for the day and night cases. Furthermore, the nighttime case (load case 3-3) has smaller amplitude and the amplitude decreases to static level in less time than the daytime case (load case 3-2) (Figures 3.8, 3.9, and 3.10). Thus, as seen with the dynamic displacement results, the external temperature has an effect on the structural response with the coldest temperature case having the greater effect on the stress response.

The maximum stress in the structure is 5.30E+08 Pa (Table 3.12). This stress is at cross-section 638, an outer chord, in the coldest temperature case (load case 3-3). The stress is predominantly caused by static pressurization and external temperature load, since the dynamic stress value is very similar to the static stress value (Table 3.8).

Table 3.10. Maximum dynamic displacements of the full structure with pressure for two temperature cases. a) Temperature Case 2; and b) Temperature Case 3.

a) Full Structure with Pressure - Temperature Case 2			
Representative Nodes	Max X Displacement (m)	Max Y Displacement (m)	Max Z Displacement (m)
781	4.22E-07	1.46E-02	-1.29E-03
779	3.27E-07	1.20E-02	-7.64E-05
1008	2.46E-03	1.79E-02	-3.39E-05
1006	5.72E-03	1.07E-02	-3.98E-04
421	1.77E-02	4.23E-02	3.39E-05
Maxima of the Frame-Membrane Structure			
Membrane	3.89E-02 Node 533 Panel GHIJ	4.38E-02 Node 221 Panel CDEF	1.63E-03 Node 199 Panel CDEF
Outer Chords	6.10E-03 Node 881 Panel GHIJ	1.46E-02 Node 781 Junction EF	-7.64E-03 Node 1182 Panel CDEF
Inner Chords	1.39E-02 Node 1043 Panel GHIJ	1.93E-02 Node 978 Panel CDEF	1.63E-03 Node 2153 Panel CDEF
Diagonals	-5.80E-03 Node 1498 Panel ABCD	1.18E-02 Node 1711 Junction EF	-6.51E-03 Node 1359 Panel GHIJ
b) Full Structure with Pressure - Temperature Case 3			
Representative Nodes	Max X Displacement (m)	Max Y Displacement (m)	Max Z Displacement (m)
781	-1.76E-06	-2.89E-02	3.16E-03
779	-1.49E-06	-2.31E-02	9.80E-05
1008	5.83E-04	-1.01E-02	4.73E-05
1006	-1.43E-03	-1.43E-02	-4.08E-04
421	2.03E-02	3.47E-02	4.45E-05
Maxima of the Frame-Membrane Structure			
Membrane	5.56E-02 Node 581 Panel GHIJ	3.81E-02 Node 261 Panel CDEF	1.57E-03 Node 169 Panel ABCD
Outer Chords	-1.03E-02 Node 847 Junction GH	-2.89E-02 Node 781 Junction EF	1.59E-02 Node 1182 Panel CDEF
Inner Chords	1.69E-02 Node 1371 Panel GHIJ	1.65E-02 Node 989 Junction EF	-1.55E-03 Node 997 Junction EF
Diagonals	-8.75E-03 Node 1879 Junction GH	-2.23E-02 Node 1359 Panel GHIJ	-1.14E-02 Node 2065 Panel GHIJ

Table 3.11. Maximum dynamic stresses of the full structure with pressure for temperature case 1.

Full Structure with Pressure - Temperature Case 1		
Element Location	Element (Cross-Section)	Stress (Pa)
Stress at Representative Nodes		
Representative Nodes	867 (781)	-3.94E+07
	868 (779)	-3.58E+07
	1078 (1008)	-1.59E+08
	1080 (1006)	-1.32E+08
	367 (421)	7.66E+07
Maxima of the Frame-Membrane Structure		
Membrane	27 (61) Panel ABCD	1.64E+08
Outer Chord	985 (902) Panel GHIJ	2.57E+08
Inner Chord	1025 (949) Junction CD	2.91E+08
Diagonal	2405 (2024) Panel GHIJ	1.15E+08

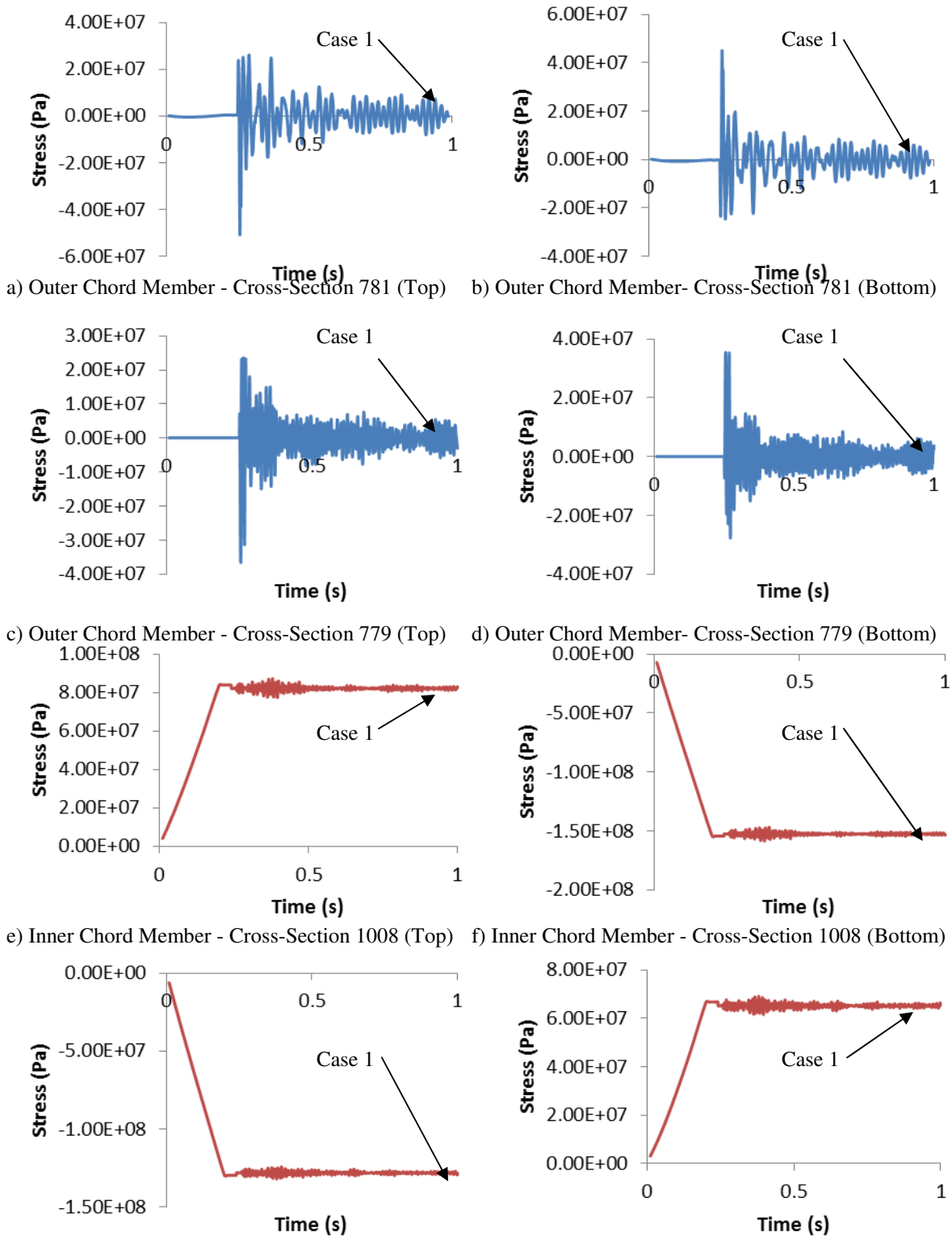

a) Outer Chord Member - Cross-Section 781 (Top) b) Outer Chord Member- Cross-Section 781 (Bottom)

c) Outer Chord Member - Cross-Section 779 (Top) d) Outer Chord Member- Cross-Section 779 (Bottom)

e) Inner Chord Member - Cross-Section 1008 (Top) f) Inner Chord Member - Cross-Section 1008 (Bottom)

g) Inner Chord Member - Cross-Section 1006 (Top) h) Inner Chord Member - Cross-Section 1006 (Bottom)

Figure 3.7. Stress time history at the top and bottom of various frame members' cross-section for temperature case 1. a) Cross-section 781 (top); b) Cross-section 781 (bottom); c) Cross-section 779 (top); d) Cross-section 779 (bottom); e) Cross-section 1008 (top); f) Cross-section 1008 (bottom); g) Cross-section 1006 (top); h) Cross-section 1006 (bottom).

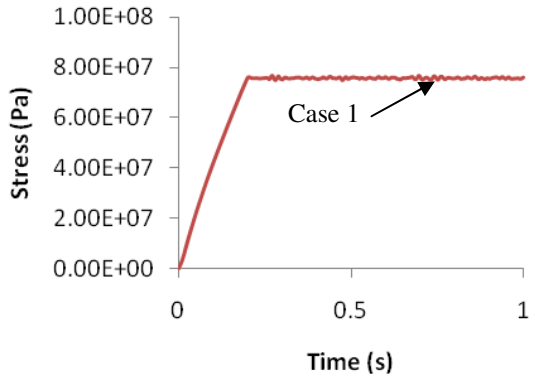

a) Temperature Case 1

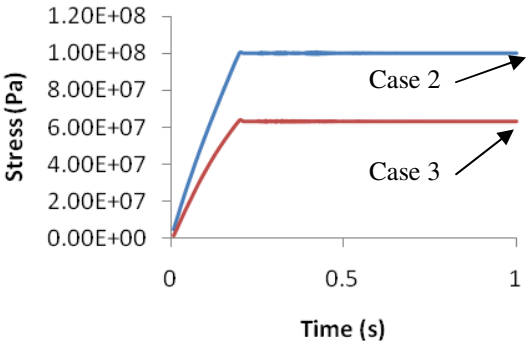

b) Temperature Cases 2 and 3

Figure 3.8. Stress time history of node 421, center of a membrane panel for three temperature cases. a) Temperature case 1; and b) Temperature cases 2 and 3.

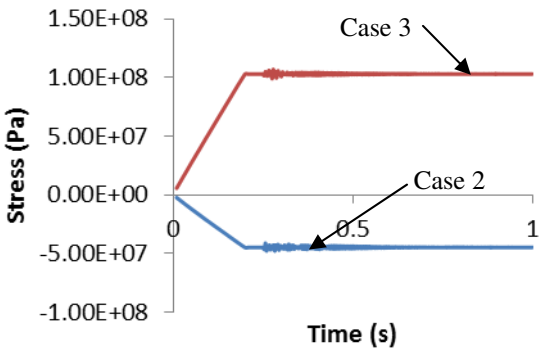

a) Outer Chord Member - Cross-Section 781 (Top)

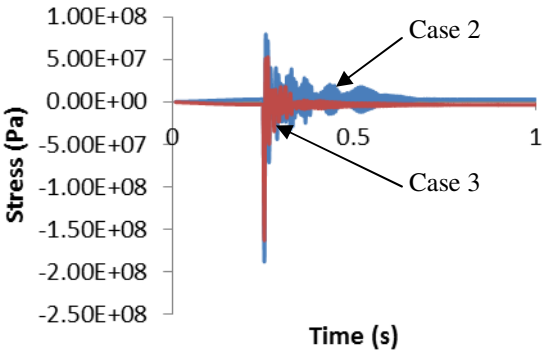

b) Outer Chord Member - Cross-Section 781 (Bottom)

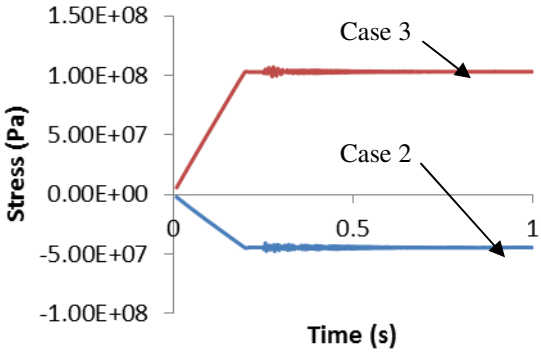

c) Outer Chord Member - Cross-Section 779 (Top)

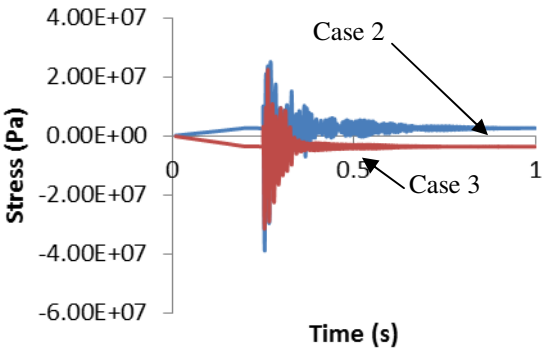

d) Outer Chord Member - Cross-Section 779 (Bottom)

Figure 3.9. Stress time history at the top and bottom of various outer frame members' cross-section for temperature cases 2 and 3. a) Cross-section 781 (Top); b) Cross-section 781 (Bottom); c) Cross-section 779 (Top); and d) Cross-section 779 (Bottom).

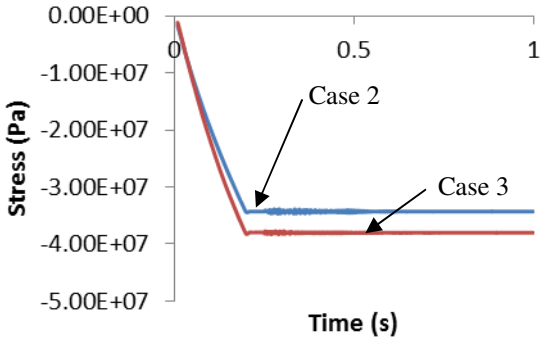

a) Inner Chord Member - Cross-Section 1008 (Top)

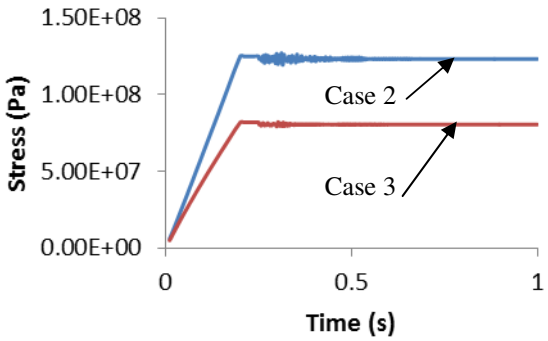

b) Inner Chord Member - Cross-Section 1008 (Bottom)

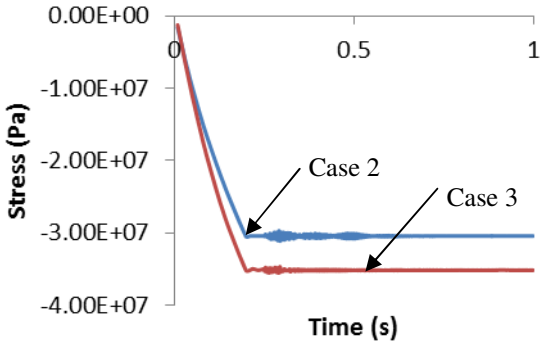

c) Inner Chord Member - Cross-Section 1006 (Top)

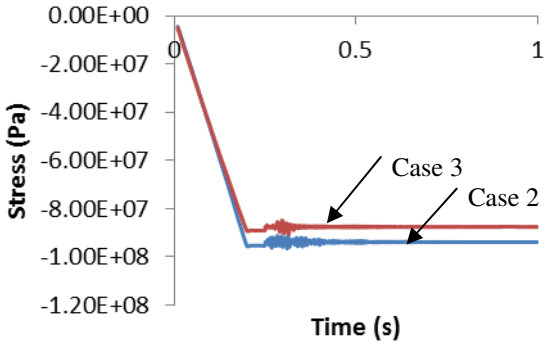

d) Inner Chord Member - Cross-Section 1006 (Bottom)

Figure 3.10. Stress time history at the top and bottom of various inner frame members' cross-section for temperature cases 2 and 3. a) Cross-section 1008 (Top); b) Cross-section 1008(Bottom); c) Cross-section 1006 (Top); and d) Cross-section 1006 (Bottom).

3.5 CONCLUSION

A 3-D frame-membrane lunar structure is subjected to internal pressure, two temperature extremes, and impact loading and analyzed to find the frequencies and static and dynamic responses.

The frequency analysis shows that the addition of the membrane to the frame dramatically increases the frequencies of the structure. However, pressurizing the membrane only leads to a slight increase in the frequencies in comparison to the unpressurized membrane case. When comparing the temperature extremes, the maximum external temperature of 123°C causes a small increase in the frequencies compared to the room temperature case. The minimum external temperature of -233°C though dramatically reduces the frequencies.

The applied temperature and internal pressure load causes substantial static displacements and stresses of the structure. For the internal pressurized case with room temperature loads (load case 3-1), there is static prestressing of the inner chords and membrane, but not for the outer chords. For the day and night temperature cases (load cases 3-2 and 3-3), a static stress is present for all chords and membrane. For all three temperature cases (load cases 3-1, 3-2, and 3-3), static displacement is seen in all chord members and the membrane.

In case of dynamic analysis under impact force on a midspan of a frame member, the dynamic response is primarily only seen at or near the point of impact. Away from the point of impact, the displacement and stress results are primarily a cause of the static loads. The dynamic displacement and stress oscillate about their initial static counterparts. Also, the external daytime and nighttime temperatures (load cases 3-2 and

3-3) are seen to reduce the maximum amplitude of oscillation and to reduce the oscillation to static value faster than with the room temperature case (load case 3-1). Furthermore, the reduction of the dynamic response is greatest for the coldest temperature case (load case 3-3).

The maximum total displacement and stress occurs in temperature case when the outside is coldest (lunar night, load case 3-3). The maximum total displacement occurs at the membrane and the maximum total stress occurs in an outer chord member. Both the maximum displacement and stress are a result of mainly the static application of the internal pressure load and temperature.

The results from this study show that the prestressing effects from the internal pressurization and temperature are critical parameters to consider while designing frame-membrane pressurized structural system. Both affect the initial static displacement and stress tremendously. The effects of lunar night (coldest temperature outside the habitat) are more critical in design.

3.6 REFERENCES

AFRL, "Inflatable Structures Can Reduce Logistics And Setup Time For Bare-based Operations," *Air Force Research Laboratory, Materials & Manufacturing Directorate*, Dayton, OH, 2007. http://www.ml.afrl.af.mil/stories/mlq-01124.html (date referred 09April2007).

ANSYS, User's *Guide, Release 12.0*, ANSYS Inc., Pennsylvania, USA, 2009.

ASCE Task Committee, "Overview of Existing Lunar Base Structural Concepts," *J. of Aerospace Engineering*, Vol. 5, No. 2, 1992, pp. 159-174.

Batelle Memorial Institute, "Metallic Materials Development and Standardization," MMPDS-04, Federal Aviation Commission, 2009.

Bedri, R. and Al-Nais, M.O., "Prestressed Modal Analysis Using Finite Element Package ANSYS," *Numerical Analysis and Its Applications*, *Third International Conference*, 3401/2005, Revised Selected Papers, NAA 2004, 2005, pp. 171-178.

Benaroya, H., Bernold, L., and Chua K., "Engineering, Design and Construction of Lunar Bases." *J. of Aerospace Engineering*, Vol. 15, No. 2, 2002, pp. 33-45.

Benaroya, H., and Ettouney, M., "Framework for Evaluation of Lunar Base Structural Concepts," J. *of Aerospace Engineering*, Vol. 5, No. 2, 1992, pp.187-198.

Castellano, A. J., Caltagirone, J. P., Sock, F. E., Dobbs, N., "Structures to Resist the Effects of Accidental Explosions," TM 5-1300, Departments of the Army, Navy, and the Air Force, Alexandria, VA, USA, 1990.

Chow, P. Y., Lin, T. Y., "Structures for the Moon," *Engineering, Construction and Operations in Space, Procs. of Space 88*, 1988, pp. 362–374.

Dayal, V., "Conceptual Design of Unpressurized Shelters on Lunar Surface." *J. of Aerospace Engineering*, Vol. 22, No. 4, 2009, pp. 396-402.

Donadon, M.V., Almeida, S.F.M. and de Faria, A.R., "Stiffening effects on the natural frequencies of laminated plates with piezoelectric actuators," *Composites: Part B*, Vol. 33, 2002, pp. 335–342.

Drake, R. M., and Richter, P. J., "Design and Construction of a Lunar Outpost Assembly Facility," *Engineering, Construction and Operations in Space II, Procs. of Space 90*, Vol. 1, 1990, pp. 449- 457.

Goldsmith, W., *Impact*, Courier Dover Publications, London, U.K, 1980, pp. 55 - 65.

Heiken, G., Vaniman, D. and French B. M., eds., *The Lunar Source Book*, Cambridge University Press, Cambridge, England, U.K., 1991.

Kapoor, H., Chun, S., Kapania, R. K., and Plaut, R. H., "Nonlinear Dynamic Response of Highly Flexible Membrane Structures to Blast Load." *Procs.*, *3rd International Conference on Structural Stability and Dynamics,* 2005, 6 pages.

"Kevlar Aramid Fiber," Dupont, Technical Guide, 2011. http://www2.dupont.com/Kevlar/en_US/assets/ downloads/KEVLAR_Technical_Guide.pdf (Accessed 15 March 2011).

Land, P., "Lunar Base Design," *In Lunar Bases and Space Activities of the 21st century* (W. W. Mendell, ed.), Lunar and Planetary Institute, Houston, Texas, 1985, pp. 363-373.

Lin, T. D., Senseney, J. A., Arp, L. D., and Lindbergh, C., "Concrete Lunar Base Investigations," *Engineering, Construction and Operations in Space, Proceedings of Space-88*, 1988, pp. 148-156.

Maier-Schneider, D., Maibach, J., Obermeier, E., "A new analytical solution for the load-deflection of square membranes," *J. of Microelectromechanical Systems,* Vol. 4, No. 4, 1995, pp. 238-241.

Malla, R., "Earthbound Civil Engineering Experience for Space Applications," *J. of Aerospace Engineering*, Vol. 4, No. 4, 1991, pp. 330-346.

Malla, R., Adib-Jahromi, H., and Accorsi, M.L., "A Simplified Design Method for Braced Double Skinned Structure in Lunar Application," *J. of Aerospace Engineering*, Vol. 8, No. 4, 1995, 189-195.

Malla, R. B. and Chaudhuri, D., "Analysis of a 3D Frame – Membrane structure for Lunar Base," *Engineering, Construction and Operations in Challenging Environments, Procs., Earth & Space 2006 Conference,* ASCE, Reston, VA , 2006.

Malla, R. B. and Chaudhuri, D., "Dynamic Analysis of a 3-D Frame-Membrane Lunar Structure Subjected to Impact," *Engineering, Science, Construction and Operations in Challenging Environments, Procs., Earth & Space 2008 Conf.*, ASCE, Reston, VA, 2008.

Malla, R. B. and Chaudhuri, D., "Effects of Pressurization on Frequencies and Impact response of Frame-Membrane Composite Structure," *Procs., ASCE Engineering Mechanics Division (EMD) conference*, ASCE, Blacksburg, VA, 2007.

Quigley, C., Horak, K., Devine, R., Dagher, H., Parent, L., Landis, E., Goslin, K, and Cassidy, E., "The Development and Evaluation of Modular Ballistic Panels for Fabric Shelters," *25th Army Science Conf.*, US Army, Orlando, Florida, 2006.

Rinehart, J.S., "Basic Design Criteria for Moon Building," *J. of the British Interplanetary Soc*., Vol. 17, 1959, pp. 126-129.

Ruess, F., Schaenzlin, J., and Benaroya, H., "Structural Design of a Lunar Habitat," *J. of Aerospace Engineering*, Vol. 19, No. 3, 2006, 133-157.

Sadeh, W. Z., and Criswell, M. E., "A generic inflatable structure for a lunar/martian base," *Engineering, Construction, and Operations in Space, Procs., SPACE 94 conf.,* ASCE*,* Reston, Va., 1994, pp. 1146–1156.

Sherwood, B., and Toups, L., "Technical Issues for Lunar Base Structures," J. *of Aerospace Engineering*, Vol. 5, No. 2, 1992, pp. 175-186.

Sowerby, P.L., "Structural Problems of the Lunar Base," *J. of the British Interplanetary Soc*., Vol. 13, 1954, pp. 36-40.

Szilard, R., "Structures for the Moon," *Civil Engineering,* Vol. 29, 1959, pp. 46-49.

Vanderbilt, M. D., Criswell, M. E., Sadeh, W. Z., "Structures for a lunar base," *Engineering, Construction and Operations in Space, Procs. of Space 88*, 1988, pp. 352- 361.

Walker, J. D. "Turning Bullets into Baseballs," *Technology Today*®. Southwest Research Institute, San Antonio, TX, 1998.

Wilde, P. D. and Draper, C., "Aircraft Protection Standards and Implementation Guidelines for Range Safety," *48th AIAA Aerospace Science Meeting Including the New Horizon Forum and Aerospace Exposition*, AIAA, Orlando, Florida, 2010.

CHAPTER 4

FREQUENCIES OF A SINGLE FRAME-MEMBRANE PANEL AND CALCULATION OF IMPACT FORCE ON A SINGLE BEAM USING HERTZ CONTACT THEORY

Abstract

In the research, four frame-membrane panels assembled in an arch shape has been proposed as a lunar habitat. However, a lunar structure may be designed using frame-membrane panels in an orientation different than the arch shape. Thus, the frequency of a single panel is presented in the following chapter. ANSYS frequency analysis is performed at extreme lunar temperatures (+123°C and -233°C) with the membrane internally pressurized to one atmosphere (96.5 kPa) to sustain life. Also, the added mass of regolith (which the frame is filled with for temperature and radiation shielding) is included. Results show that the added mass of regolith and the nighttime temperature lower the frequency, the daytime temperature increases the frequency, and the internal pressure has minimal effect on the frequency. This chapter also presents and verifies the impact analysis of a single beam using an in-house finite element code (Timoshenko, 1913) . This code uses Hertz Contact Theory to calculate the impact force function and deflection of the panel. It is more accurate and versatile than approximate method in Chapters 2 and 3, since it includes the displacement of the whole panel during the initial impact (not just the impacted member as in Chapters 2 and 3) and is applicable in locations other that the midspan of the member (unlike Chapters 2 and 3).

4.1 INTRODUCTION

Previous Chapters 2 and 3 examined the full frame-membrane lunar habitat. The structure is composed of four modular panels assembled in an arch shape. This structure has the advantages of being lightweight, easily assembled, and provides a large livable space, while still being very strong. However, it is possible that NASA may create a frame-membrane lunar structure that is not in an arch shape. The modular panels could be assembled into various other shaped structures including triangular, rectangular, and even pentagonal configurations.

Therefore, Chapter 4 presents the frequency and impact analysis of a single frame-membrane panel. The frequency analysis takes into account the effect of all criterion examined in Chapters 2 and 3. The panel is examined at lunar night temperature (-233°C), lunar day temperature (123°C), and baseline room temperature (21°C). The frequencies are presented with and without internal pressurization as well as with and without added mass of the regolith cover. Also, the frequency of the frame without the membrane attached is presented.

Additionally, the impact analysis of the single frame is presented. Chapters 2 and 3 use a force function that is found by looking at the impact of a simply supported beam struck at the midspan. The forcing function is not truly applicable at locations along the beam other than the midspan and do not take into account the flexibility of the rest of the structure. In this chapter, a finite element program coded in Matlab is presented. This program takes into account impact at locations other than the midpoint of the beam and included the rest of the panels flexibility. The code is verified by comparing it to

analytical work done by Timoshenko (1913) and then compared to the forcing function in Chapters 2 and 3.

4.2 PROPOSED STRUCTURE

The lunar habitat structure presented in Chapters 2 and 3 consisted of four connected 3-D aluminum frame modules with a 0.0075 m thick Kevlar membrane attached to the bottom of the panel (Figure 4.1). In Chapter 4, only a single panel is studied. Figure 4.1 parts (a), (b), and (d) shows a top view of the panel, a three-dimensional view of the panel, and a side view of the panel, respectively. The panel is 4.2 m x 4.2 m on the bottom, 5.6 m x 5.6 m on the top, and has a depth of 1.5 meters. The module is made up of 40 outer chords and 24 inner chords, each of length 1.4 m, and 64

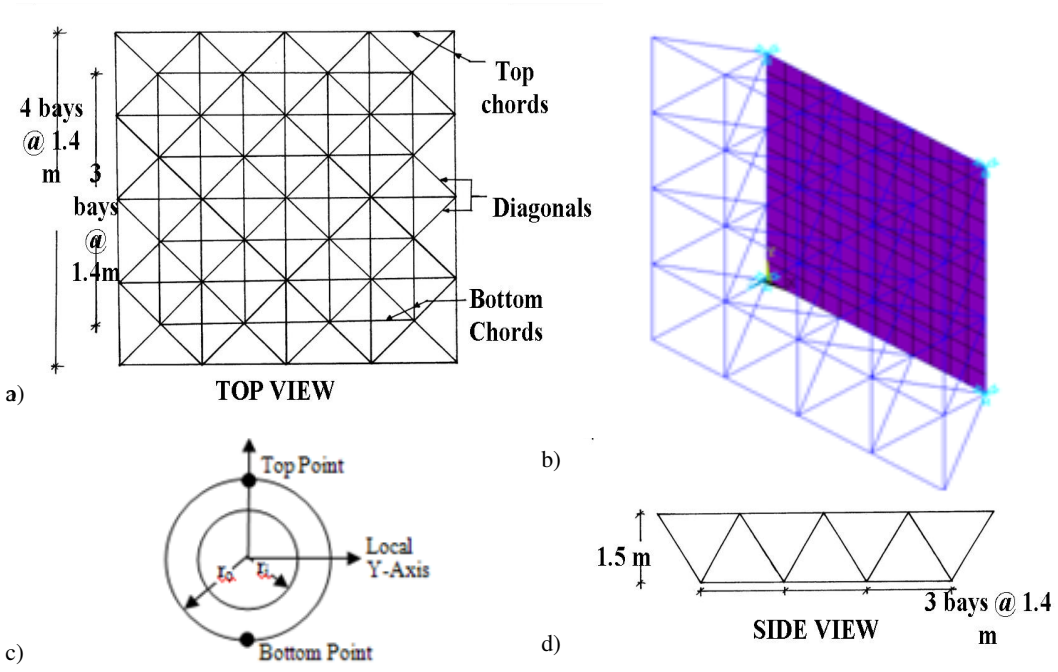

Figure 4.1. Single panel structure. a) Top view; b) 3-D view; c) Frame member cross-section with top and bottom of cross section marked; and d) Side view.

diagonal members, each 1.8 m long.

Each frame member is made of 2014-T6 aluminum and has an outer radius, r_o, of 0.0375 m and an inner radius, r_i, of 0.02 m (See Figure 4.1(c)). The structural parameters and material properties are presented in Table 4.1. As with previous Chapters, material properties were assumed to be constant at all temperatures, because the purpose of this paper is to examine the effects of temperature on the structural prestressing (not the material properties) and the change in properties with respect to the temperature range considered here is not significant. For aluminum (2014-T6) exposed to the extreme temperatures for 1,000 hours, the yield strength ranges from 476 MPa (at -233°C) to 377 MPa (+123°C) and Young's Modulus ranges from 82.7 GPa (-233°C) to 71 GPa (+123°C) (Batelle Memorial Institute, 2009). The values for Poisson's ratio (0.33) and density (2800 kg/m^3) are constant for this temperature range (Batelle Memorial Institute, 2009). For Kevlar exposed to the temperatures for 1,000 hours, the yield strength varies from 2942 GPa (-233°C) to 2905 GPa (+123°C), and Young's Modulus varies from 72.5 GPa (-233°C) to 67.4 GPa (+123°C), the density range is 1498 kg/m^3 (-233°C) to 1411 kg/m^3 (+123°C) (Dupont, 2011). The Poisson's ratio (0.35) is constant for the temperature range (Dupont, 2011).

Table 4.1. Structural dimensions, material properties at normal temperature, and finite element model information.

Parameter	Membrane	Frame
(A) Frame-Membrane Structure:		
Material Used	Kevlar	2014-T6 Aluminum
Young's Modulus[21, 22]	70.5 GPa	72.5 GPa
Density[21, 22]	1440 kg/m^3	2800 kg/m^3
Poisson's Ratio[21, 22]	0.35	0.3
Thickness/ Cross-Sectional Area	0.0075 m	0.00316 m^2
Yield Strength[21, 22]	2920 MPa	410 MPa
Coefficient of Thermal Expansion[21, 22]	-3.96E-06 m/m	23E-06 m/m

Additionally, the frame is pinned at the bottom four corners as shown in Figure 4.1(b). This boundary condition is meant to simulate the connection between modules and the module and the regolith. The bottom of the panel is pressurized to 96.5 kPa (14 psi) and set at room temperature (21°C), since the bottom of the panel would be on the inside of the structure.

4.3 ANALYSIS METHODOLOGY

Membrane structures are expected to undergo significant amount of stress stiffening due to applied pressurization and one must consider the stress state of the system during its service life for dynamic analysis (Bedri and Al-Nais, 2005). The frame is also subjected to the internal pressurization load as well as thermal loads and thus, it too can also undergo stress stiffening. The stress state influences the values of the stiffness matrix, and can therefore change the natural frequencies (Donadson et al., 2002). As a consequence of these factors, the dynamic response of the system will be affected.

The equation of motion of a structure subjected to an external excitation is given by

$$[M]\{\ddot{\delta}\} + [C]\{\dot{\delta}\} + [K + K_G]\{\delta\} = \{P\} \tag{4.1}$$

where *[K]* is the stiffness matrix, $[K_G]$ is the geometric stiffness matrix, *[M]* is the mass matrix, *[C]* is the damping matrix, *{P}* is the external force applied, which may include the impact force, $\{\delta\}$ is the nodal degree of freedom, and a dot above a character is the

derivative with respect to time. The $[K_G]$ matrix will be augmented/modified initially to account for prestress due to application of internal pressurization load and thermal load.

Restricting the study to undamped case, the above equation reduces to

$$[M]\{\ddot{\delta}\} + [K + K_G]\{\delta\} = \{P\} \tag{4.2}$$

4.3.1 Formulation of the Frequency Problem

By setting $\{P\} = 0$ in equation (4.2) and considering the free vibration motion as a simple harmonic,

$$\{\delta(t)\} = \{\delta_0\}\sin(\omega t + \phi) \tag{4.3}$$

where t is the time, $\{\delta_0\}$ is the shape of the system (which does not change with time; only the amplitude varies), ω is the natural frequency of the structure, and φ is the phase angle, the equation of motion can be expressed in the form of the eigenvalue problem as given below

$$\left([K + K_G] - \omega^2[M]\right)\{\delta_0\} = \{0\} \tag{4.4}$$

From equation (4.4), the characteristic frequency equation can be formed and is given by

$$\left|[M]^{-1}[K + K_G] - \omega^2[I]\right| = 0 \tag{4.5}$$

Where $[I]$ is the identity matrix. Equation (4.5) is used to compute the natural frequencies of the structure.

4.3.2 Solution of the Frequency Problem

Table 4.2. Loading cases used in analysis

Structural Case	Temperature Case	Load Case	Internal Temperature (°C)	External Temperature (°C)	Includes 3-D Frame	Includes Membrane	Includes Internal Pressure	Includes Added Regolith Mass
1	1	1-1	21	21	Yes	No	No	No
1	2	1-2	21	123	Yes	No	No	No
1	3	1-3	21	-233	Yes	No	No	No
2	1	2-1	21	21	Yes	Yes	No	No
2	2	2-2	21	123	Yes	Yes	No	No
2	3	2-3	21	-233	Yes	Yes	No	No
3	1	3-1	21	21	Yes	Yes	Yes	No
3	2	3-2	21	123	Yes	Yes	Yes	No
3	3	3-3	21	-233	Yes	Yes	Yes	No
4	1	4-1	21	21	Yes	Yes	No	Yes
4	2	4-2	21	123	Yes	Yes	No	Yes
4	3	4-3	21	-233	Yes	Yes	No	Yes
5	1	5-1	21	21	Yes	Yes	Yes	Yes
5	2	5-2	21	123	Yes	Yes	Yes	Yes
5	3	5-3	21	-233	Yes	Yes	Yes	Yes

As with Chapters 2 and 3, the finite element (FE) code ANSYS (2009) was used to solve the frequency problem. The membrane of the structure was modeled with SHELL181 elements, which has both bending and membrane stiffness capabilities. Since the membrane in the structure selected herein has a very small thickness (0.0075 m), the bending was negligible. This was verified by comparing the results from the FE analysis obtained in previous studies (Mallan and Chaudhuri, 2007, 2008) with analytical results (Maier-Schneider, 1995). BEAM4 elements with tension, compression, torsion, and bending capabilities were used to model the frame members. Both elements are 3-D

elements and have stress stiffening and large deflection capabilities. Table 4.1 shows the parameters used for the FE model.

The frequency analysis was performed on a total of 15 different cases (See Table 4.2). There are five structural cases: (a) the frame only (structural case 1); (b) the full frame-membrane structure without internal pressure and without added mass of regolith (structural case 2); (c) the full frame-membrane structure with internal pressure and without added mass of regolith (structural case 3); (d) the full frame-membrane structure without internal pressure and with added mass of regolith (structural case 4); and (e) the full frame-membrane structure with internal pressure and with added mass of regolith (structural case 5). The internal pressurization load of 96.5 kPa is applied on the structure's membrane pushing outward and the added regolith mass of 56129.5 kg is applied via the real constants parameter. Each of these five structural cases were performed under three temperature cases: (a) room temperature both inside and outside (both 21°C) (temperature case 1); (b) room temperature inside (21°C) and hottest external temperature (lunar day temperature of 123°C) (temperature case 2); and (c) room temperature inside (21°C) and coldest external temperature (lunar night temperature of -223°C) (temperature case 3). The internal (room) temperature was applied to the inner chords and membrane, whereas the hottest and coldest external temperatures were applied to the outer chords. The temperature varied linearly along the diagonals connecting the outer chord and inner chord.

The two prestressing loads on the structure were the internal pressure and temperature loads. In ANSYS, a stress stiffness matrix that is analogous to $[K_G]$ in equations (4.1), (4.2), (4.4), and (4.5) accounts for the stiffening effect as a result of

prestressing (ANSYS, 2009). The added mass of the regolith cover was applied as a non-structural mass equivalent to $[M_a]$ in equations (4.1), (4.2), (4.4), and (4.5). A static analysis was run with the internal pressure and temperature loads applied to determine the prestressing caused by the loads. The included prestressing option was turned on in the frequency analysis and Block Lanczos method was used to solve the eigenvalue problem in a previous section (equation (4.5)) to determine the frequencies and mode shapes. Each frame member in the FE model was divided into 10 elements and each membrane panel of size 4.2 m x 4.2 m was divided into 30 x 30 grids.

4.3.3 Formulation of the Impact Problem

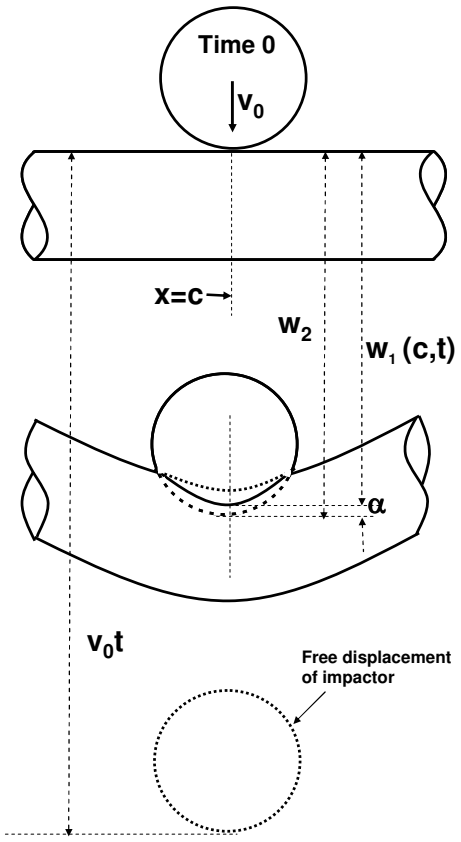

Figure 4.2. Central Transverse Impact of a Rigid Mass with a Beam

Figure 4.2 shows a simply supported beam of tubular cross section subjected to low velocity transverse projectile impact, which simulates the debris impact analyzed in previous sections. The governing equation of motion of the beam neglecting the effect of damping is:

$$[M]\{\ddot{w}_T\}+[K]\{w_T\}=\{P\},\ w_T(t=0)=0,\ \dot{w}_T(t=0)=0 \tag{4.6}$$

where:

[M]= Mass Matrix of beam element

[K]= Stiffness Matrix of beam element

$\{P\}$= External force applied (impact force)

$\{w_T\}$ = Nodal degree of freedom of target

The stiffness matrix of a three-dimensional beam element with six degrees of freedom at each node is: (Paz, 1991)

$$[K]=\begin{bmatrix}
\frac{EA}{L} & 0 & 0 & 0 & 0 & 0 & -\frac{EA}{L} & 0 & 0 & 0 & 0 & 0 \\
0 & \frac{12EI}{L^3} & 0 & 0 & 0 & \frac{6EI}{L^2} & 0 & -\frac{12EI}{L^3} & 0 & 0 & 0 & \frac{6EI}{L^2} \\
0 & 0 & \frac{12EI}{L^3} & 0 & -\frac{6EI}{L^2} & 0 & 0 & 0 & -\frac{12EI}{L^3} & 0 & -\frac{6EI}{L^2} & 0 \\
0 & 0 & 0 & \frac{GJ}{L} & 0 & 0 & 0 & 0 & 0 & -\frac{GJ}{L} & 0 & 0 \\
0 & 0 & -\frac{6EI}{L^2} & 0 & \frac{4EI}{L} & 0 & 0 & 0 & \frac{6EI}{L^2} & 0 & \frac{2EI}{L} & 0 \\
0 & \frac{6EI}{L^2} & 0 & 0 & 0 & \frac{4EI}{L} & 0 & -\frac{6EI}{L^2} & 0 & 0 & 0 & \frac{2EI}{L} \\
-\frac{EA}{L} & 0 & 0 & 0 & 0 & 0 & \frac{EA}{L} & 0 & 0 & 0 & 0 & 0 \\
0 & -\frac{12EI}{L^3} & 0 & 0 & 0 & -\frac{6EI}{L^2} & 0 & \frac{12EI}{L^3} & 0 & 0 & 0 & -\frac{6EI}{L^2} \\
0 & 0 & -\frac{12EI}{L^3} & 0 & \frac{6EI}{L^2} & 0 & 0 & 0 & \frac{12EI}{L^3} & 0 & \frac{6EI}{L^2} & 0 \\
0 & 0 & 0 & -\frac{GJ}{L} & 0 & 0 & 0 & 0 & 0 & \frac{GJ}{L} & 0 & 0 \\
0 & 0 & -\frac{6EI}{L^2} & 0 & \frac{2EI}{L} & 0 & 0 & 0 & \frac{6EI}{L^2} & 0 & \frac{4EI}{L} & 0 \\
0 & \frac{6EI}{L^2} & 0 & 0 & 0 & \frac{2EI}{L^2} & 0 & -\frac{6EI}{L^2} & .0 & 0 & 0 & \frac{4EI}{L}
\end{bmatrix} \tag{4.7}$$

where:

G = Shear modulus of beam element

E = Modulus of elasticity of beam material

I = Moment of inertia of beam

J = Polar moment of inertia of beam

L = Length of beam element

Consistent mass matrix used for formulation of the beam element is:

$$[M]=\frac{\overline{m}L}{420}\begin{bmatrix}
140 & 0 & 0 & 0 & 0 & 0 & 70 & 0 & 0 & 0 & 0 & 0 \\
0 & 156 & 0 & 0 & 0 & 22L & 0 & 54 & 0 & 0 & 0 & -13L \\
0 & 0 & 156 & 0 & -22L & 0 & 0 & 0 & 54 & 0 & 13L & 0 \\
0 & 0 & 0 & \frac{140J}{A} & 0 & 0 & 0 & 0 & 0 & \frac{70J}{A} & 0 & 0 \\
0 & 0 & -22L & 0 & 4L^2 & 0 & 0 & 0 & -13L & 0 & -3L^2 & 0 \\
0 & 22L & 0 & 0 & 0 & 4L^2 & 0 & 13L & 0 & 0 & 0 & -3L^2 \\
70 & 0 & 0 & 0 & 0 & 0 & 140 & 0 & 0 & 0 & 0 & 0 \\
0 & 54 & 0 & 0 & 0 & 13L & 0 & 156 & 0 & 0 & 0 & -22L \\
0 & 0 & 54 & 0 & -13L & 0 & 0 & 0 & 156 & 0 & 22L & 0 \\
0 & 0 & 0 & \frac{70J}{A} & 0 & 0 & 0 & 0 & 0 & \frac{140J}{A} & 0 & 0 \\
0 & 0 & 13L & 0 & -3L^2 & 0 & 0 & 0 & 22L & 0 & 4L^2 & 0 \\
0 & -13L & 0 & 0 & 0 & -3L^2 & 0 & -22L & .0 & 0 & 0 & 4L^2
\end{bmatrix} \tag{4.8}$$

where:

$\overline{m}$ = Mass per unit length

L= Length of beam element

A = Cross-section area of the beam

The element mass and stiffness matrices for the finite elements are assembled to obtain the global matrices for the simply supported beam.

The equation of motion of the impactor can be written as:

$$m_I \ddot{w}_I + F_I(t) = 0\,,\ w_I(t=0) = 0 \text{ and } \dot{w}_I(t=0) = \mathrm{v}_0 \tag{4.9}$$

where m_I is the mass of the impactor, w_I is the displacement of the impactor, and $F_I(t)$ is the contact force between the impactor and the beam target and v_0 is the initial velocity of the projectile.

The contact force can be computed using Hertz theory of contact, which is (Goldsmith, 1960; Yang and Qiao, 2005)

$$F(t) = K_c \alpha^{\frac{3}{2}} \tag{4.10}$$

where:

K_c = Hertzian contact stiffness

α = Relative indentation between the impactor and the target

Hertzian stiffness between impactor and target is estimated by contact stiffness for a half-space: (Malekzadeh, *et. al.* 2006).

$$K_C = \frac{4}{3} E R_I^{\frac{1}{2}} \ , \ \frac{1}{E} = \frac{1-\nu_I^{\ 2}}{E_I} + \frac{1-\nu_T^{\ 2}}{E_T} \tag{4.11}$$

where R_I, ν_I and E_I are respectively the radius of curvature, Poisson's ratio and elastic modulus of the impactor and ν_T and E_T are respectively the Poisson's ratio and the elastic modulus of the target.

Equations (4.6), (4.9), and (4.10) can be combined to form the following equation.

$$F(t) = K_c (w_I - w_T(x_c, y_c, t))^{\frac{3}{2}} \tag{4.12}$$

where $w_T(x_c, y_c, t)$ is the displacement of the beam at the point of impact.

4.3.4 Solution of the Impact Problem

By numerically integrating equations (4.6) and (4.9), the indentation, α, can be computed and equation (4.12) can be solved for the contact forcing function. Displacement of the projectile and beam can be computed using the Newmark-beta method. The algorithm for a 10 element beam struck by a rigid projectile at any node is given as follows.

A. Initial calculations:

i. Form stiffness matrix K, mass matrix M and damping matrix C

ii. Input initial displacement , U , velocity, $\dot{U}$, and acceleration, $\ddot{U}$, for the beam and impactor

iii. Select time step Δt and parameter α and δ and calculate integration constants :

$\delta \geq 0.50,\ \alpha \geq 0.25(0.5+\delta)^2$

The Matlab code considers δ=1/2 and α=1/4.

$$a_o = \frac{1}{\alpha \Delta t^2},\ a_1 = \frac{\delta}{\alpha \Delta t},\ a_2 = \frac{1}{\alpha \Delta t},\ a_3 = \frac{1}{2\alpha} - 1,\ a_4 = \frac{\delta}{\alpha} - 1,\ a_5 = \frac{\Delta t}{2}\left(\frac{\delta}{\alpha} - 2\right),$$

$$a_6 = \Delta t(1-\delta),\ a_7 = \delta \Delta t$$

(4.13)

iv. Form effective stiffness matrix

$$\hat{K}:\ \hat{K} = K + \alpha_0 M + \alpha_1 C \tag{4.14}$$

B. For each time step:

i. Calculate effective force at the time t+Δt

$$^{t+\Delta t}\hat{R} = ^{t+\Delta t} R + M(a_0\,{}^{t}U + a_2\,{}^{t}\dot{U} + a_3\,{}^{t}\ddot{U}) + C(a_1\,{}^{t}U + a_4\,{}^{t}\dot{U} + a_5\,{}^{t}\ddot{U}) \tag{4.15}$$

ii. Solve for the displacements at time t+Δt

$$\hat{K}\,^{t+\Delta t}U = ^{t+\Delta t}\hat{R} \tag{4.16}$$

iii. Calculate accelerations and velocities at time t+Δt

$$^{t+\Delta t}\ddot{U} = a_0(^{t+\Delta t}U - {}^{t}U) - a_2\,{}^{t}\dot{U} - a_3\,{}^{t}\ddot{U}$$

$$^{t+\Delta t}\dot{U} = {}^{t}\dot{U} + a_6\,{}^{t}\ddot{U} + a_7\,{}^{t+\Delta t}\ddot{U} \tag{4.17}$$

A Matlab program was written to solve the impact problem and a flowchart describing the code is presented below in Figure 4.3. The Matlab code is presented in APPENDIX A: Matlab Coding for Evaluation of Impact Force on a Simply Supported Beam.

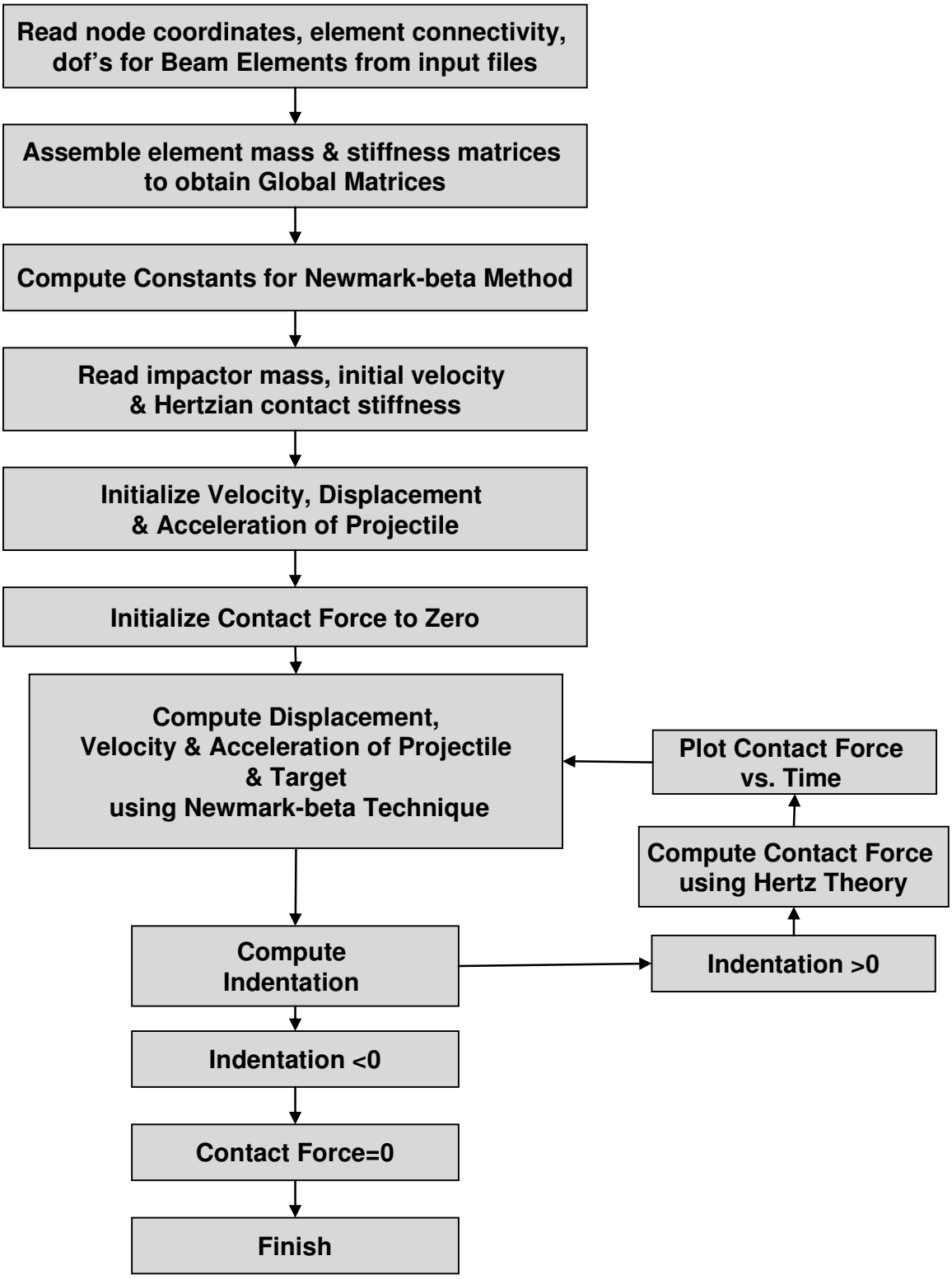

Figure 4.3. Flowchart of Algorithm for Impact Analysis of Central Transverse Impact of a Rigid Mass on a Simply Supported Beam

4.3.5 Verification of Impact Solution

In the section 4.3.3, a solution scheme for determining of contact force due to transverse impact of a rigid mass on a simply supported beam is presented. In this section, the solution method is verified with an analytical method presented in Timoshenko (1913).

In Timoshenko (1913), a simply supported rectangular beam is struck with a projectile of initial velocity, $v_{0,}$ and mass, m, at the beam's midpoint, x = c. The indentation between the projectile and striker, α, is given by

$$\alpha = w_2 - w_1(c) = v_0 t - \frac{1}{m}\int_0^t dt \int_0^t F dt - w_1(c) \tag{4.18}$$

Where w_2 is the displacement of the projectile, w_1 is the displacement of the beam at point c, and F is the contact force.

The quantity $w_1(c)$ can be given by the following equation of motion

$$w_1(c) = \frac{1}{\rho A}\sum_{i=1}^{\infty} \frac{[X_i(c)]^2}{w_i \int_0^t X_i^2 dx} \int_0^t F(\bar{\tau}) \sin\left[w_i\left(t-\bar{\tau}\right)\right] d\bar{\tau} \tag{4.19}$$

Here, the eigenfunctions, X_i, and frequencies, w_i, are determined from the equations of free vibration of the beam and depended upon the boundary conditions. Looking at the case of an elastic impact of a sphere striking the cross-section of a rectangular simply supported beam, equations (4.10), (4.18), and (4.19) combine to form:

$$\alpha = \left[\frac{F}{k_2}\right]^{2/3} = v_0 t - \frac{1}{m}\int_0^t dt \int_0^t F dt - \frac{2}{\rho A L}\sum_{i=1,3,5\ldots}^{\infty} \frac{1}{w_i}\int_0^t \mathrm{F}(\bar{\tau}) \sin w_i (t-\bar{\tau}) d\bar{\tau}$$

$$= v_0 t - \frac{1}{m}\int_0^t dt \int_0^t F dt - \frac{2L}{\rho A \pi^2 a^2}\sum_{i=1,3,5\ldots}^{\infty} \frac{1}{i^2}\int_0^t \mathrm{F}(\bar{\tau}) \sin \frac{i\pi^2 a^2}{L^2}(t-\bar{\tau}) d\bar{\tau} \qquad (4.20)$$

Where $a = \sqrt{EI/\rho A}$.

The solution of equation (4.20) was obtained by means of the small increment method where the contact force is regarded as constant during any time increment $\Delta\tau$. For the n[th] time interval $t = n\Delta\tau$, equation (4.20) could be written as

$$\alpha_n = \left[\frac{F_n}{k_2}\right]^{2/3} = v_0 n\Delta\tau - \frac{(\Delta\tau)^2}{m}\sum_{j=1}^{n} \bar{D}_{n-j+1} F_j$$
$$- \frac{2L^3}{EI\pi^4}\sum_{j=1}^{n} F_j \sum_{i=1,3,5\ldots}^{\infty} \frac{\cos\frac{i^2\pi^2 a^2}{L^2}(n-j)\Delta\tau - \cos\frac{i^2\pi^2 a^2}{L^2}(n-j+1)\Delta\tau}{i^4} \qquad (4.21)$$

where, $\Delta\tau$ was chosen as some small fraction of the fundamental period of vibration of the beam.

Timoshenko's formulation examined a 1 cm radius steel sphere impacting the midpoint of a simply supported steel beam. The projectile was travelling at an initial velocity of 1 cm/s and the beam was 1 cm x 1cm x 15.35 cm. Comparing his analytical results with the results from the Matlab coding presented in section 5.3.3, it is seen that the results match well (Figure 5.4). The Matlab code is seen to have a slightly longer duration and lower maximum force than Timoshenko (1913). The percent error is 15%

for the duration and 5.7% for the maximum force. Additionally, the impulses match within a hundredth of a percent.

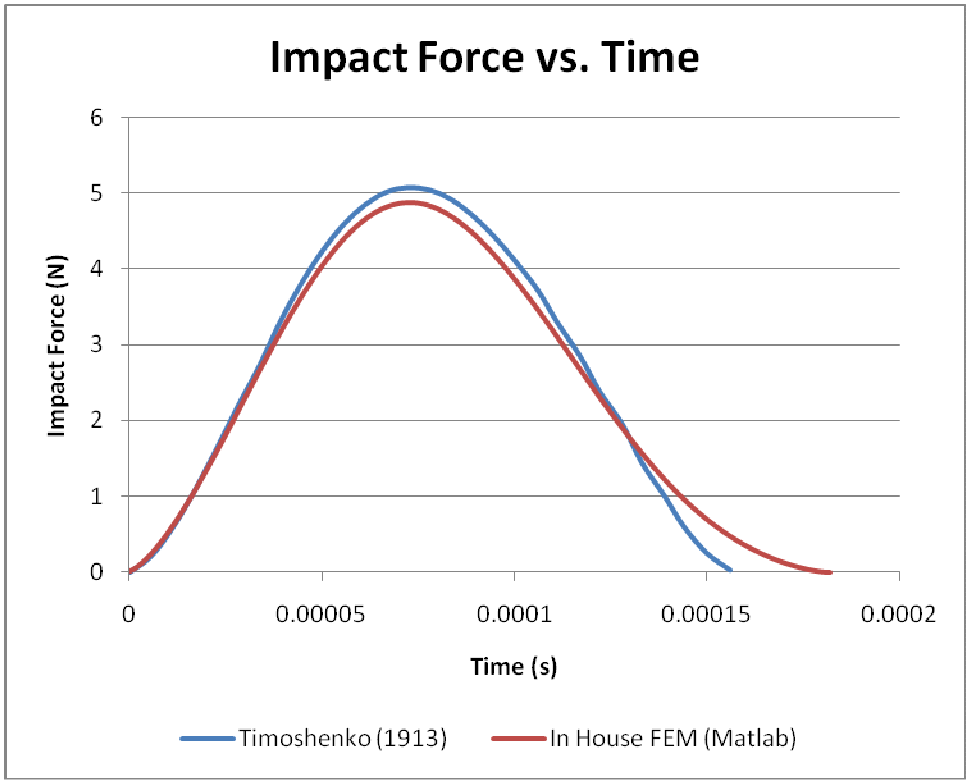

Figure 4.4. Impact forcing function using timoshenko's theoretical work and the in house finite element model (FEM, Matlab).

4.4 RESULTS AND DISCUSSION

4.4.1 Frequency Results and Discussion

Table 4.3 presents the first twenty frequencies of the single panel under the 15 load cases listed in Table 4.2. Figure 4.5 graphs the fundamental frequencies of all load cases.

The results show that the unpressurized membrane (no pressure and no added mass; load cases 2-1, 2-2, and 2-3) to the frame alone increases the frequency (load cases 1-1, 1-2, and 1-3) significantly regardless of the outside temperature. Pressurizing the membrane and having no added regolith mass (load cases 3-1, 3-2, and 3-3) is seen to reduce the frequency compared to no pressure and no added mass case. This is seen at all three temperatures and the reduction is most significant during the lunar nighttime case (-233°C). The no internal pressure and no added regolith mass cases (load cases 4-1, 4-2, and 4-3) are seen to have a frequency far lower than the no pressure and no added regolith mass cases (load cases 2-1, 2-2, and 2-3) at all three outside temperatures. The frame panel's frequency during the pressure and added mass case (load cases 5-1, 5-2, and 5-3) are seen to be slightly higher than the no internal pressure with the added mass of the regolith cover load case (load cases 4-1, 4-2, and 4-3) regardless of the temperature case. These frequencies for the pressure and added mass cases are still far lower than the no pressure and no added mass cases. Looking at the different temperature cases, it is seen that regardless of the structural cases the daytime temperature (load cases 1-2, 2-2, 3-2, 4-2, and 5-2) has a slightly higher temperature than the room temperature cases (load cases 1-1, 2-1, 3-1, 4-1, and 5-1). Conversely, the nighttime temperature case (load cases 1-3, 2-3, 3-3, 4-3, and 5-3) have drastically lower frequencies than the room temperature cases.

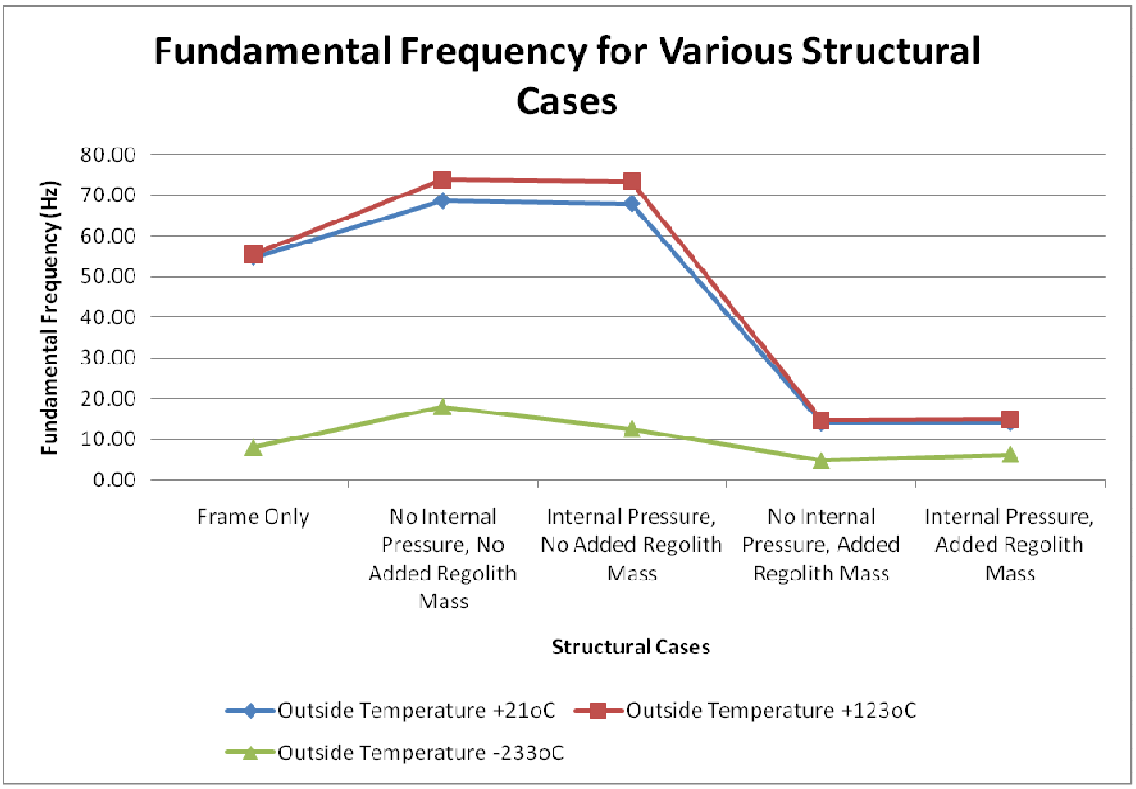

Figure 4.5. Fundamental frequencies of the single panel structure for various load cases.

Table 4.3. Frequencies of the single panel for various load cases.

Mode Number	Load Case														
	1-1	2-1	3-1	4-1	5-1	1-2	2-2	3-2	4-2	5-2	1-3	2-3	3-3	4-3	5-3
1	54.8	68.6	67.9	14.0	14.2	55.5	73.9	73.4	14.7	14.9	8.1	18.0	12.6	4.8	6.3
2	54.8	68.6	67.9	14.0	14.2	55.5	73.9	73.4	15.0	14.9	8.1	18.0	12.6	5.8	6.5
3	72.6	73.2	72.1	14.2	14.4	74.0	82.2	81.4	15.0	15.6	9.3	23.5	28.6	6.4	6.5
4	73.6	75.1	73.6	14.5	15.0	75.0	82.8	82.1	15.9	15.6	9.3	28.3	31.0	6.8	6.9
5	74.4	75.5	75.3	14.8	15.0	75.6	83.9	83.0	16.0	16.3	13.1	31.2	31.6	7.0	6.9
6	74.5	76.5	75.3	15.1	15.5	76.3	84.3	84.4	16.5	16.3	13.6	32.2	31.6	7.0	7.9
7	74.5	76.5	75.6	15.1	15.6	76.3	85.5	84.6	16.5	17.2	25.6	34.0	32.4	8.3	7.9
8	75.4	77.3	76.0	15.5	15.6	76.7	85.5	84.6	17.1	17.2	25.6	34.0	33.4	8.3	8.2
9	76.5	77.5	76.4	15.7	15.7	78.1	85.8	85.4	17.2	17.2	27.5	40.6	35.5	8.5	8.2
10	76.5	77.5	76.4	15.7	15.9	78.1	86.6	85.4	17.2	17.2	27.5	40.6	38.3	8.5	9.1
11	77.2	78.2	76.9	15.8	16.0	78.8	86.6	85.5	17.4	17.2	33.3	41.6	38.3	8.8	9.1
12	77.5	78.2	77.8	15.9	16.4	79.5	87.3	86.7	17.4	17.4	33.9	41.6	39.6	8.9	9.3
13	78.5	79.0	78.2	16.2	16.4	80.2	88.1	86.7	17.8	17.5	34.2	42.8	40.1	9.7	9.3
14	79.1	79.0	78.9	16.7	16.5	81.1	88.1	87.2	18.0	17.6	35.6	43.3	40.1	9.7	9.4
15	79.2	79.3	78.9	16.7	16.5	81.1	88.8	87.5	18.1	17.6	39.5	47.7	41.6	9.9	9.4
16	79.2	80.1	79.3	16.8	16.8	81.1	88.8	87.5	18.1	17.7	39.5	48.1	41.6	9.9	9.9
17	79.6	80.4	79.7	16.8	17.0	81.6	88.9	87.5	18.2	17.9	50.2	48.6	42.4	10.6	10.0
18	80.9	81.2	80.0	16.8	17.0	82.6	89.8	88.7	18.2	18.1	50.2	48.7	44.4	10.7	10.4
19	81.3	81.2	80.0	16.9	17.1	83.4	89.8	89.1	18.2	18.1	52.9	50.6	44.4	10.8	10.5
20	81.3	82.2	81.3	17.0	17.1	83.4	90.1	89.1	18.3	18.2	52.9	50.6	45.2	11.0	10.6

4.4.2 Impact Force Results and Discussion

For the present section, the impact loading analyzed is that from space debris impact and impacting with the single panel structure. Like in previous Chapters 2 and 3, the FAA's airplane-debris impacts codes were used to obtain the debris mass and velocity of 1.2 kg and 240 m/s, respectively (Wilde, 2010). The projectile was considered to strike the midspan of an outer frame member of the structure. However, due to computation constraints, the impact could not be examined with the impacted member being attached to the rest of the panel. Therefore, the impacted member was simply

supported in the Matlab code, meaning its endpoints could not displace downward as it would when part of the full panel (Figure 4.6).

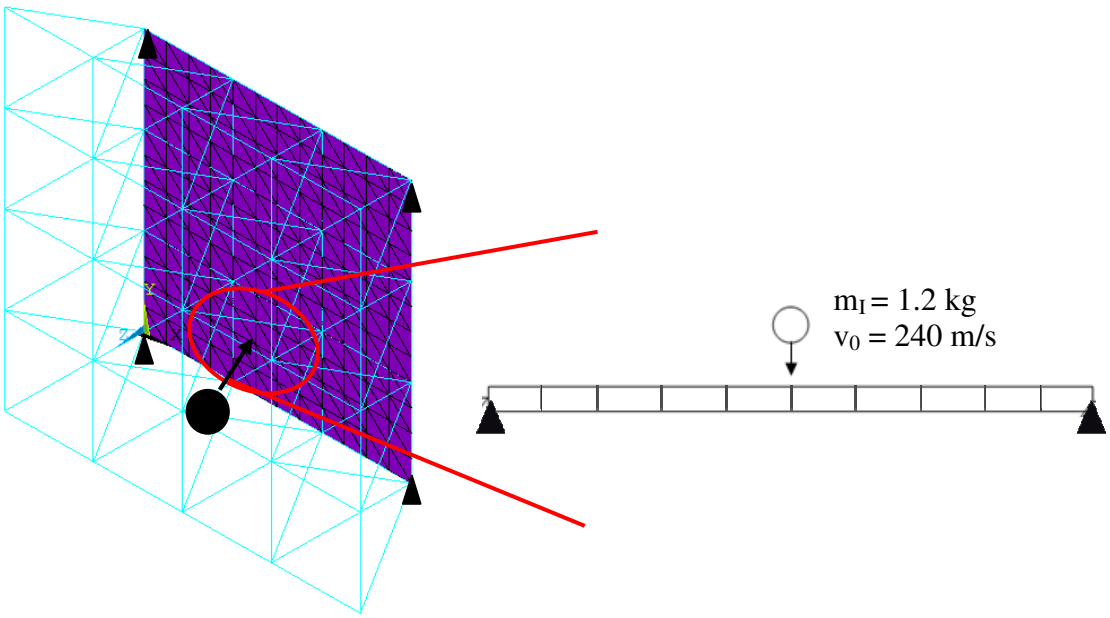

Figure 4.6. Model used for impact force evaluation on the single panel.

The impact forces from the Matlab code as well as the theoretical impact force computed in Chapters 2 and 3 are presented in Figures 4.7. The force results show that the Matlab force occurs in a much shorter duration and has a much higher maximum force than the analytical. Additionally, displacement and bending stresses at the midpoint of the beam in the Matlab code are shown in Figures 4.8 and 4.9.

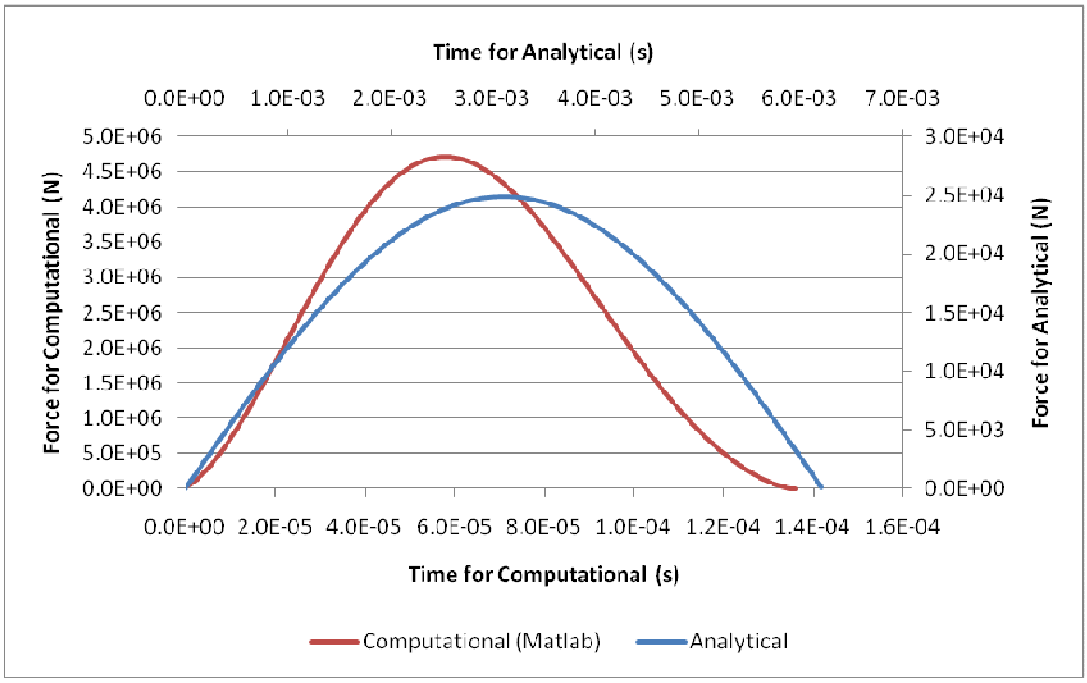

Figure 4.7. Comparison of analytical impact force (used in Chapters 2-4) and computational impact force (Matlab, Chapter 5).

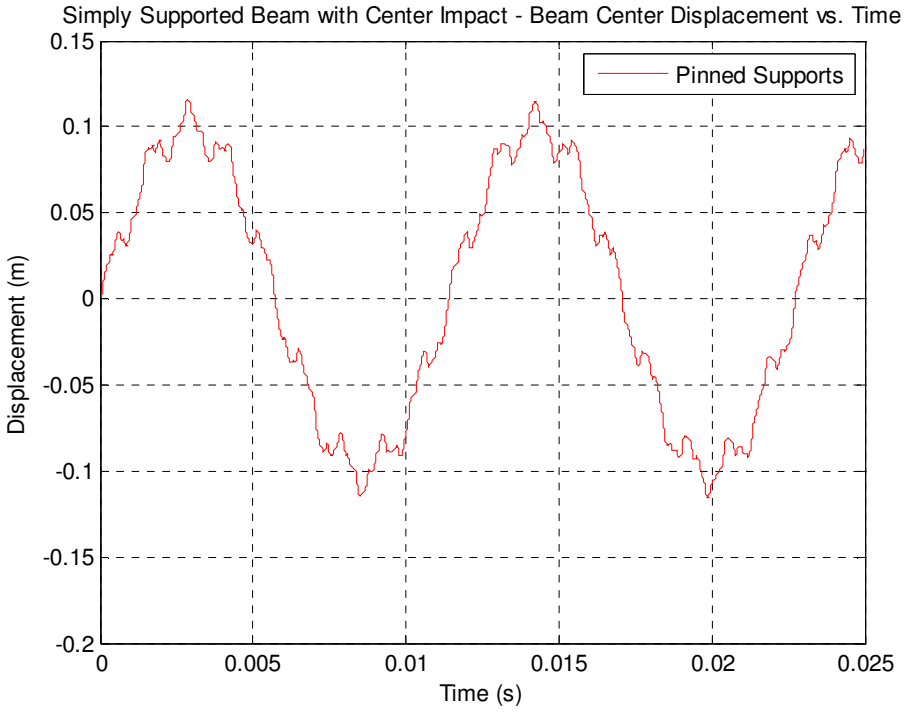

Figure 4.8. Displacement of beam's center point when subjected to impact load.

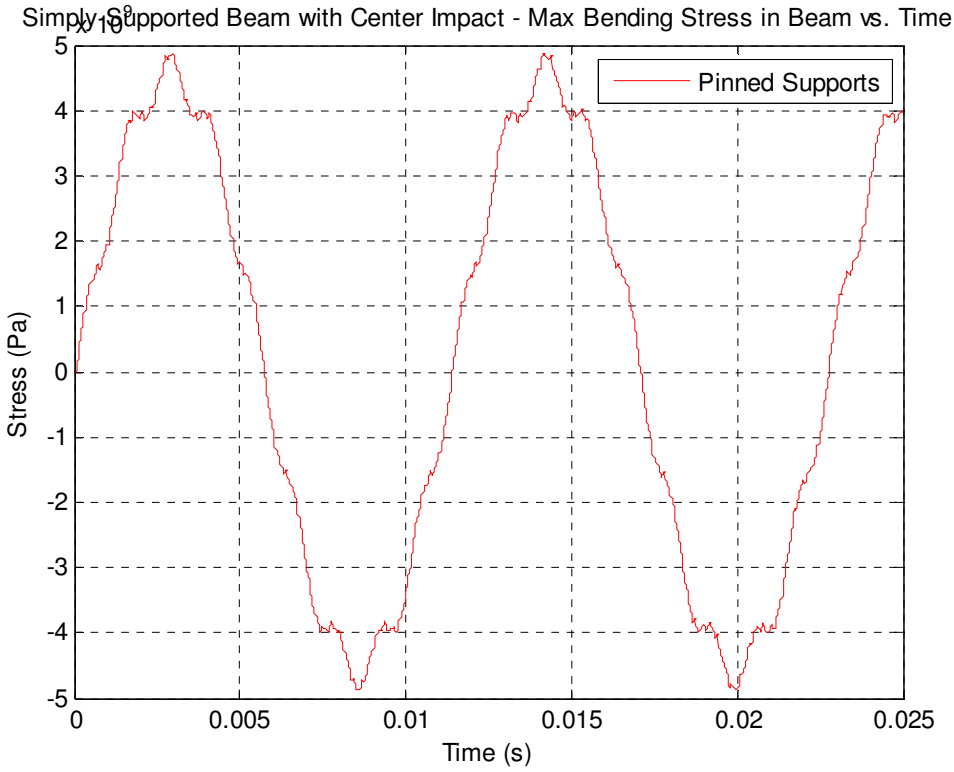

Figure 4.9. Bending of beam's center point when subjected to impact load.

4.5 CONCLUSIONS

Frequency and impact analysis were performed on a single panel of the lunar structure. The frequency was examined with and without internal pressure and added mass of regolith during the lunar temperature extremes. Due to computational constraints, the impact analysis was performed on a single simply supported beam neglect the effect that the rest of the panel would add. However, the program is capable of running the entire panel on a supercomputer.

The frequency results show the same patterns that are seen for the full structure in Chapters 2 and 3. It is seen that adding the membrane to the frame alone increases the

frequency. Additionally, the results show that pressurizing the membrane slightly increases the frequency and adding the mass of lunar regolith significantly reduces the frequency. The daytime temperature is seen to increase the frequencies a little compared to the room temperature case. The nighttime frequencies are drastically less than the room temperature frequencies.

The Matlab code used to determine the impact force was verified with Timoshenko's analytical work (1913). While Timoshenko's work and the Matlab code matched nicely, the Matlab code did not have a forcing function similar to the one used in Chapter 2 and 3. The Matlab program has the capability to determine the displacement of the beam and the stress at the beam. Additionally, the program can be used on the full single panel model, if a supercomputer was available.

CHAPTER 5

SUMMARY, CONCLUSIONS, AND RECOMMENDATION FOR THE FUTURE WORK

This research presents the structural response of an internally pressurized and regolith covered frame-membrane design subjected to impact and thermal loading. The impact loading was analytically and numerically calculated considering a moving projectile, for example space debris, hitting the midpoint of a frame member at the crest of the structure. The effects of the added mass due to the regolith cover and the stress stiffening from the internal pressurization were determined. Conclusions from the static, frequency, and dynamic nonlinear (large deformation) finite element analyses are presented in this chapter. Recommendations for future are also discussed.

5.1 CONCLUSIONS

The following covers conclusions determined based on frequency, static, and dynamic analysis presented.

- The added regolith mass and the prestressing effects from the internal pressurization and outside temperature (especially the nighttime temperature) are all critical parameters for a lunar base.
- The frequency analysis shows that the addition of the membrane to the frame dramatically increases the frequencies of the structure.
- The internal pressurization of the frame-membrane structure was found to increase the structural frequencies slightly. Conversely, the added mass of the

regolith shielding layer was found to decrease the frequencies of the system significantly.

- When comparing the frequencies due to temperature extremes, the maximum external temperature of 123°C has frequencies that are a little higher compared to the room temperature case. The lunar night temperature of -233°C though dramatically reduces the frequencies compared to the room temperature case.
- In the static analysis, the internal pressurization causes the structure to expand outward. The internal pressure is also seen to stress the inner chord members, diagonal members, and the membrane, but does not significantly stress the outer chord members. The habitat contracts a little due to the added regolith load. The added regolith mass does not significantly stress the structure.
- Both at the nighttime temperature and daytime temperature, static displacement and stresses are seen in all chord members and the membrane. The daytime temperature expands the structure and the nighttime temperature contracts the structure.
- In the dynamic analysis due to impact force on a midspan of a frame member, only at the point of impact are the dynamic displacements significant. At all other nodes, the static loads are more significant.
- Internal pressure has little effect on the dynamic displacement or stress amplitudes and periods. However, the added regolith mass increases the displacement oscillation period and reduces the displacement amplitude. Added mass also causes the stress amplitude to increase at the outer chords and decrease

at the membrane and inner chords. The stress period oscillations are increased by the added mass.

- The external daytime and nighttime temperatures are seen to reduce the maximum amplitude of oscillation and to reduce the oscillation to static value faster than with the room temperature case. The reduction of the dynamic response is greatest for the coldest temperature case.
- The maximum total (dynamic plus static) displacement and stress occurs in temperature case when the outside is coldest (lunar night) and pressure, but no added mass are applied. The maximum total displacement occurs at the membrane and the maximum total stress occurs in an outer chord member. Both the maximum displacement and stress are a result of mainly the static application of the internal pressure load and temperature.

5.2 RECOMMENDATIONS FOR FUTURE RESEARCH

This section discusses the recommendations for future research on the frame-membrane lunar structure analyzed.

- It is recommended that the impact analysis presented in Chapters 2 and 3 be carried out with the contact force determined using the Hertz contact theory (determined by the Matlab finite element code). The new force should provide more accurate results and can accurately be applied for impact occurring at places other than the midspan of a frame member.
- Different types of impact need to be examined. These include impact on the joints and membrane, hypervelocity impact, low velocity impact with much more

massive objects than 1.2 kg, and impact at multiple locations, which would simulate a meteor shower.

- The effect of regolith cover needs to be analyzed better. In the present research, only the mass of the regolith was included. However, the regolith would also absorb the impact energy and provide damping. The energy absorption would be especially important for impact, since it is likely that any debris striking the habitat would hit the regolith cover.
- When in use a lunar structure will have a significant amount of equipment, such as life support systems, communication equipment, and research computer, located inside. The effect of these equipments could be very large as they would affect the mass and the rigidity of the structure. Thus, the equipment could dramatically change the frequency and the impact response.

CHAPTER 6

REFERENCES

AFRL (2007). "Inflatable Structures Can Reduce Logistics And Setup Time For Bare-based Operations." *Air Force Research Laboratory, Materials & Manufacturing Directorate*, Dayton, OH. http://www.ml.afrl.af.mil/stories/mlq-01124.html (date referred 09April2007).

ANSYS (2009). *User's Guide, Release 12.0*, ANSYS Inc., Pennsylvania, USA, 2009.

ASCE Task Committee (1992). "Overview of Existing Lunar Base Structural Concepts." *J. of Aerospace Engineering*, 5(2), 159-174.

Barnhart, H. G. (1955). "Transverse Impact on Elastically Supported Beams," *Dissertation (Ph.D.)*, The University of California, Berkley.

Batelle Memorial Institute. (2009) "Metallic Materials Development and Standardization," MMPDS-04, Federal Aviation Commission.

Bedri, R. and Al-Nais, M.O. (2005). "Prestressed Modal Analysis Using Finite Element Package ANSYS." *Numerical Analysis and Its Applications*, Third International Conference, NAA 2004, Revised Selected Papers, 3401/2005, Springer Berlin / Heidelberg, 171-178.

Benaroya, H. and Bernold, L. (2008). "Engineering of lunar bases," *Acta Astronautica*, 62, 277-299.

Benaroya, H., Bernold, L., and Chua K. (2002). "Engineering, Design and Construction of Lunar Bases." *J. of Aerospace Engineering*, 15(2), 33-45.

Benaroya, H., and Ettouney, M. (1992). "Framework for Evaluation of Lunar Base Structural Concepts." *J. of Aerospace Engineering*, 5(2), 187-198.

Castellano, A. J., Caltagirone, J. P., Sock, F. E., Dobbs, N. (1990), "Structures to Resist the Effects of Accidental Explosions." *TM 5-1300*, Departments of the Army, Navy, and the Air Force, Alexandria, VA, USA.

Chow, P. Y., Lin, T. Y. (1988). "Structures for the Moon." *Engineering, Construction and Operations in Space- Procs. of Space 88*, 362–374.

Dayal, V. (2009). "Conceptual Design of Unpressurized Shelters on Lunar Surface." *J. of Aerospace Engineering*, 22(4), 396-402.

Donadon, M.V., Almeida, S.F.M. and de Faria, A.R. (2002). "Stiffening effects on the natural frequencies of laminated plates with piezoelectric actuators." *Composites: Part B*, **33**, 335–342.

Drake, R. M., and Richter, P. J. (1990). "Design and Construction of a Lunar Outpost Assembly Facility." *Engineering, Construction and Operations in Space II-Volume 1, Procs. of Space 90*, 449- 457.

Grandl, W. (2007). "Lunar Base 2015 Stage 1 Preliminary Design," *Acta Astronautica*, 60, 554-560.

Goldsmith, W. (1980). *Impact*, Courier Dover Publications, London, U.K.

Heiken, G., Vaniman, D. and French B. M., eds. (1991). *The Lunar Source Book*, Cambridge University Press, Cambridge, England, U.K.

John F. Kennedy Presidential Museum and Library. (1961). "Excerpt from an Address Before a Joint Session of Congress, 25 May 1961." Accession Number: TNC:200. http://www.jfklibrary.org/Asset-Viewer/xzw1gaeeTES6khED14P1Iw.aspx (Accessed on June 22, 2011).

Kapoor, H., Chun, S., Kapania, R. K., and Plaut, R. H. (2005). "Nonlinear Dynamic Response of Highly Flexible Membrane Structures to Blast Load." *Procs.*, *3rd International Conference on Structural Stability and Dynamics,* June 19-22, 2005, 6 pages.

"Kevlar Aramid Fiber," (2011) Dupont, Technical Guide. http://www2.dupont.com/Kevlar/en_US/assets/downloads/KEVLAR_Technical_Guide.pdf (Accessed 15 March 2011).

Land, P. (1985). "Lunar Base Design." *In Lunar Bases and Space Activities of the 21st century* (W. W. Mendell, ed.), Lunar and Planetary Institute, Houston, Texas, 363-373.

Lin, T. D., Senseney, J. A., Arp, L. D., and Lindbergh, C. (1988). "Concrete Lunar Base Investigations." *Engineering, Construction and Operations in Space- Proceedings of Space-88*, 148-156.

Maier-Schneider, D., Maibach, J., Obermeier, E. (1995). "A new analytical solution for the load-deflection of square membranes." J. *of Microelectromechanical Systems,* 4(4), 238-241.

Malla, R. (1991). "Earthbound Civil Engineering Experience for Space Applications." *J. of Aerospace Engineering*, 4(4), 330-346.

Malla, R., Adib-Jahromi, H., and Accorsi, M.L. (1995). "A Simplified Design Method for Braced Double Skinned Structure in Lunar Application." *J. of Aerospace Engineering*, 8(4), 189-195

Malla, R. B. and Chaudhuri, D. (2006). "Analysis of a 3D Frame – Membrane structure for Lunar Base." *Engineering, Construction and Operations in Challenging Environments (Procs., Earth & Space 2006 Conference),* ASCE, Reston, VA , March 2006, 8 pages.

Malla, R. B. and Chaudhuri, D. (2007). "Effects of Pressurization on Frequencies and Impact response of Frame-Membrane Composite Structure." *Procs., ASCE Engineering Mechanics Division (EMD) conference*, Blacksburg, VA; June, 2007, 12 pages.

Malla, R. B. and Chaudhuri, D. (2008). "Dynamic Analysis of a 3-D Frame-Membrane Lunar Structure Subjected to Impact." *Engineering, Science, Construction and Operations in Challenging Environments- Procs., Earth & Space 2008 Conf*., ASCE, Reston, VA, March, 10 pages.

NASA. (2011). "Apollo: The Apollo Missions." Yvette Smith. http://www.nasa.gov/mission_pages/apollo/ (Accessed June 24, 2011).

Quigley, C., Horak, K., Devine, R., Dagher, H., Parent, L., Landis, E., Goslin, K, and Cassidy, E. (2006). "The Development and Evaluation of Modular Ballistic Panels for Fabric Shelters." *25th Army Science Conf*., Orlando, Florida, November 27-30, 2006.

Rinehart, J.S. (1959). "Basic Design Criteria for Moon Building." *J. of the British Interplanetary Soc*., 17, 126-129.

Ruess, F., Schaenzlin, J., and Benaroya, H. (2006). "Structural Design of a Lunar Habitat." *J. of Aerospace Engineering*, 19(3), 133-157.

Sadeh, W. Z., and Criswell, M. E. (1994). "A generic inflatable structure for a lunar/martian base." *Engineering, Construction, and Operations in Space – Procs., SPACE 94 conf., ASCE,* Reston, Va., 1146–1156.

Sherwood, B., and Toups, L. (1992). "Technical Issues for Lunar Base Structures", J. *of Aerospace Engineering*, 5(2), 175-186.

Siegfried, W.H. (1999). "Lunar Base Development Missions," *Acta Astronautica*, 44, 755-767.

Sowerby, P.L. (1954). "Structural Problems of the Lunar Base." *J. of the British Interplanetary Soc*., 13, 36-40.

Szilard, R. (1959). "Structures for the Moon." *Civil Engineering,* 29, 46-49.

Timoshenko, S. P. (1913). "Zur Grage nach der Wirkung eines Stosses auf einen Balken," *Zeits. Math. Phys*., 62, 198.

Vanderbilt, M. D., Criswell, M. E., Sadeh, W. Z. (1988). "Structures for a lunar base", *Engineering, Construction and Operations in Space- Procs. of Space 88*, 352-361.

Walker, J. D. (1998). "Turning Bullets into Baseballs," *Technology Today*®. Southwest Research Institute, San Antonio, TX.

Wilde, P. D. and Draper, C. (2010). "Aircraft Protection Standards and Implementation Guidelines for Range Safety." *48th AIAA Aerospace Science Meeting Including the New Horizon Forum and Aerospace Exposition*, Orlando, Florida, January 4-7, 2010.

APPENDIX A

MATLAB CODING FOR EVALUATION OF IMPACT FORCE ON A SIMPLY SUPPORTED BEAM

The following is a finite element code created in Matlab used to compute the impact force on a simply supported beam using Hertz contact theory. The formulation of the problem solved by the program, the theory behind the program, and the verification of the program are in sections 4.3.3, 4.3.4, and 4.3.5, respectively.

```
% Global Stiffness & Mass Matrix for Beam

clear

%function[me1,me2,me3,ke1,ke2,ke3]=beam(m,I,r,E);
coordinates=load('coord_impact.txt');              % Node coordinates
member=load('elmtcon_impact.txt');                 % element
connectivity
dof=load('dof_impact.txt');                        % dofs for each node

ndof=66;                                            % total no. of dofs
(INPUT)
nel_member=size(member);                           % size of no.
elements & no. dof
nel=nel_member(1,1);                               % size of no.
elements

A=zeros(6,ndof,nel);                               % A used for
conversion to global coordinates
Mg_initial=zeros(ndof,ndof,nel);                   % initialize global
mass matrix
Kg_initial=zeros(ndof,ndof,nel);                   % initialize global
stiffness matrix

%%%%%%%%%%%%%%%%%%%%%%%%%%%%%%%%%%%%%%%%%%%%%%%%%%%%%%%%%%%%%%%%%%%%%%%%%%%%%%%%
%%%%%%%

% find corresponding nodes from element connectivity file
% find length of elements from corresponding node coordinates

for i=1:nel
   a=member(i,2);
```

```
   b=member(i,3);
   lt1=(coordinates(a,2)-coordinates(b,2));
   lt2=(coordinates(a,3)-coordinates(b,3));
   lt3=(coordinates(a,4)-coordinates(b,4));
   length(i,1)=(lt1^2+lt2^2+lt3^2)^0.5;

   %For coordinate transformation matrix
   ltxy = (lt1^2 + lt2^2)^.5;
   S1(i,1) = (coordinates(b,3)-coordinates(a,3))/ltxy;
   S2(i,1) = (coordinates(b,4)-coordinates(a,4))/length(i,1);
   C1(i,1) = (coordinates(b,2)-coordinates(a,2))/ltxy;
   C2(i,1) = ltxy/length(i,1);
end

%%%%%%%%%%%%%%%%%%%%%%%%%%%%%%%%%%%%%%%%%%%%%%%%%%%%%%%%%%%%%%%%%%%%%%%%%%%%%%%
%%%%%%%

% Input Data
% m=input('mass per unit length of element m=');   % input mass per
unit length
% I=input('moment of inertia I=');                 % input mt of
inertia
% E=input('modulus of elasticity E=');             % input modulus of
elasticity
% area=input('c/s area=');                         % input c/s area
m=8.5636;                                          % input mass per
unit length
I=1.4268e-6;                                       % input mt of
inertia
E=72500000000;                                   % input modulus of
elasticity
area=0.00316;                                        % input c/s area
G = 26e9;                                        %Shear modulus (Pa)
r_inner = .02;                                   %Inner radius (m)
r_outer = .0375;                                 %Outer radius (m)
J = pi/2*(r_outer^4 - r_inner^4);                %Polar moments of
inertia (m^4)
alpha=2.3e-5;                                        %coefficient of
thermal expansion
Temp_change = 0;                                %Change in temperature
r=(I/area)^0.5;

Q=zeros(3,3);

% Calculate Global Mass & Stiffness Matrix
for i=1:nel
    theta=member(i,4);
    S3 = sin(theta);
    C3 = cos(theta);

    T1=[C1(i,1)*C2(i,1) S1(i,1)*C2(i,1) S2(i,1);
        (-C1(i,1)*S2(i,1)*S3-S1(i,1)*C3) (-
S1(i,1)*S2(i,1)*S3+C1(i,1)*C3) S3*C2(i,1);
        (-C1(i,1)*S2(i,1)*C3-S1(i,1)*S3) (-S1(i,1)*S2(i,1)*C3-
C1(i,1)*S3) C3*C2(i,1)];
    L=[T1 Q Q Q;
```

```
       Q T1 Q Q;
       Q Q T1 Q;
       Q Q Q T1];

    %Temperature effects geometric stiffness


    % Element Mass Matrix

    me=(m*length(i,1)/420)*[140 0 0 0 0 0 70 0 0 0 0 0;
        0 156 0 0 0 22*length(i,1) 0 54 0 0 0 -13*length(i,1);
        0 0 156 0 -22*length(i,1) 0 0 0 54 0 13*length(i,1) 0;
        0 0 0 140*J/area 0 0 0 0 0 70*J/area 0 0;
        0 0 -22*length(i,1) 0 4*length(i,1)^2 0 0 0 -13*length(i,1) 0 -
3*length(i,1)^2 0;
        0 22*length(i,1) 0 0 0 4*length(i,1)^2 0 13*length(i,1) 0 0 0 -
3*length(i,1)^2;
        70 0 0 0 0 0 140 0 0 0 0 0;
        0 54 0 0 0 13*length(i,1) 0 156 0 0 0 -22*length(i,1);
        0 0 54 0 -13*length(i,1) 0 0 0 156 0 22*length(i,1) 0;
        0 0 0 70*J/area 0 0 0 0 0 140*J/area 0 0;
        0 0 13*length(i,1) 0 -3*length(i,1)^2 0 0 0 22*length(i,1) 0
4*length(i,1)^2 0;
        0 -13*length(i,1) 0 0 0 -3*length(i,1)^2 0 -22*length(i,1) 0 0
0 4*length(i,1)^2];

     % Element Stiffness Matrix

     ke_x=[E*area/length(i,1) 0 0 0 0 0 -E*area/length(i,1) 0 0 0 0 0;
         0 12*E*I/length(i,1)^3 0 0 0 6*E*I/length(i,1)^2 0 -
12*E*I/length(i,1)^3 0 0 0 6*E*I/length(i,1)^2;
         0 0 12*E*I/length(i,1)^3 0 -6*E*I/length(i,1)^2 0 0 0 -
12*E*I/length(i,1)^3 0 -6*E*I/length(i,1)^2 0;
         0 0 0 G*J/length(i,1) 0 0 0 0 0 -G*J/length(i,1) 0 0;
         0 0 -6*E*I/length(i,1)^2 0 4*E*I/length(i,1) 0 0 0
6*E*I/length(i,1)^2 0 2*E*I/length(i,1) 0;
         0 6*E*I/length(i,1)^2 0 0 0 4*E*I/length(i,1) 0 -
6*E*I/length(i,1)^2 0 0 0 2*E*I/length(i,1);
         -E*area/length(i,1) 0 0 0 0 0 E*area/length(i,1) 0 0 0 0 0;
         0 -12*E*I/length(i,1)^3 0 0 0 -6*E*I/length(i,1)^2 0
12*E*I/length(i,1)^3 0 0 0 -6*E*I/length(i,1)^2;
         0 0 -12*E*I/length(i,1)^3 0 6*E*I/length(i,1)^2 0 0 0
12*E*I/length(i,1)^3 0 6*E*I/length(i,1)^2 0;
         0 0 0 -G*J/length(i,1) 0 0 0 0 0 G*J/length(i,1) 0 0;
         0 0 -6*E*I/length(i,1)^2 0 2*E*I/length(i,1) 0 0 0
6*E*I/length(i,1)^2 0 4*E*I/length(i,1) 0;
         0 6*E*I/length(i,1)^2 0 0 0 2*E*I/length(i,1) 0 -
6*E*I/length(i,1)^2 0 0 0 4*E*I/length(i,1)];


     ke= ke_x;

     % To calculate global matrices

     a=member(i,2);
```

```
      b=member(i,3);
      d1=dof(a,2);
      d2=dof(a,3);
      d3=dof(a,4);
      d4=dof(a,5);
      d5=dof(a,6);
      d6=dof(a,7);
      d7=dof(b,2);
      d8=dof(b,3);
      d9=dof(b,4);
      d10=dof(b,5);
      d11=dof(b,6);
      d12=dof(b,7);

      A(1,d1,i)=1; A(2,d2,i)=1; A(3,d3,i)=1; A(4,d4,i)=1; A(5,d5,i)=1;
      A(6,d6,i)=1;A(7,d7,i)=1; A(8,d8,i)=1; A(9,d9,i)=1; A(10,d10,i)=1;
      A(11,d11,i)=1; A(12,d12,i)=1;
      AA(:,:,i)=A(:,:,i);

      % Coordinate Transformation

      Me=L'*me*L;
      Ke=L'*ke*L;

      % Global mass & stiffness matrices for each element

      Mg(:,:,i)=AA(:,:,i)'*Me*AA(:,:,i);
      Kg(:,:,i)=AA(:,:,i)'*Ke*AA(:,:,i);
      Mg_initial(:,:,i)=Mg_initial(:,:,i)+Mg(:,:,i);
      Kg_initial(:,:,i)=Kg_initial(:,:,i)+Kg(:,:,i);
end

% Global Mass, Stiffness Matrix

Mg_final=zeros(ndof,ndof);
Kg_final=zeros(ndof,ndof);
for i = 1:nel
    Mg_final=Mg_final+Mg_initial(:,:,i);
    Kg_final=Kg_final+Kg_initial(:,:,i);
end

% Deleting redundant dofs 1,2 & 7,8 to produce 5X5 mass & stiffness
% matrices

Mg_dof=Mg_final;
Mg_dof(:,61:63)=[];
Mg_dof(:,1:3)=[];
Mg_dof(61:63,:)=[];
Mg_dof(1:3,:)=[];

Kg_dof=Kg_final;
Kg_dof(:,61:63)=[];
Kg_dof(:,1:3)=[];
Kg_dof(61:63,:)=[];
Kg_dof(1:3,:)=[];
```

```
M=Mg_dof;
K=Kg_dof;

%%%%%%%%%%%%%%%%%%%%%%%%%%%%%%%%%%%%%%%%%%%%%%%%%%%%%%%%%%%%%%%%%%%%%%%%%
%%%%%%%

% Natural Frequency & Mode Shapes

[m wsq]=eig(K,M);
wn=sqrt(diag(wsq));                  % wn in rad/sec
wn_sorted=sort(wn);                  % sorted wn
freq=wn_sorted/(2*pi)             % freq in Hz

%%%%%%%%%%%%%%%%%%%%%%%%%%%%%%%%%%%%%%%%%%%%%%%%%%%%%%%%%%%%%%%%%%%%%%%%%
%%%%%%%

% IMPACT
%E=4.395*10^11;
dt=0.000001;
% CALCULATE CONSTANTS
alpha=0.25;
delta=0.5;
a0 = 1/(alpha*dt^2);
a1 = a0*dt;
a2 = 1.d0/(2.d0*alpha)-1.d0;
a3 = (1.d0-delta)*dt;
a4 = delta*dt;

% Initial Calculation
u_ini=load('initial_disp_impact.txt');
ud_ini=load('initial_vel_impact.txt');
udd_ini=load('initial_accl_impact.txt');

u(:,1)=u_ini;
ud(:,1)=ud_ini;
udd(:,1)=udd_ini;

% MASS & VELOCITY OF PROJECTILE
m2=1.2;                             % kg
% m_p=[m2];                           % mass 'matrix'
m_p=m2;
E1 = 72500000000;                  %Young's modulus for the beam
E2 = 72500000000;                  %Young's modulus for the projectile
delta_1 = (1 - .29^2)/E1/pi;  %Delta for beam
delta_2 = (1 - .29^2)/E2/pi;  %Delta for projectile
vo= 240;                              % m/sec
KE=4/(3*pi)*(1/(delta_1 + delta_2))*sqrt(.01);  % Hertzian contact
stiffness,rad of tip of projectile=0.00001in

% INITIALIZE DISPLACEMENT, VELOCITY & ACCELERATION FOR PROJECTILE
u_p(:,1) = [0];
ud_p(:,1) = [vo];
udd_p(:,1) = [0];
```

```
t=0:dt:25e-3;                          % time (s)
tt=size(t);

Keff=K+a0*M;                            % frame
keff_p=a0*m_p;                          % projectile
InvKeff = inv(Keff);

Ft_ind(1)=0;
F(1)=0;
R_tmp = zeros(ndof - 6);

for j=1:(tt(1,2)-1)
    % Frame
    R_tmp(29,1) = Ft_ind(1);
    R_n(:,1) = R_tmp(:,1) + M*(a0*u(:,1) + a1*ud(:,1) + a2*udd(:,1));
    u_n(:,1) = InvKeff*R_n(:,1);
    udd_n(:,1) = a0*(u_n(:,1) - u(:,1)) - a1*ud(:,1) - a2*udd(:,1);
    ud_n(:,1) = ud(:,1) + a3*udd(:,1) + a4*udd_n(:,1);

    % Projectile
    R_p_tmp(1,1) = -Ft_ind(1);
    R_p_n(1,1) = R_p_tmp(1,1) + m_p*(a0*u_p(1,1) + a1*ud_p(1,1) +
a2*udd_p(1,1));
    u_p_n(1,1) = inv(keff_p)*R_p_n(1,1);
    udd_p_n(1,1) = a0*(u_p_n(1,1) - u_p(1,1)) - a1*ud_p(1,1) -
a2*udd_p(:,1);
    ud_p_n(1,1) = ud_p(1,1) + a3*udd_p(1,1) + a4*udd_p_n(1,1);

    % Indentation
    ind=u_p_n(1,1)-u_n(29,1);
    if ind<0
        Ft_ind(2)=0;
    else
        Ft_ind(2)=KE*(ind^(1.5));
    end

    Ft_ind(1)=Ft_ind(2);
    u(:,1)=u_n(:,1);
    ud(:,1)=ud_n(:,1);
    udd(:,1)=udd_n(:,1);
    u_p(1,1)=u_p_n(1,1);
    ud_p(1,1)=ud_p_n(1,1);
    udd_p(1,1)=udd_p_n(1,1);

    %Values for plot
    T(j)=dt*(j-1);
    Force(j) = Ft_ind(1);
    u_beam2(j) = u(5,1);
    u_beam3(j) = u(11,1);
    u_beam4(j) = u(17,1);
    u_beam5(j) = u(23,1);
    u_beam6(j) = u(29,1);
    u_beam7(j) = u(35,1);
    u_beam8(j) = u(41,1);
    u_beam9(j) = u(47,1);
```

```
    u_beam10(j) = u(53,1);
    u_projectile(j) = u_p(1,1);
    ud_beam(j) = ud(29,1);
    ud_projectile(j) = ud_p(1,1);
    udd_beam(j) = udd(29,1);
    udd_projectile(j) = udd_p(1,1);
    Moment(j) = 48*u_beam7(j)*E2*I/1.4^3;
    Stress(j) = Moment(j)*.0375/I;
end

%Force plot - FEM and timo
figure(1)
plot(T,Force,'r-'),grid;
title('Simply Supported Beam with Center Impact - Force vs. Time');
ylabel('Force (N)'); xlabel('Time (s)');
legend('Pinned Supports', 'Flexible Supports')
hold on

%Beam Displacement plot - FEM and Timo
figure(2)
plot(T,u_beam6,'r-'),grid;
title('Simply Supported Beam with Center Impact - Beam Center
Displacement vs. Time');
ylabel('Displacement (m)'); xlabel('Time (s)');
legend('Pinned Supports', 'Flexible Supports')
hold on

%Projectile displacement plot - FEM and Timo
figure(3)
plot(T,u_projectile,'r-'),grid;
title('Simply Supported Beam with Center Impact - Projectile
Displacement vs. Time');
ylabel('Displacement (m)'); xlabel('Time (s)');
legend('FEM - In House')
hold on

%Overlap plot - FEM
figure(4)
plot(T,Force,'black-',T,10^7*u_projectile,'b-',T,10^7*u_beam7,'r-
');grid on;
xlabel('Time (s)'); ylabel('Force (N)/Displacement (m*10^-7)');
legend('Force', 'Displacement Projectile', 'Displacement Beam');
title('SS Beam Center Impact - Force and Displacement Overlap');

%Beam and projectile velocity plot - FEM
figure(5)
plot(T, ud_beam, 'r-', T, ud_projectile, 'black-'); grid on;
title('SS Beam with Center Impact - Beam Velocity');
ylabel('Velocity (m/s)'); xlabel('Time (s)');
legend('Beam Velocity', 'Projectile Velocity');
hold on

%Beam and Projectile acceleration plot - FEM
figure(6)
plot(T, udd_beam, 'r-', T, udd_projectile, 'black-'); grid on;
title('SS Beam with Center Impact - Beam Acceleration');
```

```
ylabel('Acceleration (m/s^2)'); xlabel('Time (s)');
legend('Beam Acceleration', 'Projectile Acceleration');
hold on

%Beam and Projectile acceleration plot - FEM
figure(7)
plot(T, u_beam2, 'b-', T, u_beam4, 'black', T, u_beam6, 'r', T,
u_beam8, 'g', T, u_beam10, 'y'); grid on;
title('SS Beam with Center Impact - Beam Nodal Displacement');
ylabel('Displacement (m)'); xlabel('Time (s)');
legend('Node 2', 'Node 4', 'Node 6', 'Node 8', 'Node 10');

%Beam Displacement plot - FEM and Timo
figure(8)
plot(T,Stress,'r-'),grid;
title('Simply Supported Beam with Center Impact - Max Bending Stress in
Beam vs. Time');
ylabel('Stress (Pa)'); xlabel('Time (s)');
legend('Pinned Supports', 'Flexible Supports')
hold on
```